Universitetet
i Stavanger

DET TEKNISK-NATURVITENSKAPELIGE FAKULTET

MASTEROPPGAVE

Studieprogram/spesialisering: **Petroleum Engineering / Reservoir Technology**	Vår.....semesteret, ..2010... Åpen / ~~Konfidensiell~~
Forfatter: **Pål Østebø Andersen**	Pål Andersen..... (signatur forfatter)

Fagansvarlig: **Steinar Evje**

Veileder(e): **Steinar Evje**

Tittel på masteroppgaven:

Matematisk modellering av vann-mineral-kjemi under vanninjeksjon og dens påvirkning på komposisjon og porøsitet i kalk

Engelsk tittel:

Mathematical modeling of water-rock chemistry during water injection and its impact on the composition and porosity of chalk

Studiepoeng: **30**

Emneord: **Water weakening** **Chalk** **Convection** **Diffusion** **Water-rock chemistry** **Strang-splitting** **Water injection**	Sidetall: .....**72**..... + vedlegg/annet: .....**18**..... Stavanger, ...**14/6, 2010**..... dato/år

Contents

Abstract

In recent years more attention has been paid to the chemical side of injected water used in chalk formations to help produce hydrocarbons. It seems the brine has a tendency to react with the formation itself if it contains the right substances, even sea water has this effect. Especially the chalk experiences the phenomenon called water weakening which affects the rocks response to external loading, but also its wettability.

Experiments have been performed in the laboratory at the University of Stavanger on chalk core plugs. Essentially the cores have been exposed to a brine under high pressure and temperature (representative reservoir conditions) a long time to reach equilibrium. Then different brines have been injected through the core at the given conditions at fixed rates typically around 1 PV (pore volume) per day by varying the inlet/outlet pressure. Responses such as core deformations and outlet concentrations have been measured. SEM images were used to study composition of the cores.

The experiments showed that results are sensitive to injection concentration of the ions Ca^{2+}, Mg^{2+} and SO_4^{2-}. Rock composition changed after flooding. Especially injecting $MgCl_2$-solution gave precipitation of a magnesium-based mineral, and flooding with seawater gave precipitation of a sulphate based mineral. The results are believed related to dissolution/precipitation reactions in an interplay with convection, diffusion and aqueous chemical reactions. A mathematical model [22] has been developed that is able to replicate the outlet measurements with good accuracy. It was developed by S. Evje, A. Hiorth, M. Madland and R. Korsnes. The same authors presented supportive experimental data and some alterations in [23].

The focus of this thesis is to expand the original model. Especially we include the mineral dolomite as a precipitate and we let rock properties such as porosity and permeability change with rock composition. Some relevant experiments are also suggested to better estimate parameters used in the model.

The water weakening effect has impact on areas such as porosity, permeability (plugging or opening of pores), compressibility (higher rock expansion means more produced pore fluid), tensile strength (can affect fracture pressure), wettability, residual saturations, water breakthrough, recovery and subsidence.

Chapter 1

Summary

In this thesis the model developed in [22, 23] has been investigated and further developed. The mineral dolomite was included to the minerals calcite, magnesite and anhydrite. Porosity was included as a function of the mineral composition. Some suggestions are given to explore effects on permeability and pressure, but under the assumptions of the model they are both eliminated from the system and no relevant data was available for testing.

Computer simulations show that dolomite by itself and magnesite by itself as the only magnesium-bearing mineral precipitating in the core can explain the effluents measured at the outlet. However, to explain SEM observations the presence of both is required. Several combinations of rate parameters are possible to fit the experimental effluent data in each model (dolomite only, magnesite only, dolomite and magnesite), but the magnesite model gave more options to determine a best fit than the dolomite model.

The simulations predicted a steady dissolution of calcite and precipitation of the minerals magnesite, dolomite and anhydrite when the environment suggested so. The net effect was a very low variation in porosity (from 0.48 to 0.47), both locally and on average, even after a period of 20 days. The reason is that the dissolved minerals are replaced by precipitating minerals and the composition changes. This conclusion is supported by the mass balance of ions where excess Ca^{2+} is produced while Mg^{2+}- and SO_4^{2-}-ions are retained in the core compared to a simulation with no reactions.

2 models were tested: one with constant porosity in the equations, with porosity only as a function of the solution of mineral composition. The other where porosity varied in the equations as well being coupled with the rest of the system. The low variation in porosity made the results from the 2 models undistinguishable.

The model does not account for available surface area in the reactions and that would probably improve the fit with experimental data at early times to a great extent.

Chapter 2

Reservoir rocks and geology

2.1 The geological aspect

When minerals are deposited, buried and compacted they become part of a sedimentary rock, per definition. The deposition can occur by transport of grains, chemicals can precipitate from solution or small organisms can leave shells and skeletons of mineral composition. During the compaction the space between the grains is reduced since the accumulating overburden forces will force the grains to pack into tighter configurations. In this process the volume occupied by fluids is reduced either because they escape or because they are compacted more easily until the pore pressure fractures an opening. Weak minerals can be ground into smaller pieces leaving a denser packing. However, most sedimentary rocks retain a relatively large fraction of pore volume, porosity, of many tens percent and that is why sedimentary rocks are good for storing hydrocarbons.

The burial process is also key to the formation of petroleum. When organic material is buried in a manner that preserves it from oxidation then it will be exposed to a gradual increase in temperature and pressure. Smaller organic molecules transform into larger complex substances. The organic material is by definition divided into kerogen and bitumen. Kerogen is the part insoluble in organic solvents, while bitumen (oil in solid state) is the soluble part. Such processes begin shallow compared to the formation of petroleum. When kerogen is exposed to high pressure and temperature over long time it turns into petroleum. The oil window is a range of temperatures where oil generation is possible. Oil begins to form at 60 ^oC with optimal conditions between 100-120 ^oC. At temperatures higher than 180 ^oC a process called cracking breaks down heavy molecules into smaller components. Gas formation is still possible above these temperatures but approaching 225 ^oC most of these processes have already happened.

Once petroleum (oil or gas) becomes mobile it will try to escape towards the surface since it has lower density than water. If it does not escape from the source rock (where the kerogen is being transformed) it will be destroyed as explained previously. The hydrocarbons will then follow a migration route along pore channels in the rock until it reaches the surface and is destroyed by bacteria or until it reaches a boundary that does not allow flow in the upward direction. This requires that a permeable and porous formation, which we call a reservoir, intersects the migration route and that a cap rock / trap overlays cuts off the route. Also, the seal must be in place before the oil can escape. The seal must keep the hydrocarbons trapped for maybe millions of years until present. Geologic activity in the crust can disturb this, but also create new possible trap configurations. The golden zone is the temperature range where oil reservoirs are actually found. It peaks around 90 ^oC but ranges from about 60 to 150 ^oC.

2.2 Reservoir rocks

2.2.1 Quantification

Although every rock is in some sense unique, we can quantify a rocks properties by performing lab tests on cores and evaluate logs and thin cuttings.

- Porosity ϕ is the volume fraction of a rock that is filled with fluids such as brine, gas and oil. High porosity indicates a high storage capacity and is given as a fraction between 0 and 1.
- Permeability k measures the ability a rock has to let a fluid flow as a single phase through the rock in a given direction. Permeability generally is anisotropic (varies with direction) and is often lower in the vertical direction. It is measured in darcy. High permeability indicates a rock with little flow restriction in the given direction, while a low permeability indicates narrow pore throats or complex pore channels.
- Wettability indicates the interplay between the rock and the pore fluids. When two fluids are placed on the rock they will be divided by an interface. One fluids tendency to spread on the rock will be given by the angle the fluid interface makes with the rock surface. If it is much less than 90 degrees the fluid is wetting, if the angle is much more than 90 the other fluid is wetting. If the angle is close to 90 degrees the rock is not preferentially wetted by either fluid. Neutral wettability is preferable for high recovery.
- Mechanical properties explain how the rock deforms to different loadings. Tests can quantify drive mechanisms such as rock expansion by pore pressure depletion and borehole stability.
- Chemical composition and the distribution of the grains can be important if the rock is chemically reactive. It is well known that clays are especially reactive due to high surface area compared to volume. They can work as catalysts for chemical reactions, can expand or compress due to ion exchange and bind water. The available surface area of the common grains is also of importance to the rate of reactions.
- Temperature and pressure at reservoir conditions is a critical factor since the behavior of rock, fluid and chemistry can change dramatically.

2.2.2 Carbonates

Carbonates are minerals containing the CO_3^{2-}-anion in combination with different cations. In reservoir engineering especially the carbonate minerals calcite, $CaCO_3$, and dolomite, $CaMg(CO_3)_2$, are of importance since limestone formations and dolomite formations respectively have these minerals as the major ingredient. Less known carbonates are aragonite $CaCO_3$ (other structure than calcite), siderite $FeCO_3$, magnesite $MgCO_3$ and ankerite $Ca(Fe, Mg, Mn)(CO_3)_2$.

Carbonate reservoirs are among the worlds largest. They are found worldwide and about 40% of the world hydrocarbon production is from carbonates.

For petroleum storage only marine carbonates matter. These carbonate sediments are products from living organisms (such as pellets), dead organisms (shells and skeletons) and precipitation of salts. The depositional environment is mostly shallow: ramps and platforms (the limestone reservoir Ghawar in Saudi Arabia is a good example), reefs or evaporites. However we also find reservoirs after great depth deposition by carbonate turbidites and as remains of pelagic creatures. Pelagic carbonates (made from ancient coccolithospheres) gives origin to chalk. The North Sea contains the giant Ekofisk oil field which mainly consists of chalk rock.

Chalk formations are characterized by high porosity (can approach 70%, but is mostly in the area $15 - 50\%$) and very low permeability (a few mD). Natural fracturing improves the effective large scale permeability to the range of 100 md. Chalks are mostly oilwetting and have a large reactive surface area.

Much of the focus in the text will be mostly relevant to chalk since the water weakening effect is most severe in these rocks. However the similar chemical composition of limestones in particular suggests that water weakening can play a role also in these formations.

Dolomites are often associated with evaporitic environments. This mineral is not formed directly, but requires the presence of $CaCO3$ (either as calcite or preferably aragonite) and magnesium ions. The transformation of a limestone into dolomite is called dolomitization and this process is believed to have formed most dolomite reservoirs. Basically Ca^{2+} is partly replaced by Mg^{2+} in the rock structure.

$$2CaCO_3 + Mg^{2+} \rightleftharpoons CaMg(CO_3)_2 + Ca^{2+} \tag{2.1}$$

The conditions for this process to move to the right is that $CaCO_3$ is unstable, the fluid is oversaturated on dolomite and Mg^{2+} is supplied adequately.

2.2.3 Sandstones

Sandstones are clastic (made of grains from pre-existing rocks). We sort clastic rocks by grain size and sandstone is on the coarse side of the scale (as opposed to claystone with much smaller grains). Sandstones contain mostly quartz, SiO_2, and feldspars (tectosilicates containing Si, O, Na, K, Al, Ca). However, mineral precipitation from fluids can contribute to fill the pore space in a process called cementation. Such minerals are calcite and other carbonates, quartz, clays and zeolites.

2.3 Chemical rock-fluid equilibrium

A rock can under normal circumstances be assumed to be in equilibrium with its pore fluids, meaning that any chemical reaction rates are negligible. The system is characterized by the local pressure and temperature on site and the local composition of the rock and fluids.

When introducing, let us say, sea water to the system it may have a low temperature, if it is injected there will be a pressure gradient and the composition of the sea water may be quite different from the one in equilibrium with the rock. A front will move from the injection site characterized by that in front the fluid is in equilibrium with the rock, while behind the front the state is different. Moving a fluid from one PT state to another can influence the solubility of its salts. Salt precipitation can reduce flow area in pores and pipes and should generally be avoided. A higher temperature will increase solubility in most cases, but an important exception is $CaCO_3$ which behaves exactly opposite. This behaviour is called retrogade solubility. So even if the compositions are the same a change in thermodynamical state can impose reactions.

Given 2 unequal fluids that can be treated as a single phase the ions will spread by diffusion (driven by concentration gradients), convection (fluid flow due to pressure gradients) and chemical reactions (working to establish a new rock-fluid equilibrium). These processes are generally very coupled since the reactions depend on local concentrations and state, the convection depends on pressure drop, rock permeability and fluid viscosity. Changes in fluid composition and state can alter viscosity, changes in the rock mechanical properties and grain distribution change permeability and porosity. Diffusion depends on component distribution, flow conditions and pore structure.

A model describing how the distribution of chemical substances progresses during injection was developed in [22] and [23]. This transport model will be explained starting in chapter 5 and reformulated during this thesis.

2.4 References

[1, 2, 3, 4, 5, 6, 22]

Chapter 3

Water weakening

3.1 Water weakening

In short words, water weakening means a rock loses some of its ability to resist deformation from the surrounding forces. This change is related to reactions with a reactive brine.

To understand water weakening one should have a basic understanding of rock mechanical theory. The sections 3.2, 3.3 and 3.4 give a summary of important concepts, relations and test methods. They are mostly based on [6], a book recommended if a more thorough description is needed.

In the last sections we will present some observations made on field scale and in the laboratory that illustrate the effects.

3.2 Stress and strain

The concept of stress is defined as force divided by area.

$$\sigma \equiv \frac{dF}{dA} \tag{3.1}$$

Stress is normal if the force works perpendicular to the surface and shear if it acts parallel to the surface. For an isotropic material stress is a tensor since a force can act in 3 directions on surfaces normal to 3 axis. Assuming force and moment equilibrium this tensor is symmetric. The stress tensor can be divided into a hydrostatic part (with only normal stresses nonzero and having the value of the mean normal stress) and a deviatoric part (which is simply the remaining part of the matrix). The hydrostatic part indicates a level of compressive or expansive load while the deviatoric part indicates how the unequal stress distribution compares.

Given a stress tensor we can find 3 perpendicular axis corresponding to zero shear stresses and thus all stresses are directed along the coordinate axis. These normal stresses are called principal stresses and define the stress state along with their direction. In any direction that is not exactly on one of the axis there will also be a shear stress, which can be expressed as a function of the principal stress values. Note that if the principal stresses are identical the loading will be hydrostatical seen from any angle. If 2 principal stresses are equal the plane that contains them contains no shear stress.

In rock mechanics it is usual to use positive stress for compression and negative stress for tension, and the principal stresses are labeled in descending order as σ_1, σ_2, σ_3.

Normal strain is defined as change in length divided by the original length L_0 of the unloaded material:

$$\varepsilon \equiv \frac{L_0 - L}{L_0} \tag{3.2}$$

It is positive for shortening and negative for extension. For small loadings, stresses and strains are linearly related.

Given a porous sample some of the load is carried by the pore fluid, given by the pore pressure, p_f times Biot's coefficient, α. The effective stress σ' that is carried by the rock grains is then

$$\sigma' \equiv \sigma - \alpha p_f \tag{3.3}$$

The deformation results from loading the rock and relates to effective stress by Youngs modulus E:

$$\sigma' = E\varepsilon \tag{3.4}$$

A load in one axial direction z causes deformation of opposite sign along the other axes x, y related by Poissons ratio ν

$$\nu \equiv -\frac{\varepsilon_x}{\varepsilon_z} \tag{3.5}$$

Volumetric deformation is given by

$$\varepsilon_V = \frac{V_0 - V}{V_0} = \varepsilon_x + \varepsilon_y + \varepsilon_z \tag{3.6}$$

If a volume is hydrostatically loaded (all principal stresses equal) by the load σ'_c the volumetric deformation is given by

$$\sigma'_c = K\varepsilon_V \tag{3.7}$$

where K is the bulk modulus.

3.3 Tests in a triaxial cell

A cylindrical core sample is placed vertically between two axial bolts and sealed from the surroundings by a thin sleeve. A confining pressure $\sigma_c = \sigma_r = \sigma_\theta$ (for a cylindrical geometry we use the coordinates r, θ, z) in the horizontal plane is provided by a confining fluid. Axial stress σ_z is provided by increasing the pressure in a fluid chamber above the upper axial bolt that pushes it down against the core sample. We must correct for friction, but in principle we know the axial load. Small openings in the bolts allow circulation of fluid and thus a pore pressure we can vary.

Axial strain is measured by displacement of the bolt (after correcting its own deformation) and radial strain is measured by sensors pointed towards the core surface.

In drained tests fluid can escape and the fluid carries a constant load p_f. In a standard triaxial compression test the load is increased hydrostatically ($\sigma'_c = \sigma'_z$) and the bulk modulus of the framework K_{fr} (representing the porous rocks ability to resist deformation) is measured as the slope

$$K_{fr} = \frac{\Delta\sigma'_z}{\Delta\varepsilon_V} = \frac{\Delta\sigma'_z}{3\Delta\varepsilon_z} \tag{3.8}$$

After this hydrostatic phase has reached a certain σ_c, the confining load is kept constant and the axial load is increased further. The Youngs modulus of the framework is then determined as

$$E_{fr} = \frac{\Delta\sigma'_z}{\Delta\varepsilon_z} \tag{3.9}$$

in this deviatoric phase.

3.4 Rock failure

Materials and rocks of low porosity do not fail hydrostatically until at very high pressures. However chalk is very porous and under enough pressure the pores can collapse by local shear failure. In the deviatoric phase we define the yield point as the effective stress that is followed by a nonlinear

stress-strain relation. The rupture stress of the rock is the stress that leads to rupture. However once this stress has been reached a relaxation of the stress allows further displacement even at lower stress before the sample finally ruptures. This explains why a process of incremental displacement is preferred over incremental loading, to observe the last phase.

Chalk can also experience creep. It is a timedependent deformation that occurs under constant stress and temperature. Note that the applied stress can be less than what causes plastic deformation (permanent strain). We can divide the creep into a transient state (decreasing strain rate), steady state (constant strain rate) and accelerating state (increasing strain rate) eventually leading to rupture.

3.5 Lab test observations

3.5.1 Simultaneous water injection and loading

In [21] several lab experiment results are presented. In one of them chalk cores at 130 ^oC are flooded with different brines while being loaded hydrostatically. The resulting stress-strain diagram is repeated left in Fig 3.1. It was observed that the cores got a lower yield stress (average of 6.5 MPa) when they were flooded with the sulphate containing brines than with the sulphate-deficient ones (average of 8.5 MPa). The sulphate exposed cores also got a much higher compaction (2.5 times the strain than those not exposed to sulphate at high stress). Note also that the bulk modulus (given by one third of the initial linear slope, as in eq. (3.8)) is less for the weakened samples (by a factor of ca 2/3).

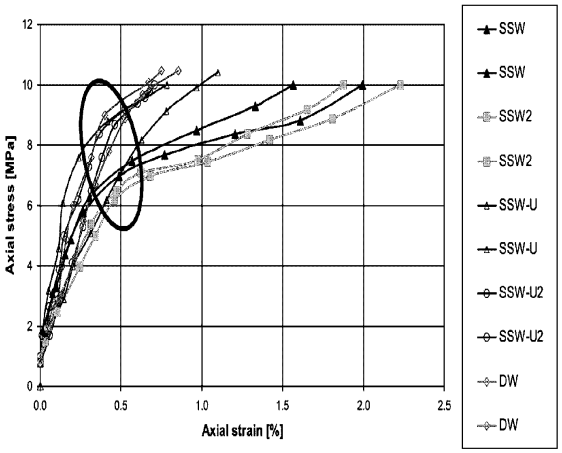

Fig. 9—Stress-strain plot during the dynamic test at 130°C for different flooding fluids.

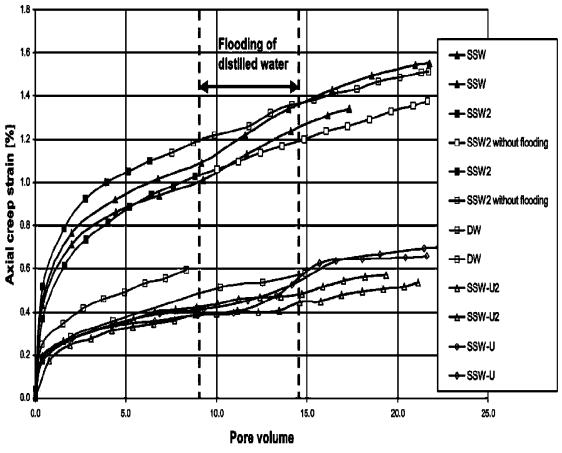

Fig. 10—Compaction during the creep phase at 130°C for different flooding fluids.

Figure 3.1: Left: Stress-strain diagram for hydrostatic loading of chalk cores at 130 ^oC while flooding brine at constant rate. Right: The following creep diagram at 10 MPa compressive stress.

When reaching 10 MPa stress this load was kept constant and the resulting creep was observed. The creep phase results are given right in Fig 3.1. Again the sulphate-exposed cores showed a much higher degree of compaction than the others. Flooding with a high concentration sulphate brine (double of seawater) led to plugging of the core, probably due to precipitation of anhydrite $CaSO_4$.

An important conclusion in the paper was that the ions Mg^{2+}, Ca^{2+} and SO_4^{2-} (in amounts comparable to that found in seawater) can impact the mechanical behavior and wettability of chalk.

3.5.2 Response to water injection in a loaded state

In [13] sandstone cores were cleaned using methanol and toluene, then dried. The cores were then saturated with decane and loaded in a triaxial cell such that $\frac{\Delta\sigma_c'}{\Delta\sigma_z'} = 0.25$. The cores were kept at a fixed stress state several days and no creep strain was observed. Slow injection with 3% KCl solution in the cores resulted in immediate response either by shear failure or quite noticeable axial and/or radial strain. Creep (continuing deformation) was also observed. This demonstrates that water weakening can be relevant also for sandstones, but that other mechanisms may be involved.

North Sea chalk was saturated with mineral oil and loaded uniaxially with a constant loading rate. The strain increase was approximately linear with time. After 290 hours North Sea water was injected into the core and a rapid increase in axial strain was observed followed by creep.

3.5.3 Potential candidates for magnesium precipitates

Flooding chalk cores with $MgCl_2$-brine result in water weakening, according to [16]. The flooding showed a lower outlet concentration of Mg^{2+} than could be explained by adsorption and ion substitution. It was concluded that a magnesium based mineral precipitating in the core could explain the observations. For the given experiment (0.219 M $MgCl_2$, T=130 ^oC, P=8 bar, $P_{CO2} = 10^{-3.5}$) simulations using EQAlt showed that several magnesium minerals were supersaturated given by the value of ion product ratio Q over solubility constant K being greater than 1. Especially huntite ($CaMg_3(CO_3)_4$) and hydro-magnesite had large such numbers, but simpler minerals such as dolomite and magnesite were also supersaturated (see Fig 3.2). Note that the large Q/K

Mineral	Log_{10} Q/K
Huntite	5.25
Hydromagnesite	4.13
Dolomite	3.25
Brucite	2.46
Magnesite	2.09
Artinite	0.94

Figure 3.2: Supersaturated magnesium minerals, table from [16]

ratio of huntite can be explained by its dependence on Mg^{2+} and CO_3^{2-} concentrations. Assume both dolomite and huntite are exactly saturated at a given state ($Q/K = 1$) in separate solutions. Doubling the concentration of Ca^{2+}, Mg^{2+} and of CO_3^{2-} would make $(Q/K)_{dolomite} = 2^1 \cdot 2^1 \cdot 2^2 = 16$ while $(Q/K)_{huntite} = 2^1 \cdot 2^3 \cdot 2^4 = 256$. If precipitation leads to the initial equilibrium concentrations the same number of moles are precipitated in each solution.

	Magnesite	Calcite	Dolomite	Huntite	Mag + Dol		Analysis
C	14.25	12.00	13.03	13.61	13.64		16.91
O	56.93	47.96	52.06	54.38	54.49		49.85
Mg	28.83	0.00	13.18	20.65	21.00		20.27
Ca	0.00	40.04	21.73	11.35	10.87		11.92
Sum	100.00	100.00	100.00	100.00	100.00		98.95

Figure 3.3: Comparison of weight distribution of analysis with weight distribution of known minerals

In [17] a presentation of composition analysis using SEM (scanning electron microscope) showed a weight distribution of the molecules in precipitated mineral grains that looked similar to huntite.

These numbers are here compared against the weight composition of the minerals dolomite, calcite, magnesite and huntite in Fig 3.3. It is seen that the analysis results can be explained as the precipitation of huntite, but a combination of the minerals magnesite and dolomite (taking the average of their distributions) gives almost exactly the same distribution as huntite (a better weighed average would fit even better to the analysis).

In the model [22, 23] magnesite is the only magnesium based mineral included. We expand this by including dolomite also. It should be considered though that huntite is just as relevant and perhaps can even be representative for the entire magnesium mineral precipitation.

3.6 Field observations

3.6.1 Valhall

In a paper [15] from 1989 rock compressibility was concluded to be an important parameter for the high porosity chalk field Valhall causing porosity reduction, compaction of reservoir intervals and seabed subsidence.

3.6.2 Ekofisk

A case study of the chalk field Ekofisk in the North Sea is presented in [14] from 1999. The field started producing in 1971, water injection began in 1987. Seafloor subsidence (see left in Fig. 3.4) increased in the 90's and the seafloor dropped at a rate of 25 to 42 cm per year. Over the years this resulted in several meters. In 94 the injection was increased to replace the produced reservoir fluid volume, but the subsidence did not decrease significantly and kept a steady rate above 35 cm/y most of the 90s. The models used so far (matching historical oil rate, water injection, GOR and water cut profiles) could not explain the observed compaction after 93, when the pressure decline was beginning to stop by increased support. Including a water weakening mechanism to the model gave just as good prediction of the previous parameters, but the compaction volume was better estimated (right in Fig. 3.4).

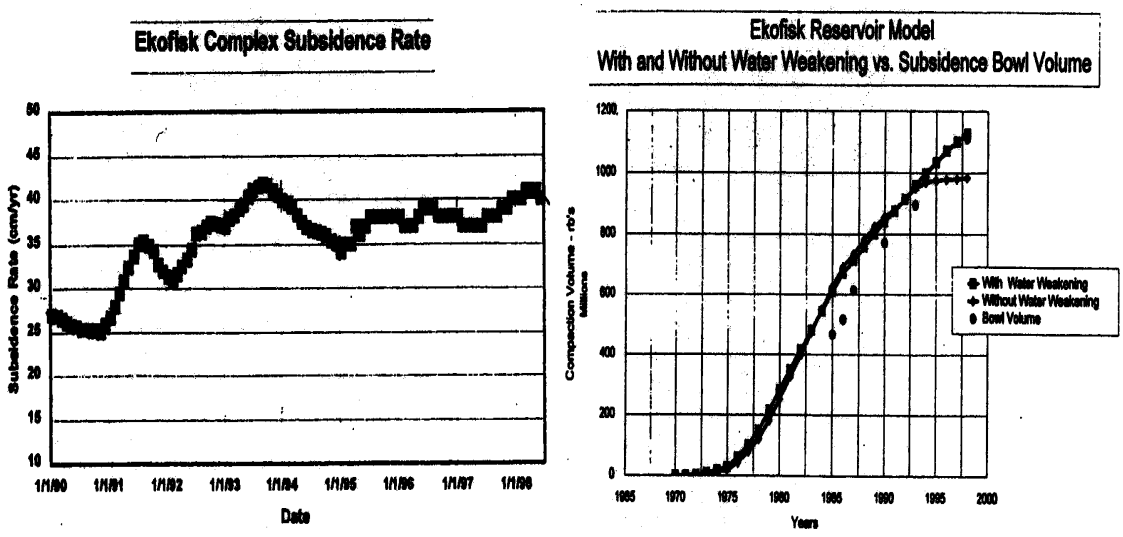

Figure 3.4: Observed subsidence rate (left) and history matching of compaction volume (right) at Ekofisk

Chapter 4

Relevant minerals in chalk replacement: Volumetric considerations

4.1 Including more minerals and volumetric considerations

We want to consider what happens if calcite $CaCO_3$ dissolves and is replaced by another precipitating mineral. If the new mineral takes less space there should be increased porosity, while minerals taking more space would reduce porosity. For simplicity we assume that the moles of ions in solution are negligible to those that have precipitated. In this way we can quickly estimate whether an increase or reduction in porosity is likely for the injected brine and which ions that should be produced. From another point of view, given the brine and outlet composition we can make a qualified guess of which reactions are taking place in the core. For the calculations we use that calcite has density 2.71 g/cm^3 and molar weight 100.087 g/mol so 1 mol calcite corresponds to

$$\frac{1mol * 100.087g/mol}{2.71(g/cm3)} = 36.93cm3 \tag{4.1}$$

In the original model [22, 23] only calcite, magnesite and anhydrite minerals were considered. We evaluate some different minerals and their possible relevance to water weakening.

4.2 Magnesium-bearing minerals

4.2.1 Magnesite

Magnesite $MgCO_3$ created from calcite can be described as

$$CaCO_3 + Mg^{2+} \rightleftharpoons MgCO_3 + Ca^{2+} \tag{4.2}$$

Magnesite has a density of ca. 3.1 g/cm^3 (actually between 3.0 and 3.2) and molar weight 84.314 g/mol. 1 mol of calcite would have a volume of 36.93 cm^3 and if it was transformed into magnesite the solid volume would be

$$\frac{1mol * 84.314g/mol}{3.1(g/cm3)} = 27.20cm3 \tag{4.3}$$

a volume reduction of 26.3%. With fluid allowed to escape it is easy to see how such a process could be relevant to water weakening. For one thing it would selfcontract the matrix and enhance compaction, despite if the fluid held the same pressure. Second, loadcarrying grain microstructures would be destabilized and the strength of the rock should decrease.

4.2.2 Dolomite

As mentioned dolomite, $CaMg(CO_3)_2$, is closely linked with calcite in its geological formation and it is reasonable to think they could transform into each other chemically under the right circumstances. Especially the supply of magnesium ions is necessary, but the rate of this transformation is also important (whether the reactions happen fast enough to matter). We can consider the transformation as a net reaction of the form

$$2CaCO_3(s) + Mg^{2+}(aq) \rightleftharpoons CaMg(CO_3)_2(s) + Ca^{2+}(aq) \tag{4.4}$$

Dolomite has density 2.85 g/cm^3 and molar weights 184.401 g/mol respectively. 2 moles of calcite has a volume of

$$2 * 36.93 = 73,86cm3 \tag{4.5}$$

while if these moles were transformed to 1 mol dolomite the volume of solid would be

$$\frac{1mol * 184.401g/mol}{2.85(g/cm3)} = 64,70cm3 \tag{4.6}$$

A complete transformation of calcite into dolomite would mean almost 12.5% reduction in rock volume.

4.2.3 Huntite

As mentioned huntite $CaMg_3(CO_3)_4$ can be a very relevant mineral for water weakening given results from SEM measurements. Calcite-huntite transformation could go as

$$4CaCO_3(s) + 3Mg^{2+}(aq) \rightleftharpoons CaMg_3(CO_3)_4(s) + 3Ca^{2+} \tag{4.7}$$

4 moles calcites has a volume of $4 * 36.93 = 147.72\ cm^3$. Huntite has density 2.87 g/cm^3 (from [26]) and molar weight 353.029 g/mol so 1 mol huntite has volume

$$\frac{1mol * 353.029g/mol}{2.87(g/cm3)} = 123.01cm3 \tag{4.8}$$

leading to a rock volume reduction of 16.73%.

The transformation of calcite into magnesium-bearing minerals seems to reduce the matrix volume.

4.3 Sulphate-bearing minerals

4.3.1 Anhydrite

The last mineral used in the original model was anhydrite: $CaSO_4$. It should be noted that anhydrite can bond with water to form gypsum $CaSO_4 \cdot 2H_2O$. A net transformation of calcite into anhydrite can be described by

$$CaCO_3 + SO_4^{2-} \rightleftharpoons CaSO_4 + CO_3^{2-} \tag{4.9}$$

Anhydrite has density 2.97 g/cm^3 and molar weight 136.139 g/mol. 1 mol calcite transformed into anhydrite would go from 36.93 cm3 solid volume to

$$\frac{1mol * 136.139g/mol}{2.97(g/cm3)} = 45.84cm3 \tag{4.10}$$

an increase of 24.1% suggesting that if this reaction is dominant we should observe a reduced permeability and perhaps even plugging. It can be mentioned that gypsum has lower density ($2.31 - 2.33\ g/cm^3$) and higher molar weight suggesting that a partial convertion of anhydrite into gypsum would further fill the pores by increasing the solid volume. Gypsum is however moderate soluble while anhydrite is less soluble and thus more relevant.

4.4 Iron-bearing minerals: ankerite and siderite

This is just for mentioning. Iron ions have not been included in the model so far, but can play a role. Especially in the case of drilling, particles from pipes or equipment can be carried with the flow either as grains or dissolved and affect a local region (iron has a negligible concentration in sea water). If this is significant a skin can develop close to the well.

Siderite $FeCO_3$ and ankerite $CaFe(CO_3)_2$ have densities 3.5 and $2.9 - 3.1$ g/cm^3 and molar weights 115.854 and 215.941 g/mol. Following the transformations of calcite as

$$CaCO_3 + Fe^{2+} \rightleftharpoons FeCO_3 + Ca^{2+} \tag{4.11}$$

$$2CaCO_3 + Fe^{2+} \rightleftharpoons CaFe(CO_3)_2 + Ca^{2+} \tag{4.12}$$

we get for siderite a volume reduction of 10.4%, while for ankerite we can get somewhere between .81% expansion and 9.4% reduction. Both cases lean toward a reduction in matrix-volume. In other words it seems iron ions will not cause chemical damage to limestone and chalk reservoirs. Near hole damage is likely more affected by mud particles plugging the pore throats.

Chapter 5

Transport-reaction model

The transport model suggested in [22] considers the process of introducing a brine into a porous rock containing an original brine in chemical equilibrium. The solution can be described by indicating the concentration of each chemical at a given location, whether it be rock minerals, water or dissolved substances. Specifically the unknowns we solve for are the pore concentrations C_i of components in fluid phase, the total volume concentrations of minerals ρ_i and pressure p. All these variables are functions of position and time (x, t). Temperature is considered constant, as is the partial pressure of dissolved gas in water.

To solve the equations we use molar balance equations, equations for instant water equilibrium and a charge balance. Incorporated into these equations are rate expressions for the rock/fluid reactions and the fluid component velocities.

The application is particularly relevant for chalk reservoirs or more generally carbonate reservoirs and this is reflected in the considered chemical reactions.

5.1 Components

We divide all chemical components into 4 groups. They are presented by name, chemical composition and primary unknown with index used for reference in equations. Dolomite has been added to the model see if it makes a better fit than magnesite or if both minerals should be included.

5.1.1 Solid state: minerals

- Calcite, $CaCO_3$, ρ_c
- Anhydrite, $CaSO_4$, ρ_g
- Magnesite, $MgCO_3$, ρ_m
- Dolomite, $CaMg(CO_3)_2$, ρ_d

5.1.2 Aqueous state: ions

- Calcium, Ca^{2+}, C_{ca}
- Magnesium, Mg^{2+}, C_{mg}
- Sulphate, SO_4^{2-}, C_{so}
- Sodium, Na^{+}, C_{na}
- Cloride, Cl^{-}, C_{cl}

- Hydron, H^+, C_h
- Hydroxide, OH^-, C_{oh}
- Bicarbonate, HCO_3^-, C_{hco}
- Carbonate, CO_3^{2-}, C_{co}

5.1.3 Dissolved gas

- Carbon dioxide, CO_2, P_{CO2} (assumed given by temperature)

5.1.4 Liquid state

- Water, H_2O, C_l

Note that the minerals are assumed to exist only in solid phase while the other components are assumed to be part of the water phase, either as ions, dissolved gas or water.

5.2 Reactions

5.2.1 Dissolution and precipitation of minerals

- Calcite: $CaCO_3 + H^+ \rightleftharpoons Ca^{2+} + HCO_3^-$
- Anhydrite: $CaSO_4 \rightleftharpoons Ca^{2+} + SO_4^{2-}$,
- Magnesite: $MgCO_3 + H^+ \rightleftharpoons Mg^{2+} + HCO_3^-$,
- Dolomite: $CaMg(CO_3)_2 + 2H^+ \rightleftharpoons Ca^{2+} + Mg^{2+} + 2HCO_3^-$

These reactions between fluid and rock occur with a finite rate defined in section 5.6. We use them to define the rate terms in the differential equations.

5.2.2 Aqueous reactions

- $CO_2 + H_2O \rightleftharpoons HCO_3^- + H^+$
- $HCO_3^- \rightleftharpoons CO_3^{2-} + H^+$
- $H_2O \rightleftharpoons H^+ + OH^-$

The reactions in the fluid phase occur at high rates compared to the mineral reactions and are assumed to be in equilibrium. They are used as constraints, that is 3 equations to determine 3 unknowns.

5.3 Porosity and volume balance

In the former models [22, 23] a variable porosity has not been fully considered. This section will attempt to make a physically meaningful definition of porosity as a function of the local variables.

Given all the components we can separate them into those existing in solid phase (minerals) and those in the fluid phase (water, dissolved ions and gas). Consider a small part of the core sample with volume V. At a given time all components have defined their total concentration ρ_i, where i represents the given component. If we also know the molar masses, $M_i = \frac{\text{mass}}{\text{mol}}$, and effective densities, $\omega = \frac{\text{mass}}{\text{effective volume}}$ (by effective volume we mean the volume the component

would fill if we could isolate it from the other components), we can calculate each components number of moles n_i, mass m_i and volume V_i:

$$n_i = \rho_i V \tag{5.1}$$
$$m_i = M_i \rho_i V \tag{5.2}$$
$$V_i = \frac{M_i \rho_i V}{\omega_i} \tag{5.3}$$
$$\frac{V_i}{V} = \frac{M_i \rho_i}{\omega_i} \tag{5.4}$$

Note that the last equation is the volume fraction of component i. Since the total volume is the sum of effective volumes

$$V = A\Delta x = \sum_i V_i = \sum_i \frac{M_i \rho_i V}{\omega_i} \tag{5.5}$$
$$\sum_i \frac{M_i \rho_i}{\omega_i} = 1 \tag{5.6}$$

The volume fraction of solid phase is then

$$\frac{V_{minerals}}{V} = \sum_{i:minerals} \frac{M_i \rho_i}{\omega_i} \tag{5.7}$$

and the porosity is per definition the remaining volume fraction

$$\phi = 1 - \sum_{i:minerals} \frac{M_i \rho_i}{\omega_i} \tag{5.8}$$

Eqn (5.6) can in theory be used as a constraint on the unknowns (just as the sum of saturations should be 1 in a multiphase problem). In practice there are a few difficulties though. If we have properly defined the chemical structure of each component then all M_i can be found from tables. (Effective) density for rocks and water is also available in the literature and it can be adjusted for temperature and pressure using the minerals coefficient of thermal expansion ($\alpha = \frac{dV}{VdT}$), the pressure compressibility ($\beta = -\frac{dV}{Vdp}$) and the deviations from the reference state. Increased pressure and increased temperature tend to have opposite effect, and both values are typically of low order (percents) for solid rocks and liquids and we assume the densities remain constant for simplicity. There will be more uncertainty related to how much effective volume is occupied by the dissolved ions and gas. Water is polar and could sometimes be pushed away by equal charges to increase the effective volume. In just the same way it could work to shrink. The ions themselves will perhaps occupy more effective space if they are more charged. One possibility is to assume the atoms are so far apart due to low concentrations that their effective volume is the same, especially the same as water, which is known with great accuracy since its density is known. We will give a better definition of volume balance later using the water phase as a whole.

The mentioned uncertainties do not effect (5.8) since the ions are not included, but the volume balance must be a constraint to define the porosity the way we do.

In the original model [22, 23] it was assumed that porosity was constant. Letting it vary will increase the coupling of variables in the differential equations.

5.4 Permeability and possible hysteresis

In short words we treat local permeability as a function of local porosity. In [22, 23] it has been assumed constant.

Chalk has narrow pore throats, but large pores, resulting in high porosity and low permeability. When grains are forced against each other they will tend to dissolve at the contact points and

smoothen to reduce the stress locally. Given fluid flow through the pore network and using Bernoulli's law it is clear that the velocity will be greater in the pore throats and the pore pressure less. Higher velocity will drag on the grains and reduced pore pressure will increase the load carried by the rock. These mechanisms would favor an improvement in permeability by increased porosity. On the other hand, when the flow enters the wide pores and the pressure is larger and velocity smaller, grains should settle and possibly precipitation would occur more easily in these regions. Following this reasoning deposition should not effect the size of the pore throats very much. A reduction in porosity should reduce permeability less than a cleaning effect would increase it. This would lead to a form of hysteresis, meaning that a porosity increase, followed by a porosity reduction to the same level would give a better permeability. We neglect any such behavior, partly for simplification, and partly because the porosity should go mainly in one direction. The model assumes no movement of solid particles carried by the fluid. That means particles larger than the pore throats do not cause any plugging effect.

It should be noted that the processes described will depend on fluid velocity, its ability to carry grains (involves viscosity), the variation in area from pore to throat, rates of dissolution/precipitation, stresses in the rock, fluid pressure and probably other factors. Since it would be practically impossible to make accurate measurements relating such pore scale effects to permeability which is measured on core scale we settle for a more uncertain relation that just relates permeability to porosity, that is $k = k(\phi)$. This can be justified by thinking of low permeability as a region of locally low porosity. The measured permeability over the core length will depend on the whole distribution, especially on the smallest values.

Assume we have an initial distribution of both permeability and porosity: $k(x, t = 0) = k_0$ and $\phi(x, t = 0) = \phi_0$. We assume there is a function $f(\cdot)$ such that

$$\frac{k}{k_0} = f(\frac{\phi}{\phi_0}) \tag{5.9}$$

With no hysteresis initial ϕ corresponds to initial k, so $f(1) = 1$. Improving one should improve the other so $f' > 0$. Both should be zero at the same time so $f(0) = 0$. If it is true that the throats are attacked first then the effect should be most rapid close to the original state when the throats are small compared to the pores. Also the effect should be less powerful when they are comparable in size, suggesting that $f'' < 0$.

Some suggestions are evaluated in appendix **??** with references. It is shown that depending on the choice of formulation of f we require a correlation to fit

$$f(x) = \begin{cases} x^a & 0 < x < 1 \\ bx^c + 1 - b & x > 1 \end{cases} \tag{5.10}$$

with

$$a > 1; \quad b > 0; \quad 0 < c < 1 \tag{5.11}$$

$$\text{or} \quad a > 1; \quad b, c < 0 \tag{5.12}$$

or we can use the correlation

$$f = \begin{cases} \frac{e^{ax}-1}{e^a-1} & 0 < x < 1 \\ be^{cx} + 1 - be^c & x > 1 \end{cases} \tag{5.13}$$

with

$$a > 0; \quad b, c < 0 \tag{5.14}$$

These are derived from typical permeability-porosity correlations where parameters should depend on lithology and the mechanism of the structural changes involved.

5.5 Molar balance

The assumptions are that moles are transported in the fluid phase with a certain velocity. The velocity depends both on fluid velocity and diffusion. Solid components are not transported by the flow, but accumulate or diminish locally by precipitation or dissolution.

Assume a thin cutting of a core that has crossectional area A (assumed constant with time and position) and length Δx. At position x fluid enters the volume, and at $x+\Delta x$ fluid leaves. During the time Δt there is a change in the total content of moles of the substance due to transport and chemical reaction. We denote porosity as ϕ, component velocity in the pore space v (positive in the x-direction), concentration of component as moles per volume fluid C and chemical production of moles per volume fluid per time as $\dot{r}$. For a component in the fluid phase we have:

$$(A\phi Cv)_x\Delta t - (A\phi Cv)_{x+\Delta x}\Delta t = \text{moles added by flow} \tag{5.15}$$

$$A\Delta x\dot{r}\Delta t = \text{moles created by reactions inside the volume} \tag{5.16}$$

$$(A\Delta x\phi C)_{t+\Delta t} - (A\Delta x\phi C)_t = \text{change in number of moles} \tag{5.17}$$

Since the accumulation is the sum of chemical generation and transport across boundaries we have

$$(A\Delta x\phi C)_{t+\Delta t} - (A\Delta x\phi C)_t = (A\phi Cv)_x\Delta t - (A\phi Cv)_{x+\Delta x}\Delta t + A\Delta x\dot{r}\Delta t \tag{5.18}$$

Divide by $A\Delta x\Delta t$ and let both $\Delta x, \Delta t \to 0$

$$\frac{(\phi C)_{t+\Delta t} - (\phi C)_t}{\Delta t} = \frac{(\phi Cv)_x - (\phi Cv)_{x+\Delta x}}{\Delta x} + \dot{r} \tag{5.19}$$

$$\frac{\partial(\phi C)}{\partial t} = -\frac{\partial(\phi Cv)}{\partial x} + \dot{r} \tag{5.20}$$

$$\frac{\partial(\phi C)}{\partial t} + \frac{\partial(\phi Cv)}{\partial x} = \dot{r} \tag{5.21}$$

Fluid concentration is defined as $C = \frac{\text{mol}}{\text{pore volume}}$. Since porosity is $\phi = \frac{\text{pore volume}}{\text{total volume}}$ we can define total concentrations as

$$\rho = \frac{\text{mol}}{\text{total volume}} = \frac{\text{pore volume}}{\text{total volume}}\frac{\text{mol}}{\text{pore volume}} = \phi C \tag{5.22}$$

Eqn (5.21) can then be written in terms of total concentrations as

$$\frac{\partial\rho}{\partial t} + \frac{\partial(\rho v)}{\partial x} = \dot{r} \tag{5.23}$$

For the solid components there is only chemical contribution to the accumulation so a similar derivation results in

$$\frac{\partial\rho}{\partial t} = \dot{r} \tag{5.24}$$

Equations (5.21) and (5.24) are those originally used. We will make a small alteration by noting that the rate terms should be related to the pore volumes, since that is where reactions take place. In other words $\dot{r}$ means moles generated per time per pore volume from now on. To convert this into rates per total volume again so the balance is correct, the terms are multiplied by porosity:

$$\frac{\text{moles}}{\text{time}\cdot\text{total volume}} = \frac{\text{pore volume}}{\text{total volume}}\frac{\text{moles}}{\text{time}\cdot\text{pore volume}} \tag{5.25}$$

$$\dot{r}_{tot} = \phi\cdot\dot{r}_{pore} \tag{5.26}$$

The molar balance equations are now

$$\frac{\partial(\phi C)}{\partial t} + \frac{\partial(\phi Cv)}{\partial x} = \phi\dot{r} \quad \text{for nonsolid components} \tag{5.27}$$

$$\frac{\partial\rho}{\partial t} = \phi\dot{r} \quad \text{for solid components} \tag{5.28}$$

5.6 Reaction rates

Assume a reaction of the form

$$aA + bB \rightleftharpoons cC + dD \tag{5.29}$$

of chemical reactants A and B and products C and D where a, b, c, d are stoichiometric coefficients that preserve molar and charge balance. The rate of the reaction is defined (see also [10, 11]) by

$$\dot{r} = -\frac{1}{a}\frac{dn_A}{Vdt} = -\frac{1}{b}\frac{dn_B}{Vdt} = \frac{1}{c}\frac{dn_C}{Vdt} = \frac{1}{d}\frac{dn_D}{Vdt} \tag{5.30}$$

where n is moles and V is pore volume. The rate is positive when the reaction is shifted to the right (A and B are consumed, C and D are produced).

We are really interested in the derivatives on the right side which is the reactions contribution to the component rates used in the equations. For example we can say that for A

$$\dot{r}_A = \frac{dn_A}{Vdt} = \frac{dC_A}{dt} = -a\dot{r} \tag{5.31}$$

stating that if the reaction moves to the right ($\dot{r}$ positive) then A is consumed by an amount of a compared to the reaction rate.

The reaction rate is a function of the chemical activity, a_i of the involved components. Activity is directly related to fluid concentration C_i by

$$a_i = \gamma_i C_i \tag{5.32}$$

where γ_i is the activity coefficient of component i, to be discussed later.

The rate of which the left and right side components transform can be given as $k_{+1}a_A^a a_B^b$ and $k_{-1}a_C^c a_D^d$ where k_{+1} and k_{-1} are positive constants, but specific for the given reaction and the temperature of consideration. The net rate of the reaction is

$$\dot{r} = k_{+1}a_A^a a_B^b - k_{-1}a_C^c a_D^d \tag{5.33}$$

Such a formulation was made in [22].

In [23], a rate expression of the form

$$\dot{r} = k(1 - \Omega)^n \tag{5.34}$$

was adopted from [10], only using $n = 1$ for simplicity. This model will also be applied here. Its application is dissolution reactions and Ω is defined as the activity product ratio divided by the solubility constant.

$$\Omega = Q/K \tag{5.35}$$

We will show which assumptions can lead to such a model: The point of view is that the reactions of consideration are dissolution reactions with component A being the mineral. Minerals, water and CO_2 are here assumed to have activity equal to 1. Gas components are normally represented by their partial pressure in reaction rates, but it is assumed here that all gas exists dissolved in the water phase and that this amount is given by the constant temperature.

Dissolution has rate $k_{+1}a_A^a = k_{+1}$ while precipitation has rate $k_{-1}\frac{a_C^c a_D^d}{a_B^b}$. The net reaction rate is then

$$\dot{r} = k_{+1} - k_{-1}\frac{a_C^c a_D^d}{a_B^b} \tag{5.36}$$

Having defined the reactions the exponents are known and given the current state, so are the activities. If we know k_{+1} and k_{-1} we can specify the reaction rate and thus the chemical production/consumption of a given component due to this specific reaction. k_{+1} and k_{-1} are related by

the solubility product K which can be found experimentally or perhaps even in chemistry tables. At equilibrium the reaction rate is 0 and we define

$$K \equiv \frac{k_{+1}}{k_{-1}} = \frac{a_C^c a_D^d}{a_B^b} \tag{5.37}$$

The same value of K results from both rate formulations, but the specific values of k_{+1} and k_{-1} can be different.

We then write the reaction rate as

$$\dot{r} = k_{+1}(1 - \frac{a_C^c a_D^d}{a_B^b K}) \tag{5.38}$$

and note that the mentioned Ω is the ratio of activity products divided by the equilibrium constant for the reaction.

Dissolution can happen only as long as the mineral exists. Each dissolution reaction rate will therefore be modified so that if the concentration of the mineral is 0 the reaction rate cannot be positive, but is set to 0.

The rate expression is written as a function F times the k_{+1} factor. We then separate F into 2 terms according to when it is positive or negative. When F is positive and mineral concentration is zero, rate is set to 0.

$$F \equiv 1 - \Omega = (1 - \frac{a_C^c a_D^d}{a_B^b K}) = F^+ - F^- \tag{5.39}$$

$$F^+ \equiv \max(0, F), \quad F^- \equiv \max(0, -F), \quad sgn^+(x) = \begin{cases} 1 & \text{if } x \geq 0 \\ 0 & \text{else} \end{cases} \tag{5.40}$$

$$\dot{r} = k_{+1}[sgn^+(\rho)F^+ - F^-] \tag{5.41}$$

5.6.1 Chemical activity

Ion activities a_i are related to fluid concentrations C_i as $a_i = \gamma_i C_i$. γ_i is component i's activity coefficient, given by the Debye-Huckel formula (see [10, 12])

$$-\log_{10}(\gamma_i) = \frac{A(T) Z_i^2 \sqrt{I_0}}{1 + a_i^0 B(T) \sqrt{I_0}} \tag{5.42}$$

$$I_0 = \frac{1}{2} \sum_i C_i Z_i^2 \tag{5.43}$$

where I_0 is the ionic activity and Z_i are the ionic charges. a_i^0 are component specific constants indicating the effective size of the hydrated ion measured on angstrom and can be found from tables such as in [12]. The constants we use are

$$\begin{aligned} &Z_{ca} = +2, \quad Z_{mg} = +2, \quad Z_{so} = -2, \quad Z_{na} = +1, \quad Z_{cl} = -1, \quad Z_h = +1, \\ &Z_{oh} = -1, \quad Z_{hco} = -1, \quad Z_{co} = -2 \\ &a_{ca}^0 = 6, \quad a_{mg}^0 = 8, \quad a_{so}^0 = 4, \quad a_{na}^0 = 4, \quad a_{cl}^0 = 3, \quad a_h^0 = 9, \\ &a_{oh}^0 = 3.5, \quad a_{hco}^0 = 4, \quad a_{co}^0 = 4.5 \end{aligned}$$

$A(T)$ and $B(T)$ are correlations of the density of water, the dielectric constant of water which depends on temperature and temperature itself. Such relations are given in [12].

The temperature we consider is a constant 130 degrees Celsius and we have

$$A(T = 130) = 0.6623 \quad B(T = 130) = 0.3487 \tag{5.44}$$

which were calculated in [22, 23] using the simulator EQAlt. I_0, the ionic activity is evaluated with the composition of the injected fluid and assumed constant. In total all activity coefficients are then treated as constants for a given simulation.

5.6.2 Reaction rates for the model

The final rate expressions for the reactions in subsection 5.2.1 become

$$\text{Calcite:} \quad \dot{r}_c = k_1^c[sgn^+(\rho_c)F_c^+ - F_c^-] \quad F_c = 1 - \frac{\gamma_{ca}\gamma_{hco}}{\gamma_h K^c}\frac{C_{ca}C_{hco}}{C_h} \tag{5.45}$$

$$\text{Anhydrite:} \quad \dot{r}_g = k_1^g[sgn^+(\rho_g)F_g^+ - F_g^-] \quad F_g = 1 - \frac{\gamma_{ca}\gamma_{so}}{K^g}C_{ca}C_{so} \tag{5.46}$$

$$\text{Magnesite:} \quad \dot{r}_m = k_1^m[sgn^+(\rho_m)F_m^+ - F_m^-] \quad F_m = 1 - \frac{\gamma_{mg}\gamma_{hco}}{\gamma_h K^m}\frac{C_{mg}C_{hco}}{C_h} \tag{5.47}$$

$$\text{Dolomite:} \quad \dot{r}_d = k_1^d[sgn^+(\rho_d)F_d^+ - F_d^-] \quad F_d = 1 - \frac{\gamma_{ca}\gamma_{mg}\gamma_{hco}^2}{\gamma_h^2 K^d}\frac{C_{ca}C_{mg}C_{hco}^2}{C_h^2} \tag{5.48}$$

5.6.3 Aqueous reactions and charge balance

The aqueous reactions in subsection 5.2.2 are instantly at equilibrium and we write

$$C_1 = P_{CO2}K = a_{hco}a_h = \gamma_{hco}\gamma_h C_{hco}C_h \tag{5.49}$$

$$C_2 = \frac{a_{co}a_h}{a_{hco}} = \frac{\gamma_{co}\gamma_h}{\gamma_{hco}}\frac{C_{co}C_h}{C_{hco}} \tag{5.50}$$

$$C_w = a_h a_{oh} = \gamma_h\gamma_{oh}C_h C_{oh} \tag{5.51}$$

$$C_3 = C_{hco} + 2C_{co} + C_{oh} - C_h \tag{5.52}$$

for 3 constants $C_1(T), C_2(T), C_w(T)$ and a function C_3 that are all independent of $C_{hco}, C_{co}, C_{oh}, C_h$. C_1 in eq (5.49) is constant based on the equilibrium constant for the reaction, K, and the assumption that the partial pressure of CO_2 is constant. C_2 and C_w are also equilibrium constants. Eq (5.52) is based on the charge balance

$$\sum_{i:ions} C_i Z_i = 0 \Rightarrow C_3 \equiv 2(C_{ca} + C_{mg} - C_{so}) + (C_{na} - C_{cl}) = C_{hco} + 2C_{co} + C_{oh} - C_h \tag{5.53}$$

The reactions are assumed to happen so fast that changes in some concentrations will instantly shift the concentrations $C_{hco}, C_{co}, C_{oh}, C_h$ to fit aqueous equilibrium. In other words, at a given temperature and time the 4 values can be calculated. We define 3 new constants based on our knowledge of $C_1(T), C_2(T), C_w(T)$ and the activity coefficients:

$$\tilde{C_1} = \frac{C_1}{\gamma_{hco}\gamma_h} = C_{hco}C_h \quad \tilde{C_2} = \frac{C_2\gamma_{hco}}{\gamma_{co}\gamma_h} = \frac{C_{co}C_h}{C_{hco}} \quad \tilde{C_w} = \frac{C_w}{\gamma_h\gamma_{oh}} = C_h C_{oh} \tag{5.54}$$

Assuming a pH between 6 and 8 we follow the assumption in [22] that we can neglect C_{co} in (5.52) and get

$$C_3 = C_{hco} + C_{oh} - C_h = \frac{\tilde{C_1}}{C_h} + \frac{\tilde{C_w}}{C_h} - C_h \tag{5.55}$$

$$\Rightarrow \quad C_h^2 + C_3 C_h - (\tilde{C_1} + \tilde{C_w}) = 0 \tag{5.56}$$

$$\Rightarrow \quad C_h = \frac{1}{2}\left(-C_3 + \sqrt{C_3^2 + 4(\tilde{C_1} + \tilde{C_w})}\right) \tag{5.57}$$

$$\Rightarrow \quad C_{hco} = \frac{\tilde{C_1}}{C_h} \quad C_{co} = \frac{\tilde{C_2}C_{hco}}{C_h} = \frac{\tilde{C_1}\tilde{C_2}}{C_h^2} \quad C_{oh} = \frac{\tilde{C_w}}{C_h} \tag{5.58}$$

These concentrations will affect the reaction rates. They change according to the transport of the other ions requiring updated values for C_3.

5.7 Transport equations

The following equations are the ones we need to solve in the most general case we consider.

$$\begin{aligned}
\partial_t(\phi C_l) + \partial_x(\phi C_l v_l) &= 0 && H_2O \text{ flowing water} && (5.59)\\
\partial_t(\phi C_{na}) + \partial_x(\phi C_{na} v_{na}) &= 0 && Na^+\text{-ions in water} && (5.60)\\
\partial_t(\phi C_{cl}) + \partial_x(\phi C_{cl} v_{cl}) &= 0 && Cl^-\text{-ions in water} && (5.61)\\
\partial_t(\phi C_{ca}) + \partial_x(\phi C_{ca} v_{ca}) &= \phi(\dot{r}_c + \dot{r}_g + \dot{r}_d) && Ca^{2+}\text{-ions in water} && (5.62)\\
\partial_t(\phi C_{so}) + \partial_x(\phi C_{so} v_{so}) &= \phi\dot{r}_g && SO_4^{2-}\text{-ions in water} && (5.63)\\
\partial_t(\phi C_{mg}) + \partial_x(\phi C_{mg} v_{mg}) &= \phi(\dot{r}_m + \dot{r}_d) && Mg^{2+}\text{-ions in water} && (5.64)\\
\partial_t \rho_c &= -\phi\dot{r}_c && CaCO_3\text{-mineral} && (5.65)\\
\partial_t \rho_g &= -\phi\dot{r}_g && CaSO_4\text{-mineral} && (5.66)\\
\partial_t \rho_m &= -\phi\dot{r}_m && MgCO_3\text{-mineral} && (5.67)\\
\partial_t \rho_d &= -\phi\dot{r}_d && CaMg(CO_3)_2\text{-mineral} && (5.68)
\end{aligned}$$

As we have shown, including more reactions and minerals can easily be implemented. Including new ions can be a little trickier. The charge balance is changed and we need another transport equation if the ions presence is controlled by flow and rock-fluid reactions. If it is controlled by aqueous equilibrium we get a more complicated system of algebraic equations that needs to be solved.

5.7.1 Component velocities

In the transport equations we still need to determine each components interstitial velocity, v_i. We divide the water phase into water component l and ion group g such that

$$C_g = C_{na} + C_{cl} + C_{ca} + C_{mg} + C_{so} \tag{5.69}$$

Only the ions whose concentration are determined by flow and rock-fluid reactions are involved. The total concentration of flowing ions in the water phase is then

$$C = C_l + C_g \tag{5.70}$$

The seepage velocities V_l for water and V_g for ions are related to the interstitial velocities as

$$V_l = \phi v_l \quad V_g = \phi v_g \tag{5.71}$$

so that the transport equations for water and ions take the form

$$\begin{aligned}
\partial_t(\phi C_l) + \partial_x(C_l V_l) &= 0 && \text{Water component} && (5.72)\\
\partial_t(\phi C_i) + \partial_x(C_i V_g) &= \phi\dot{r}_i && i = na, cl, ca, so, mg && (5.73)
\end{aligned}$$

The water phase seepage velocity V is related to the component seepage velocities by

$$CV = C_g V_g + C_l V_l \tag{5.74}$$

and obeys Darcy's law

$$V = -\frac{k}{\nu}\partial_x p \tag{5.75}$$

where ν is fluid phase dynamic viscosity and k is the permeability along the core. The ions move relative to the phase speed due to diffusion with relative velocity

$$U_g = V_g - V \tag{5.76}$$

According to Ficks law we have for each ion that the molar flux is proportional to the concentration gradient.

$$C_i \frac{U_g}{\phi} = -D\partial_x C_i \qquad i = na, cl, ca, so, mg \tag{5.77}$$

Note that the mechanism works to create a smooth concentration profile and even the distribution locally. The proportionality factor D is called the effective dispersion coefficient and is assumed equal for all components. It varies with porosity and phase seepage velocity as

$$D = D_m\phi + \frac{F_I d_p}{2}\frac{V}{\phi} = D_m\phi + \alpha\frac{V}{\phi} \tag{5.78}$$

where constants D_m, F_I and d_p are molecular diffusion coefficient, formation inhomogeneity factor and average particle diameter respectively. $\alpha = \frac{F_I d_p}{2}$ is called the dispersion length. More information and references about diffusion is found in appendix C.

We update the transport equations with this information:

$$\begin{aligned}
& \partial_t(\phi C_i) + \partial_x(C_i V_g) && = \phi\dot{r}_i && (5.79)\\
\Rightarrow\quad & \partial_t(\phi C_i) + \partial_x(C_i U_g) && = \phi\dot{r}_i - \partial_x(C_i V) && (5.80)\\
\Rightarrow\quad & \partial_t(\phi C_i) - \partial_x(D\phi\partial_x C_i) && = \phi\dot{r}_i - \partial_x(C_i V) && (5.81)\\
& i = na, cl, ca, so, mg
\end{aligned}$$

We now wish to replace the equation for the water component with an equation for the water phase. First we add the equations for the ions

$$\begin{aligned}
\sum_i [\partial_t(\phi C_i) - \partial_x(D\phi\partial_x C_i)] &= \sum_i [\phi\dot{r}_i - \partial_x(C_i V)] && (5.82)\\
\Rightarrow \partial_t(\phi\sum_i C_i) - \partial_x(D\phi\partial_x\sum_i C_i) &= \phi\sum_i \dot{r}_i - \partial_x(\sum_i C_i V) && (5.83)\\
\Rightarrow \partial_t(\phi C_g) - \partial_x(D\phi\partial_x C_g) &= \phi\sum_i \dot{r}_i - \partial_x(C_g V) && (5.84)
\end{aligned}$$

The water component flux is related to V and U_g as follows

$$C_l V_l = CV - C_g V_g = CV - C_g(U_g + V) = (C - C_g)V - C_g U_g = C_l V - C_g U_g = C_l V + D\phi\partial_x C_g \tag{5.85}$$

This is used in the equation for the water component

$$\begin{aligned}
\partial_t(\phi C_l) + \partial_x(C_l V_l) &= 0 && (5.86)\\
\partial_t(\phi C_l) + \partial_x(C_l V) + \partial_x(D\phi\partial_x C_g) &= 0 && (5.87)\\
\partial_t(\phi C_l) + \partial_x(D\phi\partial_x C_g) &= -\partial_x(C_l V) && (5.88)
\end{aligned}$$

Adding eqs. (5.84) and (5.88) gives

$$\begin{aligned}
\partial_t(\phi C_g) - \partial_x(D\phi\partial_x C_g) + \partial_t(\phi C_l) + \partial_x(D\phi\partial_x C_g) &= \phi\sum_i \dot{r}_i - \partial_x(C_g V) - \partial_x(C_l V) && (5.89)\\
\Rightarrow \partial_t(\phi C) &= \phi\sum_i \dot{r}_i - \partial_x(CV) && (5.90)
\end{aligned}$$

5.7.2 Volume conservation

In addition to these equations we must have volume preservation. We assume that the total water phase has the same volume as the volume defined by the concentration C, that is the ions involved in aqueous reactions are assumed to have negligible volume. Given molar weight M and density ω of the water phase and minerals we must have that the sum of all volume fractions equals 1:

$$\frac{M_w}{\omega_w}\phi C + \frac{M_c}{\omega_c}\rho_c + \frac{M_g}{\omega_g}\rho_g + \frac{M_m}{\omega_m}\rho_m + \frac{M_d}{\omega_d}\rho_d = 1 \tag{5.91}$$

Note that this equation expresses local volume conservation in space. It does not imply that the volume is constant in time and can be used also if the crossection of the core is compressed.

5.7.3 Updated equation system

Our system of equations then becomes

$$\begin{aligned}
\partial_t(\phi C) + \partial_x(CV) &= \phi(\dot{r}_c + 2\dot{r}_g + \dot{r}_m + 2\dot{r}_d) && (5.92)\\
\partial_t(\phi C_{na}) - \partial_x(D\phi\partial_x C_{na}) &= -\partial_x(C_{na}V) && (5.93)\\
\partial_t(\phi C_{cl}) - \partial_x(D\phi\partial_x C_{cl}) &= -\partial_x(C_{cl}V) && (5.94)\\
\partial_t(\phi C_{ca}) - \partial_x(D\phi\partial_x C_{ca}) &= \phi(\dot{r}_c + \dot{r}_g + \dot{r}_d) - \partial_x(C_{ca}V) && (5.95)\\
\partial_t(\phi C_{so}) - \partial_x(D\phi\partial_x C_{so}) &= \phi\dot{r}_g - \partial_x(C_{so}V) && (5.96)\\
\partial_t(\phi C_{mg}) - \partial_x(D\phi\partial_x C_{mg}) &= \phi(\dot{r}_m + \dot{r}_d) - \partial_x(C_{mg}V) && (5.97)\\
\partial_t\rho_c &= -\phi\dot{r}_c && (5.98)\\
\partial_t\rho_g &= -\phi\dot{r}_g && (5.99)\\
\partial_t\rho_m &= -\phi\dot{r}_m && (5.100)\\
\partial_t\rho_d &= -\phi\dot{r}_d && (5.101)\\
\frac{M_w}{\omega_w}\phi C &= 1 - \left(\frac{M_c}{\omega_c}\rho_c + \frac{M_g}{\omega_g}\rho_g + \frac{M_m}{\omega_m}\rho_m + \frac{M_d}{\omega_d}\rho_d\right) && (5.102)\\
D &\equiv D_m\phi + \alpha\frac{V}{\phi} && (5.103)\\
V &\equiv -\frac{k}{\nu}\partial_x p && (5.104)\\
\phi &\equiv 1 - \frac{M_c}{\omega_c}\rho_c + \frac{M_g}{\omega_g}\rho_g + \frac{M_m}{\omega_m}\rho_m + \frac{M_d}{\omega_d}\rho_d && (5.105)\\
k &\equiv k_0 f(\frac{\phi}{\phi_0}) && (5.106)
\end{aligned}$$

Equations (5.92)-(5.102) are 11 equations used to solve for the 11 unknowns $C, C_{na}, C_{cl}, C_{ca}, C_{so}$, $C_{mg}, \rho_c, \rho_g, \rho_m, \rho_d, p$.

This is a 1-dimensional version of the model derived in [23] except we have included dolomite, treated the reaction rates as defined per pore volume, included total volume conservation given by eq. (5.102) and let the dispersion coefficient depend on interstitial velocity. Following the steps in [23] similar to here a 3D model can be derived and is given in appendix A.

We note that the given system still allows us to implement and find solutions for pH, aqueous concentrations, nonconstant densities $\omega_i(p)$, porosity $\phi(\rho_{minerals})$, permeability $k(\phi)$, diffusion coefficient $D(\phi, V)$ and more.

Chapter 6

Case definitions

6.1 Case I: Constant core properties and incompressible fluid

This is a direct continuation of the model tested in [23]. We specify the assumptions and consequences:

- The water phase is assumed incompressible: C is constant

$$C = \frac{\omega_w}{M_w} = \frac{1000 \text{ g/liter}}{18.015 \text{ g/mol}} = 55.5 \text{ mol/liter} \tag{6.1}$$

  In general density ω increases with salinity, but so does average molar weight when heavy ions such as sulphate and carbonate become a bigger part of the solution, so the effects on C are assumed to cancel out.

- The contribution from reactions in eq (5.92) is assumed negligible to the overall concentration and set to 0.
- Porosity ϕ is assumed constant: The left term in eq (5.92) vanishes and since C is constant we get $\partial_x(V) = 0$, stating that $V \equiv -\frac{k}{\nu}\partial_x p$ is uniform over x although it can change with time.
- $D \equiv D_m\phi + \alpha V$ can be treated as the sum of a constant part and a time-dependent part.
- Permeability k is constant (with the assumptions we have used this would also follow from constant porosity). That means the pressure gradient is constant from the definition of V.
- Pressure p is eliminated since its distribution is given by Darcys law.

From this we can remove eqn 5.92 (it reduces to $0 = 0$). Eq 5.102 reduces to

$$\frac{M_w}{\omega_w}\phi\frac{\omega_w}{M_w} = \phi = 1 - \left(\frac{M_c}{\omega_c}\rho_c + \frac{M_g}{\omega_g}\rho_g + \frac{M_m}{\omega_m}\rho_m + \frac{M_d}{\omega_d}\rho_d\right) = \phi \tag{6.2}$$

and can also be removed.

$$\partial_t(\phi C_{na}) - \partial_x(D\phi\partial_x C_{na}) = \partial_x(C_{na}\frac{k}{\nu}\partial_x p) \tag{6.3}$$

$$\partial_t(\phi C_{cl}) - \partial_x(D\phi\partial_x C_{cl}) = \partial_x(C_{cl}\frac{k}{\nu}\partial_x p) \tag{6.4}$$

$$\partial_t(\phi C_{ca}) - \partial_x(D\phi\partial_x C_{ca}) = \phi(\dot{r}_c + \dot{r}_g + \dot{r}_d) + \partial_x(C_{ca}\frac{k}{\nu}\partial_x p) \tag{6.5}$$

$$\partial_t(\phi C_{so}) - \partial_x(D\phi\partial_x C_{so}) = \phi\dot{r}_g + \partial_x(C_{so}\frac{k}{\nu}\partial_x p) \tag{6.6}$$

$$\partial_t(\phi C_{mg}) - \partial_x(D\phi\partial_x C_{mg}) = \phi(\dot{r}_m + \dot{r}_d) + \partial_x(C_{mg}\frac{k}{\nu}\partial_x p) \tag{6.7}$$

$$\partial_t\rho_c = -\phi\dot{r}_c \tag{6.8}$$

$$\partial_t\rho_g = -\phi\dot{r}_g \tag{6.9}$$

$$\partial_t\rho_m = -\phi\dot{r}_m \tag{6.10}$$

$$\partial_t\rho_d = -\phi\dot{r}_d \tag{6.11}$$

C, ϕ, k, ν are constant, D, V can change with time. This case requires solving the above 9 equations for the 9 unknowns $C_{na}, C_{cl}, C_{ca}, C_{so}, C_{mg}, \rho_c, \rho_g, \rho_m, \rho_d$.

The purpose of this case is to see what effect dolomite can have on the system: does it make a better fit than magnesite or should both minerals be included to get the correct behavior? Especially we are interested in determining a good fit for the rate constants.

Although we assume both k and ϕ constant it is interesting to see how they will behave as functions of the resulting redistribution of components. In other words in this case we treat the initial values as representative in the calculations and see what changes will occur.

6.2 Case II: Variable porosity and permeability

We now let ϕ and k change simultaneously with the concentrations. In general this should be solved by the equations (5.92-5.102). However solving this complete set of differential equations is more complicated than Case I since we would need to include numerical pressure-gradients in the expressions. To achieve numerical stability it is vital to use a correct numerical inclusion of this term and this will not be pursued further. We can however simplify the solution to this problem considerably even if the pressure gradient is nonconstant.

- As in Case I the water phase is still assumed incompressible: C is constant and equal to 55.5 mol/liter. As shown in the last section we can remove eq (5.102).
- The contribution from reactions in eq (5.92) is assumed to exactly balance the change in porosity caused by the dissolution/precipitation. Rock/fluid reactions are in other words assumed not to cause any net volume changes. Mathematically we assume

  $$\partial_t(\phi C) = \phi(\dot{r}_c + 2\dot{r}_g + \dot{r}_m + 2\dot{r}_d) \tag{6.12}$$

  which reduces eq (5.92) to

  $$\partial_x(CV) = 0 \Leftrightarrow V(t) = \text{constant} \Leftrightarrow \partial_x(k\partial_x p) = 0 \tag{6.13}$$

  Since the equation set only depends on V which is given by a freely defined function we can eliminate p as an unknown.
- Porosity will now vary according to mineral concentrations as defined.
- $D \equiv D_m\phi + \alpha V$ will not just be time dependent any more but vary with porosity
- Permeability k depends on porosity.

$$\partial_t(\phi C_{na}) - \partial_x(D\phi\partial_x C_{na}) = \partial_x(C_{na}\frac{k}{\nu}\partial_x p) \tag{6.14}$$

$$\partial_t(\phi C_{cl}) - \partial_x(D\phi\partial_x C_{cl}) = \partial_x(C_{cl}\frac{k}{\nu}\partial_x p) \tag{6.15}$$

$$\partial_t(\phi C_{ca}) - \partial_x(D\phi\partial_x C_{ca}) = \phi(\dot{r}_c + \dot{r}_g + \dot{r}_d) + \partial_x(C_{ca}\frac{k}{\nu}\partial_x p) \tag{6.16}$$

$$\partial_t(\phi C_{so}) - \partial_x(D\phi\partial_x C_{so}) = \phi\dot{r}_g + \partial_x(C_{so}\frac{k}{\nu}\partial_x p) \tag{6.17}$$

$$\partial_t(\phi C_{mg}) - \partial_x(D\phi\partial_x C_{mg}) = \phi(\dot{r}_m + \dot{r}_d) + \partial_x(C_{mg}\frac{k}{\nu}\partial_x p) \tag{6.18}$$

$$\partial_t\rho_c = -\phi\dot{r}_c \tag{6.19}$$

$$\partial_t\rho_g = -\phi\dot{r}_g \tag{6.20}$$

$$\partial_t\rho_m = -\phi\dot{r}_m \tag{6.21}$$

$$\partial_t\rho_d = -\phi\dot{r}_d \tag{6.22}$$

$$D \equiv D_m\phi + \alpha\frac{V}{\phi} \tag{6.23}$$

$$V(t) \equiv -\frac{k}{\nu}\partial_x p \tag{6.24}$$

$$\phi \equiv 1 - \frac{M_c}{\omega_c}\rho_c + \frac{M_g}{\omega_g}\rho_g + \frac{M_m}{\omega_m}\rho_m + \frac{M_d}{\omega_d}\rho_d \tag{6.25}$$

$$k \equiv k_0 f(\frac{\phi}{\phi_0}) \tag{6.26}$$

C, ν are constant, $V(t)$ can change with time. This case requires solving the first 9 equations above for the 9 unknowns $C_{na}, C_{cl}, C_{ca}, C_{so}, C_{mg}, \rho_c, \rho_g, \rho_m, \rho_d$, similar to case I.

6.3 Reformulating the problem

For the numerical solution of the problem it is advantageous to use either pore concentrations or total concentrations, but not both since it increases the number of variables. We decide to solve for total concentrations (this has an advantage that becomes apparent in a while). The equations can be written as 2 sorts:

$$\partial_t(\phi C_i) - \partial_x(D\phi\partial_x C_i) = \phi\dot{r}_i + \partial_x(C_i\frac{k}{\nu}\partial_x p) \tag{6.27}$$

$$\partial_t\rho_j = \phi\dot{r}_j \tag{6.28}$$

where i is for ions and j for minerals. Note that the last equation is just a special case of the first. We replace all pore concentrations by total concentrations. Porosity and permeability can vary.

$$\partial_t(\phi C_i) - \partial_x(D\phi\partial_x C_i) = \phi\dot{r}_i - \partial_x(C_i V) \tag{6.29}$$

$$\partial_t(\phi C_i) - \partial_x(D\phi\partial_x\frac{\phi C_i}{\phi}) = \phi\dot{r}_i - \partial_x(\frac{\phi C_i}{\phi}V) \tag{6.30}$$

$$\partial_t(\rho_i) - \partial_x(D\phi\partial_x\frac{\rho_i}{\phi}) = \phi\dot{r}_i - \partial_x(\frac{\rho_i}{\phi}V) \tag{6.31}$$

6.4 Units and dimensioning

It has been taken for granted that the units in the equations are consistent, but practically we do not acquire measurements in these units. Working with SI units we introduce the following units in the solution and convert all other measurements into them:

$$[x] = [\alpha] = m, \quad [t] = s, \quad [D] = [D_m] = m^2/s, \quad [k] = m^2, \quad [p] = Pa, \tag{6.32}$$

$$[\nu] = Pa \cdot s, \quad [\dot{r}] = mol/m^3 s \quad [C] = [\rho] = mol/liter, \quad [\phi] = 0, \tag{6.33}$$

Note that concentrations are given in moles per liter. The reason is that we will not scale the concentrations, but let the equations have the dimension of mol/liter after dimensioning.

To scale the problem we introduce positive constant reference values $\widehat{x}$, $\widehat{t}$, $\widehat{D}_m$, $\widehat{k}$ and $\widehat{p}$ that can be chosen arbitrarily, but should fit the dimensions of the analysis. From this we make dimensionless variables and parameters:

$$x' = \frac{x}{\widehat{x}} \quad t' = \frac{t}{\widehat{t}} \quad D'_m = \frac{D_m}{\widehat{D}_m} \quad k' = \frac{k}{\widehat{k}} \quad p' = \frac{p}{\widehat{p}} \tag{6.34}$$

$$x = \widehat{x}\,x' \quad t = \widehat{t}\,t' \quad D_m = \widehat{D}_m\,D'_m \quad k = \widehat{k}\,k' \quad p = \widehat{p}\,p' \tag{6.35}$$

We now transform V, D and then eq. (6.31) using the dimensionless variables.

$$V = -\frac{k}{\nu}\frac{\partial p}{\partial x} = -\frac{\widehat{k}k'}{\nu}\frac{\widehat{p}\partial p'}{\widehat{x}\partial x'} = -\frac{\widehat{k}\widehat{p}}{\widehat{x}\nu}\frac{k'\partial p'}{\partial x'} = \frac{\widehat{k}\widehat{p}}{\widehat{x}\nu}V' \tag{6.36}$$

$$V' \equiv -\frac{k'\partial p'}{\partial x'} \tag{6.37}$$

$$D = D_m\phi + \alpha\frac{V}{\phi} = \widehat{D}_m D'_m\phi + \frac{\alpha}{\phi}\frac{\widehat{D}_m}{\widehat{D}_m}\frac{\widehat{k}\widehat{p}}{\widehat{x}\nu}V' \tag{6.38}$$

$$D' \equiv \frac{D}{\widehat{D}_m} = D'_m\phi + \frac{\alpha}{\phi}\frac{1}{\widehat{D}_m}\frac{\widehat{k}\widehat{p}}{\widehat{x}\nu}V' = D'_m\phi + \frac{\alpha}{\phi\widehat{x}}\frac{\widehat{k}\widehat{p}}{\nu\widehat{D}_m}V' = D'_m\phi + \frac{\mu}{\phi}\varepsilon V' \tag{6.39}$$

$$\varepsilon \equiv \frac{\widehat{k}\widehat{p}}{\nu\widehat{D}_m} \qquad \mu \equiv \frac{\alpha}{\widehat{x}} \tag{6.40}$$

$$\partial_t(\rho_i) - \partial_x(D\phi\partial_x(\frac{\rho_i}{\phi})) = \phi\dot{r}_i - \partial_x(\frac{\rho_i}{\phi}V) \tag{6.41}$$

$$\frac{1}{\widehat{t}}\frac{\partial\rho_i}{\partial t'} - \frac{1}{\widehat{x}}\frac{\partial}{\partial x'}(\widehat{D}_m D'\phi\frac{1}{\widehat{x}}\frac{\partial}{\partial x'}(\frac{\rho_i}{\phi})) = \phi\dot{r}_i - \frac{1}{\widehat{x}}\frac{\partial}{\partial x'}(\frac{\rho_i}{\phi}\frac{\widehat{k}\widehat{p}}{\widehat{x}\nu}V') \tag{6.42}$$

$$\frac{\partial\rho_i}{\partial t'} - \frac{\partial}{\partial x'}\left(\frac{\widehat{D}_m\widehat{t}}{\widehat{x}^2}D'\phi\frac{\partial}{\partial x'}(\frac{\rho_i}{\phi})\right) = \widehat{t}\phi\dot{r}_i - \frac{\partial}{\partial x'}(\frac{\widehat{D}_m\widehat{t}}{\widehat{x}^2}\frac{\widehat{k}\widehat{p}}{\nu\widehat{D}_m}\frac{\rho_i}{\phi}V') \tag{6.43}$$

Since we can choose reference values arbitrarily we constraint $\widehat{D}_m$ by having

$$\widehat{D}_m \equiv \frac{\widehat{x}^2}{\widehat{t}} \tag{6.44}$$

From the definition of ε in eq (6.40) we get

$$\frac{\partial\rho_i}{\partial t'} - \frac{\partial}{\partial x'}\left(D'\phi\frac{\partial}{\partial x'}(\frac{\rho_i}{\phi})\right) = \widehat{t}\phi\dot{r}_i - \frac{\partial}{\partial x'}(\varepsilon\frac{\rho_i}{\phi}V') \tag{6.45}$$

In addition we choose $\widehat{x} = L$, the length of the core (so $0 \le x' \le 1$) and $\widehat{t} = \tau$, the timescale of the experiment. We use $\tau = 1d = 24 \cdot 60 \cdot 60s$ (one weeks test is equivalent to $t' = 7$). In compact form without the $'$s the system is described by normalized equations of the form

$$\partial_t\rho_i - \partial_x\left(D\phi\partial_x(\frac{\rho_i}{\phi})\right) = \tau\phi\dot{r}_i - \partial_x(\varepsilon\frac{\rho_i}{\phi}V) \tag{6.46}$$

Chapter 7

Solution procedure

7.1 Operator splitting

The solution of the equation system follows the approach used in [22, 23]. Note that the variables in this chapter are normalized as specified in section 6.4. Let

$$\mathbf{C} = (\rho_{na}, \rho_{cl}, \rho_{ca}, \rho_{so}, \rho_{mg}) \tag{7.1}$$
$$\mathbf{U} = (\rho_c, \rho_g, \rho_m, \rho_d) \tag{7.2}$$

We want to solve the system of equations

$$\partial_t \mathbf{C} + \partial_x(\mathbf{C}\frac{\varepsilon V}{\phi}) = \tau\phi\dot{\mathbf{r}}_{\mathbf{C}} + \partial_x\left(D\phi\partial_x(\frac{\mathbf{C}}{\phi})\right) \tag{7.3}$$
$$\partial_t \mathbf{U} = \tau\phi\dot{\mathbf{r}}_{\mathbf{U}} \tag{7.4}$$

and do so by splitting the system into a reaction part (convection and diffusion neglected):

$$\partial_t \mathbf{C} = \tau\phi\dot{\mathbf{r}}_{\mathbf{C}} \tag{7.5}$$
$$\partial_t \mathbf{U} = \tau\phi\dot{\mathbf{r}}_{\mathbf{U}} \tag{7.6}$$

and a convection/diffusion part (reactions neglected):

$$\partial_t \mathbf{C} + \partial_x(\mathbf{C}\frac{\varepsilon V}{\phi}) = \partial_x\left(D\phi\partial_x(\frac{\mathbf{C}}{\phi})\right) \tag{7.7}$$
$$\partial_t \mathbf{U} = 0 \tag{7.8}$$

Let T be the simulation time, T_{sol} the total simulation time (when the experiment is over) and let t be the time variable in the solvers, with t_{sol} the amount of time the solver should calculate ahead. We solve one timestep ΔT ahead by solving half a step ($t_{sol}^{con/dif,1} = \Delta T/2$) with convection/diffusion, then use this information to solve a time step ahead ($t_{sol}^{reac} = \Delta T$)for reactions and then use this information to solve half a time step ahead ($t_{sol}^{con/dif,2} = \Delta T/2$) with convection/diffusion, so called Strang splitting. Letting the reaction solver be called S_t and the convection/diffusion solver be called D_t this corresponds to

$$(\mathbf{C}^{n+1}, \mathbf{U}^{n+1}) = [D_{\Delta T/2} S_{\Delta T} D_{\Delta T/2}](\mathbf{C}^n, \mathbf{U}^n) \tag{7.9}$$

We discretize the core length into grid cells with boundaries at $x = 0$ and 1. With I grid cells we have grid length

$$dx = \frac{1}{I} \tag{7.10}$$

Cell number i from the left has its center value x_i given as

$$x_i = dx/2 + (i-1)dx, \qquad i = 1, ..., I \tag{7.11}$$

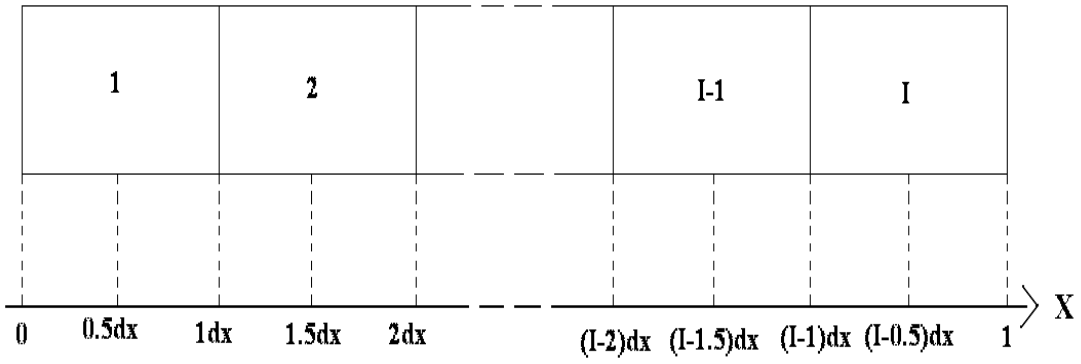

Figure 7.1: Relation between cell number and position on x-axis.

7.2 The reaction solver

Removing the convection/diffusion terms our equation set is

$$\begin{aligned}
\partial_t(\rho_{na}) &= 0 && (7.12)\\
\partial_t(\rho_{cl}) &= 0 && (7.13)\\
\partial_t(\rho_{ca}) &= \phi\tau(\dot{r}_c + \dot{r}_g + \dot{r}_d) && (7.14)\\
\partial_t(\rho_{so}) &= \phi\tau\dot{r}_g && (7.15)\\
\partial_t(\rho_{mg}) &= \phi\tau(\dot{r}_m + \dot{r}_d) && (7.16)\\
\partial_t\rho_c &= -\phi\tau\dot{r}_c && (7.17)\\
\partial_t\rho_g &= -\phi\tau\dot{r}_g && (7.18)\\
\partial_t\rho_m &= -\phi\tau\dot{r}_m && (7.19)\\
\partial_t\rho_d &= -\phi\tau\dot{r}_d && (7.20)
\end{aligned}$$

This set of equations can be considered as a system of ordinary differential eqations (ODE's). That is a system of the form

$$\frac{d\mathbf{Y}}{dt} = f(\mathbf{Y}) \tag{7.21}$$

At any given position and time the development in the solution vector depends only on the current state. This is a very useful property because it allows us to solve the system for each location separately. We can reduce the number of variables in the system by recombining the equations

$$\begin{aligned}
\partial_t(\rho_{na}) &= 0 && (7.22)\\
\partial_t(\rho_{cl}) &= 0 && (7.23)\\
\partial_t(\rho_g + \rho_{so}) &= 0 && (7.24)\\
\partial_t(\rho_m + \rho_d + \rho_{mg}) &= 0 && (7.25)\\
\partial_t(\rho_c - \rho_{so} + \rho_d + \rho_{ca}) &= 0 && (7.26)\\
\partial_t(\rho_{so}) &= \phi\tau\dot{r}_g && (7.27)\\
\partial_t(\rho_{mg}) &= \phi\tau(\dot{r}_m + \dot{r}_d) && (7.28)\\
\partial_t\rho_d &= -\phi\tau\dot{r}_d && (7.29)\\
\partial_t(\rho_{ca}) &= \phi\tau(\dot{r}_c + \dot{r}_g + \dot{r}_d) && (7.30)
\end{aligned}$$

and we see that some unknowns are easily given as the solutions of other:

$$\begin{aligned}
\rho_{na}(t) &= \rho^0_{na} && (7.31)\\
\rho_{cl}(t) &= \rho^0_{cl} && (7.32)\\
\rho_g(t) &= (\rho^0_g + \rho^0_{so}) - \rho_{so}(t) && (7.33)\\
\rho_m(t) &= (\rho^0_m + \rho^0_d + \rho^0_{mg}) - (\rho_d(t) + \rho_{mg}(t)) && (7.34)\\
\rho_c(t) &= (\rho^0_c - \rho^0_{so} + \rho^0_d + \rho^0_{ca}) - (-\rho_{so}(t) + \rho_d(t) + \rho_{ca}(t)) && (7.35)\\
\partial_t\rho_{so} &= \phi\tau\left[k^g_1[sgn^+(\rho_g)F^+_g - F^-_g]\right] && (7.36)\\
\partial_t\rho_{mg} &= \phi\tau\left[k^m_1[sgn^+(\rho_m)F^+_m - F^-_m] + k^d_1[sgn^+(\rho_d)F^+_d - F^-_d]\right] && (7.37)\\
\partial_t\rho_d &= -\phi\tau\left[k^d_1[sgn^+(\rho_d)F^+_d - F^-_d]\right] && (7.38)\\
\partial_t\rho_{ca} &= \phi\tau\left[k^c_1[sgn^+(\rho_c)F^+_c - F^-_c] + k^g_1[sgn^+(\rho_g)F^+_g - F^-_g] + k^d_1[sgn^+(\rho_d)F^+_d - F^-_d]\right] && (7.39)
\end{aligned}$$

Earlier we specified the functions F_i using pore concentrations of all reaction relevant ions. In the system above we focus on the total concentrations $\rho_{ca}, \rho_{so}, \rho_{mg}$ and correct for this using $C_j = \rho_j/\phi$. We now show how the other ions are eliminated. C_3 is calculated as

$$C_3 \equiv 2(C_{ca} + C_{mg} - C_{so}) + (C_{na} - C_{cl}) = \frac{1}{\phi}\left(2(\rho_{ca} + \rho_{mg} - \rho_{so}) + (\rho_{na} - \rho_{cl})\right) \tag{7.40}$$

The aqueous concentrations are then

$$C_h = \frac{1}{2}\left(-C_3 + \sqrt{C_3^2 + 4(\tilde{C_1} + \tilde{C_w})}\right) \tag{7.41}$$

$$C_{hco} = \frac{\tilde{C_1}}{C_h} \quad C_{co} = \frac{\tilde{C_1}\tilde{C_2}}{C_h^2} \quad C_{oh} = \frac{\tilde{C_w}}{C_h} \tag{7.42}$$

The rate functions F_i can then be expressed as

$$\begin{aligned}
F_c &= 1 - \frac{\gamma_{ca}\gamma_{hco}}{\gamma_h K^c}\frac{C_{ca}C_{hco}}{C_h} = 1 - \frac{\gamma_{ca}\gamma_{hco}\tilde{C_1}}{\gamma_h K^c}\frac{\rho_{ca}}{\phi C_h^2} = 1 - \frac{\gamma_{ca}C_1}{\gamma_h^2 K^c}\frac{\rho_{ca}}{\phi C_h^2} && (7.43)\\
F_g &= 1 - \frac{\gamma_{ca}\gamma_{so}}{K^g}C_{ca}C_{so} = 1 - \frac{\gamma_{ca}\gamma_{so}}{K^g}\frac{\rho_{ca}\rho_{so}}{\phi^2} && (7.44)\\
F_m &= 1 - \frac{\gamma_{mg}\gamma_{hco}}{\gamma_h K^m}\frac{C_{mg}C_{hco}}{C_h} = 1 - \frac{\gamma_{mg}\gamma_{hco}\tilde{C_1}}{\gamma_h K^m}\frac{\rho_{mg}}{\phi C_h^2} = 1 - \frac{\gamma_{mg}C_1}{\gamma_h^2 K^m}\frac{\rho_{mg}}{\phi C_h^2} && (7.45)\\
F_d &= 1 - \frac{\gamma_{ca}\gamma_{mg}\gamma_{hco}^2}{\gamma_h^2 K^d}\frac{C_{ca}C_{mg}C_{hco}^2}{C_h^2} = 1 - \frac{\gamma_{ca}\gamma_{mg}\gamma_{hco}^2\tilde{C_1}^2}{\gamma_h^2 K^d}\frac{\rho_{ca}\rho_{mg}}{\phi^2 C_h^4} && (7.46)\\
&= 1 - \frac{\gamma_{ca}\gamma_{mg}C_1^2}{\gamma_h^4 K^d}\frac{\rho_{ca}\rho_{mg}}{\phi^2 C_h^4} && (7.47)
\end{aligned}$$

The idea is that the solver receives initial values $\rho^0_{na}, \rho^0_{cl}, \rho^0_{ca}, \rho^0_{so}, \rho^0_{mg}, \rho^0_c, \rho^0_g, \rho^0_m, \rho^0_d$ and is told how far in time t_{sol} to calculate the given system. In practice t_{sol} is the time step ΔT as described in section 7.1. It can also be a longer period such as when we want to calculate an equilibrium state (ideally diffusion (and not convection) should be included in such a case but it has not been done).

The solution is made iteratively by dividing t_{sol} into several time steps δt. Given the solution at a time t these values are used to update the rate expressions and estimate the solution at $t + \delta t$.

The solutions of $\rho_{ca}, \rho_{so}, \rho_{mg}$ are essential to update the F_i functions and C_3 (C_3 also depends on ρ_{na} and ρ_{cl} but these are constant parameters during the solution procedure). $\rho_c, \rho_g, \rho_m, \rho_d$ update the porosity ϕ if it is assumed to vary, but they are also relevant in the $sgn^+(\cdot)$ terms.

When t_{sol} has been reached and the solution is within acceptable error bounds, the solver returns the updated solution.

To solve the problem we have used the Matlab ODE solver called ode23.

7.2.1 A test of the reaction solver

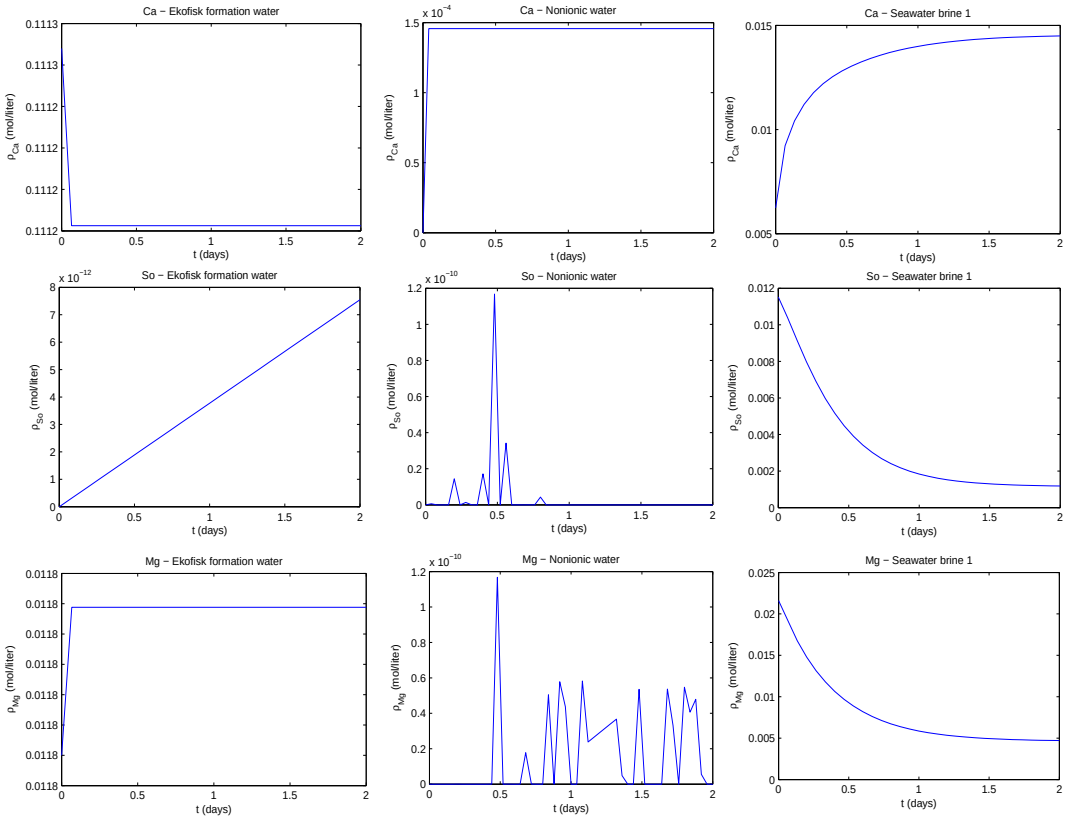

Figure 7.2: Concentrations of Ca^{2+}, SO_4^{2-} and Mg^{2+} (mol/liter) with time (days) for Ekofisk formation water (left), nonionic water (middle) and seawater SW1 (right)

The reaction solver is tested on 3 different fluids: nonionic water, Ekofisk formation brine and seawater SW1 (experimental data are specified in chapter 8). We specify a fluid composition and the surrounding rock and then observe how they change with time due to the exposure. The first 2 fluids are considered low reactive (since the minerals are "insoluble" in water and formation brine is in equilibrium) while seawater is considered more reactive. The simulation ran 30 times to give the state at different times t_{sol} in the interval 0 to 2 days. Remember that the internal time steps are chosen by the Matlab ode23 routine.

The rate constants determined in [23] were used in the test (corrected for porosity and including the dolomite constant) as given below

$$k_1^c = 3.125 \cdot 10^{-6} \text{ (mol/liter)/sec}, \quad k_1^g = 0.03k_1^c, \quad k_1^m = 0.09k_1^c, \quad k_1^d = 0.00k_1^c \tag{7.48}$$

As seen in Fig 7.2 the 2 less reactive brines very quickly reach an equilibrium state that would be better captured if more points were used. On a first look they seem to be very reactive, but when you look at the concentration scale their state changes little in absolute value. Especially sulphate ion concentrations appear to change, but are only the result of the error limitations of the routine. In both cases it should theoretically be 0, but is calculated to be of an order equal or less than 10^{-10} mol/liter.

Seawater SW1 is seen to change more in response to the rock and only after 1.5-2 days the reactions have reached equilibrium. This shows that a reactive fluid will spend days to reach equilibrium so using outer time steps on the order of hours seems reasonable.

7.3 The convection/diffusion solver

$$\partial_t \rho + \partial_x(\rho \frac{\varepsilon V}{\phi}) = \partial_x \left(D\phi \partial_x (\frac{\rho}{\phi}) \right) \tag{7.49}$$

$$\partial_t \rho = 0 \tag{7.50}$$

Without reaction terms our equations take the form

$$\partial_t \rho_{na} + \partial_x(\rho_{na} \frac{\varepsilon V}{\phi}) = \partial_x \left(D\phi \partial_x (\frac{\rho_{na}}{\phi}) \right) \tag{7.51}$$

$$\partial_t \rho_{cl} + \partial_x(\rho_{cl} \frac{\varepsilon V}{\phi}) = \partial_x \left(D\phi \partial_x (\frac{\rho_{cl}}{\phi}) \right) \tag{7.52}$$

$$\partial_t \rho_{ca} + \partial_x(\rho_{ca} \frac{\varepsilon V}{\phi}) = \partial_x \left(D\phi \partial_x (\frac{\rho_{ca}}{\phi}) \right) \tag{7.53}$$

$$\partial_t \rho_{so} + \partial_x(\rho_{so} \frac{\varepsilon V}{\phi}) = \partial_x \left(D\phi \partial_x (\frac{\rho_{so}}{\phi}) \right) \tag{7.54}$$

$$\partial_t \rho_{mg} + \partial_x(\rho_{mg} \frac{\varepsilon V}{\phi}) = \partial_x \left(D\phi \partial_x (\frac{\rho_{mg}}{\phi}) \right) \tag{7.55}$$

$$\partial_t \rho_c = 0 \tag{7.56}$$

$$\partial_t \rho_g = 0 \tag{7.57}$$

$$\partial_t \rho_m = 0 \tag{7.58}$$

$$\partial_t \rho_d = 0 \tag{7.59}$$

We see the mineral concentrations do not change with time. Since

$$\phi \equiv 1 - \frac{M_c}{\omega_c}\rho_c + \frac{M_g}{\omega_g}\rho_g + \frac{M_m}{\omega_m}\rho_m + \frac{M_d}{\omega_d}\rho_d \tag{7.60}$$

$$D \equiv D_m \phi + \alpha \varepsilon \frac{V}{\phi} \tag{7.61}$$

and V can be assumed constant over the solution time t_{sol} (here normally taken to be a half timestep $\Delta T/2$) both ϕ and D have constant spatial distributions during the solution. Especially only the minerals initial distributions are required for the solver. The differential equations equations are not coupled since each equation has no parameters depending on the solution of the other variables. This means each solution can be solved separately.

At the start we specify porosity distribution $\phi_0(x)$ and the constant V_0 (both given at the time specified in the fullscale simulation by T). Let

$$J \equiv \varepsilon V_0 \tag{7.62}$$

The distribution of D is then calculated as

$$D_0(x) = D_m \phi_0(x) + \mu\varepsilon \frac{V_0}{\phi_0(x)} = D_m \phi_0(x) + \frac{\mu J}{\phi_0(x)} \tag{7.63}$$

For each ion we must specify the initial concentration distribution $\rho_i(x, t = 0) = \rho_{i0}(x)$. The left boundary condition is given by the inlet fluid concentration $C_{i,brine}$ and the porosity at that position as

$$\rho_i(0, t) = C_{i,brine}\phi_0(0) \tag{7.64}$$

For the right boundary condition we would use $\rho_i(\infty, t) = \rho_{i0}(\infty)$ but since we must consider a finite system in practice we let

$$\partial_x \rho_i(1, t) = 0 \tag{7.65}$$

which in practice means the right boundary adopts the neighbors value. Each ion then requires the solution of

$$\partial_t \rho(x,t) + \partial_x (J\frac{\rho(x,t)}{\phi_0(x)}) = \partial_x \left(D_0(x)\phi_0(x)\partial_x (\frac{\rho(x,t)}{\phi_0(x)}) \right) \tag{7.66}$$

We solve the equations simultaneously by performing the same operations to the ion vector as we would to each ion variable.

7.3.1 Numerical solution

For simplicity we consider the equation of one ion variable

$$\partial_t \rho(x,t) = \partial_x \left(D_0(x)\phi_0(x)\partial_x (\frac{\rho(x,t)}{\phi_0(x)}) \right) - \partial_x (J\frac{\rho(x,t)}{\phi_0(x)}) \tag{7.67}$$

We now assume we know the solution at a time t in discrete points so that

$$\rho_i^n \equiv \rho(x_i, t_n) \tag{7.68}$$

for integers $1 \leq i \leq I$ such that $I\Delta x = 1$ and $t_n = n\Delta t$. Based on this information we want to estimate the solution at the next timestep ρ_i^{n+1}.

We discretize the separate terms as follows

$$\partial_t \rho(x,t) = \frac{\rho_i^{n+1} - \rho_i^n}{\Delta t} \tag{7.69}$$

$$\partial_x \left(D_0(x)\phi_0(x)\partial_x (\frac{\rho(x,t)}{\phi_0(x)}) \right) = \frac{1}{\Delta x} \left((D_0\phi_0\partial_x \frac{\rho}{\phi_0})_{i+1/2} - (D_0\phi_0\partial_x \frac{\rho}{\phi_0})_{i-1/2} \right) \tag{7.70}$$

$$\partial_x (J\frac{\rho(x,t)}{\phi_0(x)}) = \frac{1}{\Delta x} \left((J\frac{\rho}{\phi_0})_{i+1/2} - (J\frac{\rho}{\phi_0})_{i-1/2} \right) \tag{7.71}$$

We use an explicit 3-point formulation (meaning that the solution at a point for the next time step is based on the solution in the point and its neighbors at the previous time). In other words all values on the right side are given at t^n. The values of interface expression must be selected in a proper manner for numerical stability. A good starting point is to let fluxes be based on the direction the points they come from. In this way we assume the flow is running from left to right (since we inject at the left boundary) and so for the convective terms we use an upwind formulation

$$(\frac{\rho}{\phi_0})_{i+1/2} = \frac{\rho_i}{\phi_{0,i}} \qquad (\frac{\rho}{\phi_0})_{i-1/2} = \frac{\rho_{i-1}}{\phi_{0,i-1}} \tag{7.72}$$

If we had based this flux on the values on both sides of the interface it would cause stability problems.

The diffusive terms are somewhat simpler when it comes to stability. We need representative values of ϕ_0 and D_0 based on the neighboring cell values. This can be done in a number of ways:

- Arithmetic mean:

$$D_{0,i+1/2} = \tfrac{1}{2}(D_{0,i} + D_{0,i+1}), \quad D_{0,i-1/2} = \frac{1}{2}(D_{0,i-1} + D_{0,i}), \tag{7.73}$$

$$\phi_{0,i+1/2} = \tfrac{1}{2}(\phi_{0,i} + \phi_{0,i+1}), \quad \phi_{0,i-1/2} = \frac{1}{2}(\phi_{0,i-1} + \phi_{0,i}). \tag{7.74}$$

- Harmonic mean:

$$D_{0,i+1/2} = \tfrac{2D_{0,i}D_{0,i+1}}{D_{0,i}+D_{0,i+1}}, \quad D_{0,i-1/2} = \frac{2D_{0,i-1}D_{0,i}}{D_{0,i-1} + D_{0,i}}, \tag{7.75}$$

$$\phi_{0,i+1/2} = \tfrac{2\phi_{0,i}\phi_{0,i+1}}{\phi_{0,i}+\phi_{0,i+1}}, \quad \phi_{0,i-1/2} = \frac{2\phi_{0,i-1}\phi_{0,i}}{\phi_{0,i-1} + \phi_{0,i}}. \tag{7.76}$$

- Geometric mean:

$$D_{0,i+1/2} = \sqrt{D_{0,i}D_{0,i+1}}, \quad D_{0,i-1/2} = \sqrt{D_{0,i-1}D_{0,i}}, \tag{7.77}$$

$$\phi_{0,i+1/2} = \sqrt{\phi_{0,i}\phi_{0,i+1}}, \quad \phi_{0,i-1/2} = \sqrt{\phi_{0,i-1}\phi_{0,i}}. \tag{7.78}$$

The gradients are discretized as

$$\partial_x(\tfrac{\rho}{\phi_0})_{i+1/2} = \tfrac{1}{\Delta x}(\tfrac{\rho_{i+1}}{\phi_{0,i+1}} - \tfrac{\rho_i}{\phi_{0,i}}), \qquad \partial_x(\frac{\rho}{\phi_0})_{i-1/2} = \frac{1}{\Delta x}(\frac{\rho_i}{\phi_{0,i}} - \frac{\rho_{i-1}}{\phi_{0,i-1}}) \tag{7.79}$$

Now let

$$\lambda \equiv \frac{\Delta t}{\Delta x} \tag{7.80}$$

With the notation above in mind the convection/diffusion solver takes the form

$$\begin{aligned} \rho_i^{n+1} &= \rho_i + \lambda\left([D_{0,i+1/2}\phi_{0,i+1/2}(\partial_x\frac{\rho}{\phi_0})_{i+1/2}] - [D_{0,i-1/2}\phi_{0,i-1/2}(\partial_x\frac{\rho}{\phi_0})_{i-1/2}]\right) \\ &\quad -\lambda\left(J(\frac{\rho}{\phi_0})_{i+1/2} - J(\frac{\rho}{\phi_0})_{i-1/2}\right) \end{aligned} \tag{7.81}$$

These equations are computed for each cell $i = 1..I$, but we must specify values at the boundary interfaces. Specifically the average values of D_0 and ϕ_0 are taken as the cell value at the edges.

At the outlet the pore concentration is assumed the same at the center of the cell as at the right boundary so we neglect diffusion there and keep the upwind flux.

At the inlet the convective flux in is naturally given by the injection fluid composition. The left side diffusive flux is given by assuming a cell to the left with injection fluid composition.

$$D_{0,1/2} = D_{0,1} \qquad D_{0,I+1/2} = D_{0,I} \tag{7.82}$$

$$\phi_{0,1/2} = \phi_{0,1} \qquad \phi_{0,I+1/2} = \phi_{0,I} \tag{7.83}$$

$$(\tfrac{\rho}{\phi_0})_{1/2} = C_{inj} \qquad (\frac{\rho}{\phi_0})_{I+1/2} = \frac{\rho_I}{\phi_{0,I}} \tag{7.84}$$

$$\partial_x(\tfrac{\rho}{\phi_0})_{1/2} = \tfrac{1}{\Delta x}(\tfrac{\rho_1}{\phi_{0,1}} - C_{inj}) \qquad \partial_x(\frac{\rho}{\phi_0})_{I+1/2} = 0 \tag{7.85}$$

To determine a good volume rate for the experiment we want the front to pass through the core during the time scale of the experiment. Let Q be volume rate and q be the number of pore volumes per day injected. To let this be determined uniquely we relate it to the initial porosity ϕ_{init}.

$$Q = q\frac{AL\phi_{init}}{\tau} \tag{7.86}$$

Q is also related to Darcys law.

$$Q = -\frac{k_{tot}A}{\nu}\frac{\Delta P}{L} = -\frac{\widehat{k}k'_{tot}A}{\nu}\frac{\Delta P}{L} = -\frac{\widehat{k}k'A}{\nu}\frac{\widehat{p}}{L}\frac{\partial p'}{\partial x'} \tag{7.87}$$

Combining this we get

$$q\frac{L\phi_{init}}{\tau} = -\frac{\widehat{k}k'_{tot}}{\nu}\frac{\Delta P}{L} \tag{7.88}$$

$$\frac{k'\partial p'}{\partial x'} = \frac{k'_{tot}\frac{\Delta P}{\widehat{p}}}{\frac{L}{L}} = k'_{tot}\frac{\Delta P}{\widehat{p}} = -q\phi_{init}\frac{L^2}{\tau\widehat{D}_m}\frac{\widehat{D}_m\nu}{\widehat{k}\widehat{p}} = -\frac{q\phi_{init}}{\varepsilon} \tag{7.89}$$

$$J = -\varepsilon\frac{k'\partial p'}{\partial x'} = q\phi_{init} \tag{7.90}$$

This simple relation is used so that q is an input parameter to determine J. We will typically consider injection rates of 1 PV/day, corresponding to $q = 1$.

7.3.2 Simplification: Constant porosity

With ϕ constant and equal over time and space and V_0 considered constant over the solver simulation time (as before) we can simplify the system and better evaluate stability. D_0 will be constant and uniform over a simulation. Let

$$V \equiv \frac{\varepsilon V_0}{\phi} = \frac{J}{\phi} \tag{7.91}$$

(not to be confused with the seepage velocity which is not dimensionless). Note that for constant porosity

$$V = q \tag{7.92}$$

so V adopts the value of number pore volumes injected per day directly. The PDE becomes

$$\partial_t \rho(x,t) = D_0 \partial_{xx}(\rho(x,t)) - V \partial_x(\rho(x,t)) \tag{7.93}$$

With the chosen discretization we have

$$\begin{aligned}
\rho_i^{n+1} &= \rho_i + \lambda D_0 \left((\partial_x \rho)_{i+1/2} - (\partial_x \rho)_{i-1/2} \right) - \lambda V \left(\rho_{i+1/2} - \rho_{i-1/2} \right) && (7.94)\\
&= \rho_i + \lambda D_0 \left(\frac{\rho_{i+1} - \rho_i}{\Delta x} - \frac{\rho_i - \rho_{i-1}}{\Delta x} \right) - \lambda V \left(\rho_i - \rho_{i-1} \right) && (7.95)\\
&= \rho_i - \lambda \left([V\rho_i - D_0 \frac{\rho_{i+1} - \rho_i}{\Delta x}] - [V\rho_{i-1} - D_0 \frac{\rho_i - \rho_{i-1}}{\Delta x}] \right) && (7.96)
\end{aligned}$$

with boundary conditions

$$\begin{aligned}
\rho_{1/2} &= C_{inj}\phi_0 \qquad & \rho_{I+1/2} &= \rho_I && (7.97)\\
\partial_x \rho_{1/2} &= \tfrac{1}{\Delta x}(\rho_1 - C_{inj}\phi) \qquad & \partial_x \rho_{I+1/2} &= 0 && (7.98)
\end{aligned}$$

used to solve for the first and last cell.

In [9] solutions to the problem

$$\partial_t \rho(x,t) + \partial_x(f(\rho(x,t))) = 0 \tag{7.99}$$

(corresponding to $f(\rho) = V\rho$ and $D_0 = 0$) are investigated and especially the upwind formulation used above for the convection gives stable convergence if

$$V\lambda \leq 1 \quad \Leftrightarrow \quad \Delta t \leq \Delta x / V \tag{7.100}$$

A test of this criterion (using $\Delta t = \Delta x/V$) was performed on (7.96). Settings for the simulation was

$$dx = 0.05, \quad \phi = 0.3, \quad \Delta T = 0.0, 0.2, ..., 1.0, \quad V = 1.0, \quad \rho_{initial} = 1, \quad C_{inj} = 50 \tag{7.101}$$

For $D_0 = 0$ the result (left in Fig 7.3) is a function with smooth fronts indicating how far the injected fluid has traveled, imposed by the convective flow. The initial distribution is here a flat line. As seen the fronts are here far from vertical as expected theoretically. The smear depends on the method used (upwind is considered relatively good) and the grid refinement (the grid is a bit coarse). Including diffusion soon makes the solution unstable.

For $D_0 = 0.01$ (bottom in Fig 7.3) it really diverges to unreasonable values, but for $D_0 = 0.001$ (right in Fig 7.3) it seems okay. However for such low values of D it is little difference between the solutions (unless one looks closely). The value of V will typically be around 1 but simulations show that a finer grid is required for the fronts and we need a better limitation on Δt for stability.

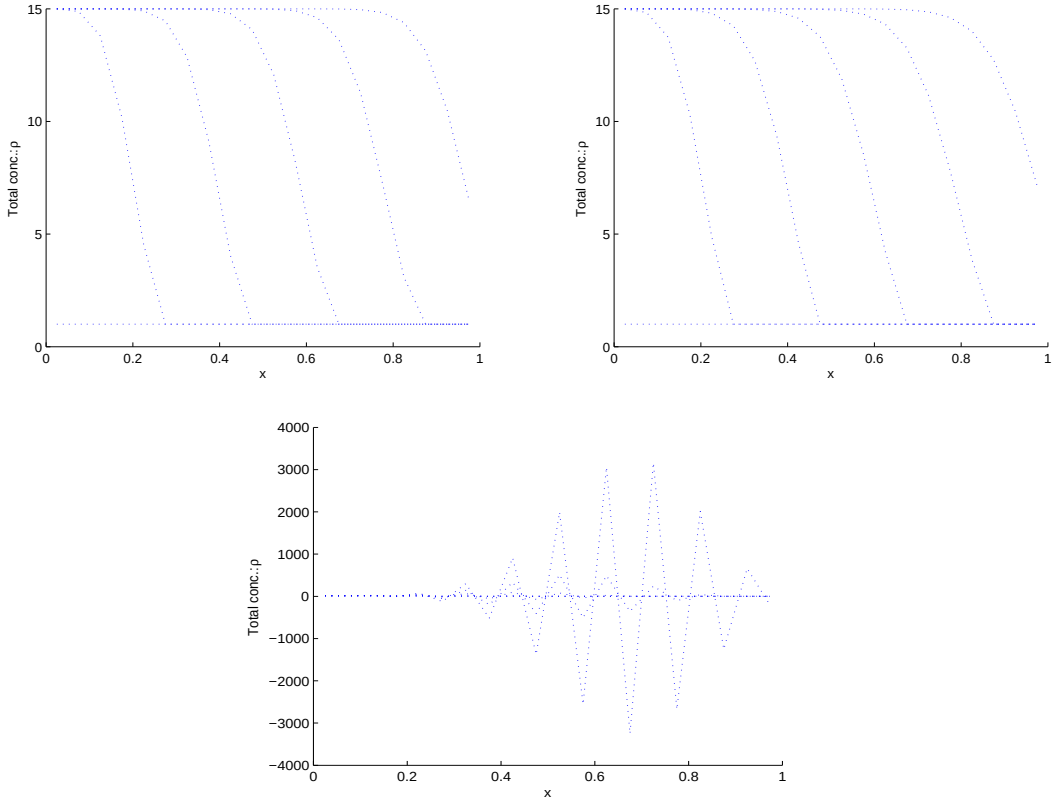

Figure 7.3: Numerical results for convective/diffusive displacement: Concentration distribution at times 0.0, 0.2, ..., 1.0 . Left: $D_0 = 0$. Right: $D_0 = 0.001$. Bottom: $D_0 = 0.01$

7.3.3 TVD-analysis for stability

Our measure of stability will be total variation (TV). It is defined as

$$TV^n = \sum_{i=-\infty}^{\infty} |\rho_{i+i}^n - \rho_i^n| \Delta x \tag{7.102}$$

We seek a limitation on the time steps so that the method is total variation diminishing (TVD). A method is TVD if

$$TV^{n+1} \leq TV^n \quad \text{for all } n \tag{7.103}$$

This ensures that the solution at a later time will not oscillate or blow up.

We will now give a criterion to ensure that our method is TVD. A numerical procedure for the solution of (7.99) can be written as

$$\rho_i^{n+1} \quad = \quad \rho_i - \lambda[f_{i+1/2} - f_{i-1/2}] = \rho_i - \lambda[F(\rho_i, \rho_{i+1}) - F(\rho_{i-1}, \rho_i)] \tag{7.104}$$

Notice that eq (7.96) is of exactly this form with

$$F(\rho_i, \rho_{i+1}) = V\rho_i - D_0 \frac{\rho_{i+1} - \rho_i}{\Delta x} \tag{7.105}$$

Define

$$q_{i+1/2} \equiv \lambda \frac{f(\rho_i) - 2F(\rho_i, \rho_{i+1}) + f(\rho_{i+1})}{\rho_{i+1} - \rho_i} \tag{7.106}$$

If

$$\lambda|\frac{f(\rho_{i+1})-f(\rho_i)}{\rho_{i+1}-\rho_i}| \leq q_{i+1/2} \leq 1 \tag{7.107}$$

the method is TVD. It will also be monotonicity preserving (MP), meaning that if the solution is nondecreasing or -increasing at some point it will be the same at all later times. If the rightside limit of 7.107 is replaced by $1/2$ the solution at the next time step is limited by the infimum and supremum of the previous solution (from [9]).

With our algorithm we get

$$\lambda|\frac{f(\rho_{i+1})-f(\rho_i)}{\rho_{i+1}-\rho_i}| = \lambda|\frac{V\rho_{i+1}-V\rho_i}{\rho_{i+1}-\rho_i}| = \lambda V \tag{7.108}$$

$$q_{i+1/2} = \lambda\frac{V\rho_i - 2(V\rho_i - D_0\frac{\rho_{i+1}-\rho_i}{\Delta x}) + V\rho_{i+1}}{\rho_{i+1}-\rho_i} \tag{7.109}$$

$$= \lambda\frac{V\rho_{i+1} - V\rho_i + 2D_0\frac{\rho_{i+1}-\rho_i}{\Delta x}}{\rho_{i+1}-\rho_i} \tag{7.110}$$

$$= \lambda(V + \frac{2D_0}{\Delta x}) \tag{7.111}$$

Clearly the left inequality of (7.107) is held since $D_0 \geq 0$. Our criterion becomes

$$\lambda(V + \frac{2D_0}{\Delta x}) \leq 1 \quad \Leftrightarrow \quad \Delta t \leq \frac{\Delta x^2}{V\Delta x + 2D_0} \tag{7.112}$$

Note that for low D_0 it takes the same form as 7.100. Also of importance is that for high D_0 we get small Δt and a large number of time steps. This criterion is also derived from the definition in app D. If $V = 0$ and D is very low the time step can become larger than the simulation time. To make sure we always finish the simulation with at least 2 steps and exactly on the simulation time we select Δt as follows

$$steps = round(t_{sol}/\Delta t_{max} + 1.5) \qquad \Delta t = t_{sol}/steps \tag{7.113}$$

A new simulation test was performed with the highest allowed Δt from (7.112). Settings for the simulation was

$$dx = 0.01, \quad \phi = 0.3, \quad \Delta T = 0.0, 0.33, 0.67, 1.0, \quad \rho_{initial} = 1, \quad C_{inj} = 50 \tag{7.114}$$

and both D_0 and V were varied. First the case $V = 1$ and $D_0 = 0$ was repeated and as seen left in Fig 7.4 the fronts are better defined with steeper edges than the case left in 7.3.

When we include diffusion the effect is clear as seen right in Fig 7.4. $V = 1$ still, but we vary D over the values 0.0, 0.001, 0.01 and 0.1. The fronts move with approximately the same velocity, but the concentration profile is smoothed out more for higher D_0. If D_0 is high the front actually changes speed because the diffusive wave out to the left travels faster than the convective speed and has reached the left boundary. Since the algorithm tells the left side to keep a constant value the wave is reflected at the edge and the mass is pushed ahead of the convective front. This solution is not very physical since a physical system would let the diffusion continue.

To see the effects of diffusion only we let $V = 0$ and vary D_0 from 0 to 1. The solutions are given at time 1.0 in Fig 7.5. We see that in all cases the diffusion works to average out any differences in concentration (in this case the concentration in the core is increased because ions travel into it by diffusion from the concentrated brine). The higher the value of D_0 the more rapid this process happens. Also this example is not entirely physical since diffusion should be allowed to proceed out of the core. However we are mostly interested in situations where convection reduces this error.

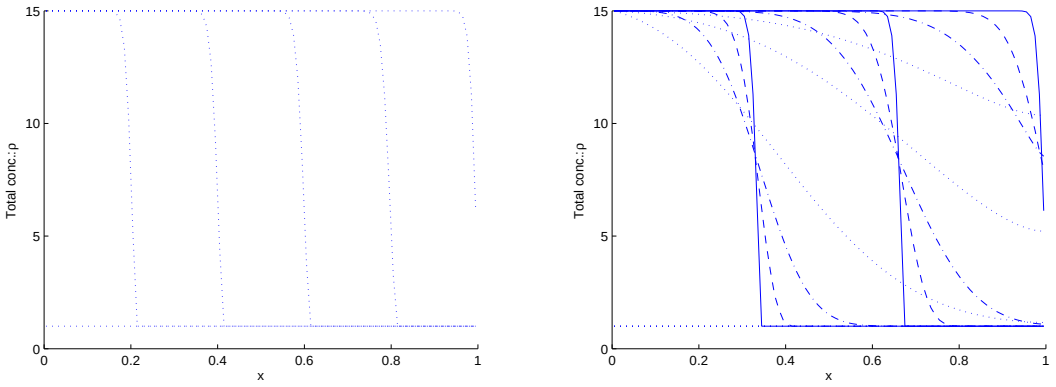

Figure 7.4: Concentration distribution at times between 0.0 and 1.0 . Left: $V = 1$ and $D_0 = 0$. Right: $V = 1$, $D_0 = 0, 0.001, 0.01, 0.1$ (lines with higher D_0 have more dots).

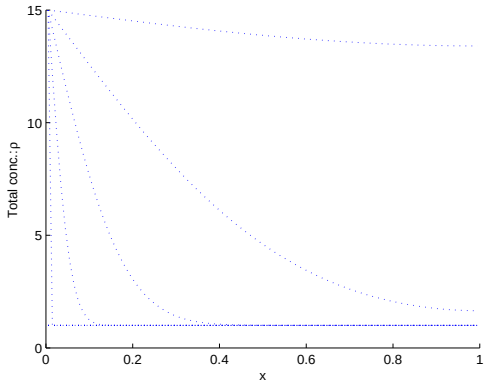

Figure 7.5: Concentration distribution at time 1.0 with $V = 0$ and $D_0 = 0$, 0.001, 0.01, 0.1, 1.0 (graphs corresponding to higher D are more to the right).

7.4 Consequences of operator splitting

As seen in this chapter the splitting of the original problem into a convection/diffusion solver and a reaction solver offers great advantages when it comes to solving the equations. But it also has a price when we want the overall solution to converge to the solution of the initial problem. The external numerical discretization has some key effects and we must try to keep the number of time steps and cells as low as possible without affecting the end result to seriously.

7.4.1 Too high ΔT: Washout

If $t_{sol} = \Delta T/2$ is too high the flow will push out any initial fluid composition distribution and replace it with the injection brine composition uniformly. When the reaction solver starts, the reactions respond to the local fluid composition and therefore the result will also be a uniform reaction. The entire core will show a uniform distribution throughout the simulation that changes only with time. This phenomena could also be limited to a smaller portion of the core. This means that for long time simulations it is still important to keep ΔT on a level that allows for heterogeneous reactions.

7.4.2 Too high ΔT: Chemical equilibrium

If the reactions are allowed to occur isolated over a long enough period they will reach equilibrium. However we wish to capture the effects that reactions are constantly disturbed by the flow. In other words a sample of fluid may react at one location and approach equilibrium and then be transported further downstream the core. Since this sample is closer to equilibrium it reacts slower and there should be less precipitation/dissolution. The choice of Δt decides then if the reactions happen everywhere in the core or primarily at the inlet. Note that this dependence can also be linked to the reaction rates and the rate constants.

7.4.3 Too low ΔT: Left side boundary condition

We want to permit reactions to happen near the inlet, so that the composition there changes during the reaction procedure. However, it is expected that on an average basis the fluid composition there is similar to the injection composition. This is a paradox since the place which will change the injection composition most rapidly will also be constant over time.

The answer to this paradox is that we are looking a finite distance into the rock and so there will be a change in the fluid composition. However, the reacting fluid is also being transported away, carrying dissolved ions and the inlet position is refueled with reactive brine. It is natural to expect that moving closer to the inlet one would always find the composition close to the injection brine. This point is not captured if the time step is taken to short. Consider the distribution after the reaction solver has finished. The convection/diffusion solver uses this distribution as input and returns a new distribution after $\Delta t/2$. If the solver has not given cell 1 a composition equal to the injection composition it will be closer to equilibrium between the injection fluid and the rock. This effect will lead the inlet composition further away from its supposed value until it reaches a stable value between inlet composition and equilibrium composition, depending on the numerics. Given the spatial grid for x we should ideally keep $\Delta t/2$ large enough to let cell 1 reach the injection composition. A numerical test was performed in Excel to test how long steps would be required. First we looked at a case with low diffusion.

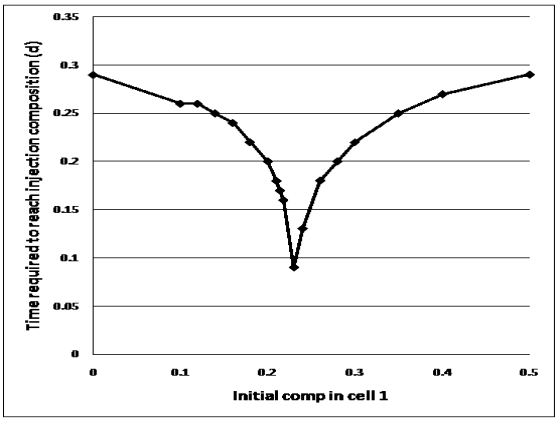

Time	rho0	rho1	rho2	rho3	rho4
0.00	0.2180	0.1600	0.0000	0.0000	0.0000
0.02	0.2180	0.1802	0.0608	0.0067	0.0000
0.04	0.2180	0.1933	0.1056	0.0313	0.0047
0.06	0.2180	0.2017	0.1381	0.0619	0.0175
0.08	0.2180	0.2073	0.1615	0.0921	0.0369
0.10	0.2180	0.2109	0.1782	0.1189	0.0600
0.12	0.2180	0.2133	0.1901	0.1415	0.0840
0.14	0.2180	0.2149	0.1984	0.1598	0.1070
0.16	0.2180	0.2159	0.2043	0.1743	0.1279
0.18	0.2180	0.2166	0.2084	0.1854	0.1461
0.20	0.2180	0.2171	0.2113	0.1939	0.1614
0.22	0.2180	0.2174	0.2133	0.2003	0.1740
0.24	0.2180	0.2176	0.2148	0.2050	0.1842
0.26	0.2180	0.2177	0.2157	0.2086	0.1922
0.28	0.2180	0.2178	0.2164	0.2112	0.1985
0.30	0.2180	0.2179	0.2169	0.2131	0.2033

Figure 7.6: Left: Simulation time required for solver to reach 0.218 M concentration in cell 1 (3 correct decimals). Right: solution for $\rho_1^0 = 0.16$ and $\Delta t = 0.01$ (only every second step shown)

The settings were

$$V = 1 \quad D = 0.001 \quad dx = 0.05 \quad \rho_0 = 0.218 \quad \rho_{2,3,4}^0 = 0 \quad \rho_1^0 \text{ variable} \quad t_{sol} = 0.02 \tag{7.115}$$

a simple system indicating injection of 0.218 M $MgCl_2$ solution (with ρ indicating Mg^{2+} concentration in mol/liter) into a core filled with pure water where only look at the first 4 cells. Given

the data above (note that the simulation time $t_{sol} = 0.02 \approx 0.5 * 1/24$ is equivalent to a half hour) and the stability criterium (7.112) we find the inner time step Δt using

$$steps = round(t_{sol}/\Delta t_{max} + 1.5) = 2 \qquad \Delta t = t_{sol}/steps = 0.01 \tag{7.116}$$

Then for a given t_{sol} we compute the solution in space and time and see how long it takes for cell 1 to get composition equal to the injection composition to 2 or 3 decimals. We want this time to be less then the simulation time of the solver.

What is clear from the results left in Fig 7.6 is that cell 1 does not copy the injection solution properly before 0.3 days have gone, although 0.25 days would cover most practical situations. For example the equilibrium concentration of Mg^{2+} is around 0.16 mol/liter and after 0.24 days it reaches the wanted 0.218 as seen in the table to the right in Fig 7.6 with the complete solution. The required time well outside the typical time for the solver. Note that the values only approach the boundary condition, but the error is minimal after a long enough period.

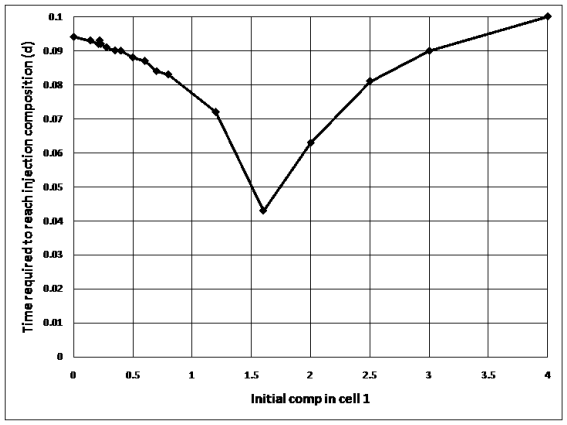

Time	rho0	rho1	rho2	rho3	rho4
0.00	0.2180	0.1600	0.0000	0.0000	0.0000
0.01	0.2180	0.1700	0.1269	0.0928	0.0749
0.02	0.2180	0.1906	0.1656	0.1463	0.1358
0.03	0.2180	0.2023	0.1879	0.1769	0.1708
0.04	0.2180	0.2090	0.2007	0.1944	0.1909
0.05	0.2180	0.2128	0.2081	0.2045	0.2025
0.06	0.2180	0.2150	0.2123	0.2102	0.2091
0.07	0.2180	0.2163	0.2147	0.2135	0.2129
0.08	0.2180	0.2170	0.2161	0.2154	0.2151
0.09	0.2180	0.2174	0.2169	0.2165	0.2163
0.10	0.2180	0.2177	0.2174	0.2172	0.2170

Figure 7.7: Left: Simulation time required for solver to reach 0.218 M concentration in cell 1 (3 correct decimals). Right: solution for $\rho_1^0 = 0.16$ and $\Delta t = 0.0011$ (only every 9th step shown)

Consider now the same example with $D = 1.0$. An immediate numerical consequence of increasing D is that Δt decreases from 0.01 to 0.0011 to keep stability, while the number of time steps increases from 2 to 18.

The increased diffusion reduces the time to get the proper boundary data to less than 0.1 days (see Fig 7.7) for any practical initial value in cell 1, but as we see in the table, after the simulation time of 0.02 has ended, the difference is little.

7.4.4 Correction at the boundary

The convection/diffusion solver is of the form

$$\begin{aligned} \rho_i^{n+1} &= \rho_i + \lambda \left([D_{0,i+1/2}\phi_{0,i+1/2}(\partial_x \frac{\rho}{\phi_0})_{i+1/2}] - [D_{0,i-1/2}\phi_{0,i-1/2}(\partial_x \frac{\rho}{\phi_0})_{i-1/2}] \right) \\ &\quad -\lambda \left(J(\frac{\rho}{\phi_0})_{i+1/2} - J(\frac{\rho}{\phi_0})_{i-1/2} \right) \end{aligned} \tag{7.117}$$

$$(\partial_x \frac{\rho}{\phi_0})_{1/2} = \frac{1}{\Delta x}(\frac{\rho_1}{\phi_{0,1}} - C_{inj}) \quad (\partial_x \frac{\rho}{\phi_0})_{I+1/2} = 0 \quad (\frac{\rho}{\phi_0})_{1/2} = C_{inj} \quad (\frac{\rho}{\phi_0})_{I+1/2} = \frac{\rho_I}{\phi_{0,I}} \tag{7.118}$$

and it is based on mass preservation/transport. Especially we see that when summing over all cells and multiplying with $\Delta V = A\Delta x$ we get

$$A\sum_i \rho_i^{n+1}\Delta x = A\sum_i \rho_i \Delta x + A\Delta t\left([D_{0,I+1/2}\phi_{0,I+1/2}(\partial_x \frac{\rho}{\phi_0})_{I+1/2}] - [D_{0,1/2}\phi_{0,1/2}(\partial_x \frac{\rho}{\phi_0})_{1/2}]\right)$$
$$-A\Delta t\left(J(\frac{\rho}{\phi_0})_{I+1/2} - J(\frac{\rho}{\phi_0})_{1/2}\right) \quad (7.119)$$

It states that the number of moles at the next time step is equal to the previous number of moles plus the difference of moles transported in and out by convection and diffusion at the boundaries of the core. In this way no moles disappear since fluxes leaving a cell enter another.

We now want to alter this method to obtain the correct boundary condition on the left hand side at the end of the simulation. We could do this by increasing the simulation time $t_{sol} = \Delta T/2$ or perhaps refining the grid, but we treat them for now as given.

As seen in the example (especially the tables in Fig 7.6 and 7.7) cell 1 approaches the boundary condition during the simulation. After a certain fraction of t_{sol} we then replace cell 1 with the boundary condition after each iteration. Compared to the total mass this is a negligible error when $\Delta x \to 0$. The remaining fraction of t_{sol} is spent on smoothing out any discontinuities. This is also a good approximation of the diffusion is of same order as the convection (D similar to V).

Note also that this procedure gives a diffusive flux from cell 2 to cell 1 that is not carried any further, but as seen in the table, after some time the two cell values are similar and the diffusive flux is not very significant. If we could use $t_{sol} = \Delta T/2 = 0.3$ days the error would be very small in first our example. Had we let it be infinite there would be no error at the boundary. Since diffusion works to average out any deviations we must force the correct boundary condition in place in finite time.

A test of the full simulator was performed with data corresponding to the paper [23]

$$V = 1.3 \quad D = 1.058 \quad \Delta T = 0.5hr \quad T_{sol} = 2days \quad (7.120)$$

The rate constants in (7.48) were also used. Seawater SW1 was injected into a core that had reached equilibrium with nonionic water.

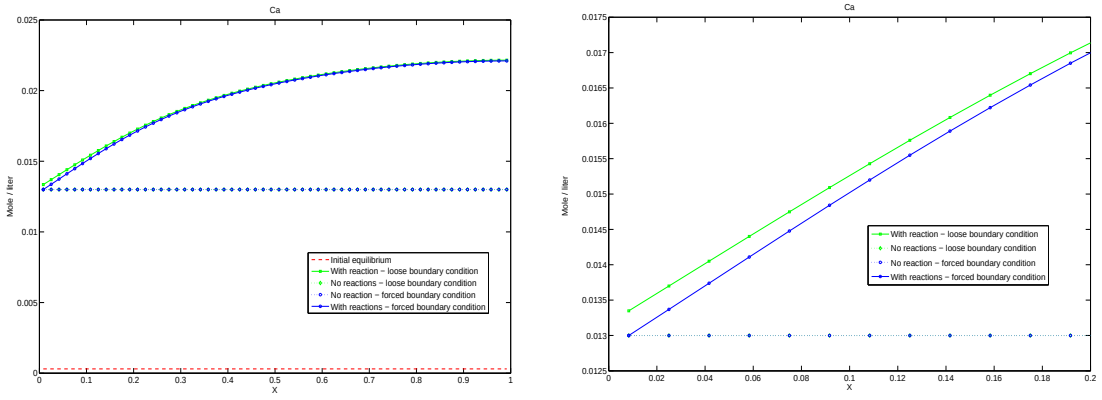

Figure 7.8: Comparison of left boundary conditions. Closer view in the right picture.

The distribution of Ca-ion concentration in the core after 2 days is given in Fig 7.8. We have plotted 5 curves: the initial equilibrium is used as a reference, 2 curves have only convection and diffusion taking place but one used the loose boundary condition and the other the forced. The 2 are inseparable at the given time but might have been more distinguished before the core was completely flooded. The 2 remaining curves include reactions also and there is a small but noticeable difference between the 2 curves at the inlet that is reduced further out in the core. With the forced condition the solutions with and without reactions always join at the left side.

7.4.5 Choice of ΔT

As seen in the example of the reaction solver and the discussion above we should use time steps not exceeding a few hours to capture the interplay between convection/diffusion and reactions. We will typically use 0.5 to 2.5 hr as external time steps corresponding to $\Delta T = 0.02 - 0.10$.

Chapter 8

Experimental data

8.1 Experimental setting

The experimental data were obtained at the University of Stavanger and is also given in [22, 23].

Cores of chalk were filled with nonionic water at a temperature of 130^oC, while being pressurized by a confining pressure. The core saturation is performed a long time so equilibrium can be reached. Injection of a brine with given composition into the core results in disturbance of the equilibrium and chemical reactions. Ion concentrations of Ca, So, Mg, Na and Cl are measured at the outlet at different times after start of injection. Also this process is performed at high temperature and pressure. Pressure at the inlet and outlet are adjusted to keep the flowrate constant during the experiment. The flooding processes were kept going for several days.

The relevant core properties were

Initial porosity	$\phi_{init} = 0.48$
Length	$L = 0.07m$
Bulk volume	$V_b = 75ml$
Pore volume	$V_p = 36ml$
Matrix volume	$V_m = 39ml$
Rock mass	$m_m = 100g$

The initial calcite concentration can be calculated as

$$\rho_c = \frac{m_m}{M_c V_b} = \frac{100g}{100g/mol \cdot 0.075liter} = 13.33mol/liter \tag{8.1}$$

However we will use eq (5.105) to calculate the initial concentration since that is used later in the program.

$$\rho_c = (1 - \phi_{init})\frac{\omega_c}{M_c} = (1 - 0.48)\frac{2710}{100.087} = 14.08mol/liter \tag{8.2}$$

The values are similar indicating that the formula can be used.

All experiments use a volume rate of 1.3 pore volumes per day, which is equivalent to

$$q = 1.3 \quad J = q\phi_{init} = 0.624 \tag{8.3}$$

We assume a constant viscosity of

$$\nu = 0.7cP = 0.7 \cdot 10^{-3} Pa \cdot s \tag{8.4}$$

	Nonionic water	Ekofisk formation water	Seawater SW1	Seawater SW2	0.109 M MgCl2	0.218 M MgCl2	0.657 M NaCl
Ca (mol/liter)	0.0	0.2318	0.013	0.013	0.000	0.000	0.000
So (mol/liter)	0.0	0.0000	0.024	0.024	0.000	0.000	0.000
Mg (mol/liter)	0.0	0.0246	0.045	0.045	0.109	0.218	0.000
Na (mol/liter)	0.0	0.6849	0.450	0.050	0.000	0.000	0.657
Cl (mol/liter)	0.0	1.1975	0.525	0.125	0.218	0.436	0.657

Figure 8.1: Brines used in experiments and simulations

8.2 Fluid compositions

In the calculations we must specify an initial fluid and an injection fluid. Each composition is identified by the fluid concentration of Ca, So, Mg, Na and Cl. The experiments available for comparison are chalk cores saturated with nonionic water and then flooded with the 5 brines to the right in Fig 8.1. Note that the 2 seawater brines have identical composition of Ca, So and Mg but differ in Na and Cl. The 3 remaining injection brines are simple solutions containing only 2 of the 5 ions in each. In all simulations being compared to experiments we will use nonionic water as initial fluid that is saturated with the rock to equilibrium before simulation starts.

8.3 Activity coefficients and ionic strength

For any simulation the activity coefficients of every ion and the ionic strength of the solution must be calculated using the theory in subsection 5.6.1. These values are set to depend only on the temperature and the injection fluid composition. Note that brines 1, 4 and 5 in Fig 8.2 have

Injection fluid	I_0	γ_ca	γ_so	γ_mg	γ_na	γ_cl	γ_h	γ_oh	γ_co	γ_hco
SW 1	0.6515	0.1602	0.0987	0.2200	0.5604	0.5130	0.7058	0.5379	0.1139	0.5604
SW 2	0.2515	0.2247	0.1653	0.2794	0.6376	0.6055	0.7429	0.6222	0.1805	0.6376
0.109 M MgCl2	0.3270	0.2043	0.1436	0.2608	0.6156	0.5795	0.7319	0.5983	0.1591	0.6156
0.218 M MgCl2	0.6540	0.1600	0.0985	0.2198	0.5601	0.5127	0.7057	0.5376	0.1137	0.5601
0.657 M NaCl	0.6570	0.1598	0.0982	0.2196	0.5598	0.5123	0.7055	0.5372	0.1135	0.5598

Figure 8.2: Ionic strength I_0 and activity coefficients of the ions calculated in simulations with injection of the specified brine

almost identical ionic strength and activity coefficients.

8.4 Reaction equilibrium constants

These are assumed to depend only on temperature and are given at $T = 130^oC$

$$K_c = 10^{+0.35}, \quad K_g = 10^{-5.94}, \quad K_m = 10^{-0.01}, \quad K_d = 10^{-0.82}, \tag{8.5}$$

$$P_{CO2} = 10^{-3.5}, \quad K = 10^{-9.01} \tag{8.6}$$

$$C_1 = P_{CO2} * K, \quad C_2 = 10^{-10.15}, \quad C_w = 10^{-12.26} \tag{8.7}$$

The units are based on (mole/liter) except P_{CO2} and K which also require pressure units, but C_1 removes this unit from the system since C_1 is only based on (mole/liter).

8.5 Reference values

We use

$$\widehat{x} = L = 0.07m \tag{8.8}$$

$$\widehat{t} = \tau = 1d = 24 \cdot 60 \cdot 60 = 86400s \tag{8.9}$$

$$\widehat{D}_m = \frac{L^2}{\tau} = \frac{0.07^2}{86400} = 5.67 \cdot 10^{-8} m^2/s \tag{8.10}$$

$$\widehat{k} = 2mD = 0.002 \cdot 0.987 \cdot 10^{-12} = 1.974 \cdot 10^{-15} m^2 \tag{8.11}$$

$$\widehat{p} = 1bar = 10^5 Pa \tag{8.12}$$

$$\varepsilon = \frac{\widehat{k}\widehat{p}}{\nu \widehat{D}_m} = \frac{1.974 \cdot 10^{-15} m^2 10^5 Pa}{0.7 \cdot 10^{-3} Pa \cdot s 5.67 \cdot 10^{-8} m^2/s} = 4.97 \tag{8.13}$$

in SI units for the calculations.

Chapter 9

Case I: Constant core properties and incompressible fluid

9.1 Assumptions and goals

The basic assumptions for this case are that we can treat permeability and porosity as uniform and constant in the equation and that the velocity is uniform. In the section we will explain how to use and actually use experimental results to determine parameters in the model. It is important to notice that the statement of constant porosity means constant in the equations. We still want to calculate porosity as a function of mineral concentration, but do not treat porosity as a variable.

An important technique to determine parameters is elimination. We find cases where only 1 or a few parameters act and determine them with high accuracy. Then the parameters can be taken as given and more complicated cases are suddenly simplified to contain less variable parameters.

We will find the components of the diffusion coefficient and evaluate whether magnesite or dolomite is best suited to explain the observations or if both minerals should be included.

The development of the solid structure of the core is of great interest and we will see how porosity changes and if it is reasonable to treat it as constant. Also the assumption of a uniform velocity will be checked.

9.2 Simple pressure analysis

As mentioned in section 6.1 pressure p can be eliminated using Darcys law ($V(t) \equiv \frac{Q}{A}$) and a boundary condition (let us say the inlet pressure, p_{inlet}). The steps below are given assuming consistent units with Q volumetric rate, A crossectional area, L the core length and V the seepage velocity. We are especially interested in the pressure drop over the core $\Delta P(t) = p_{inlet} - p_{outlet}$. $Q(t)$ is controlled externally and induces the pressure drop. The overall permeability k falls out of this relation.

$$V(t) \equiv \frac{Q}{A} = -\frac{k}{\nu}\frac{dp}{dx} \Rightarrow \frac{dp}{dx} = -\frac{Q\nu}{kA} \Rightarrow \int_{p_{inlet}}^{p} dp = \int_{x=0}^{x} -\frac{Q\nu}{kA}dx \tag{9.1}$$

$$p(x,t) = p_{inlet} - \frac{Q(t)\nu}{kA}x \tag{9.2}$$

$$\Delta P = p_{inlet} - p(L,t) = Q(t)\frac{\nu L}{kA} \tag{9.3}$$

An important implication of eq (9.3) is that if the injection rate is constant so is the pressure drop. We should expect fluctuations, but if we see any notable changes with time this suggests permeability is affected by the chemical processes.

Such a test can indicate whether the brine is really affecting the permeability and porosity (assuming they are connected locally). This is not pursued further, but can easily be implemented into the algorithm.

9.3 Determination of D and α

The determination of D can be made by comparing the outlet concentrations of Na^+ and Cl^- from experiments with simulations where we select the best value of D. These ions are not participating in the reactions and the concentration movement should only depend on the convection which is constant and the diffusion. D is here fit to Cl^- curve from the experiments of injecting 0.109 M

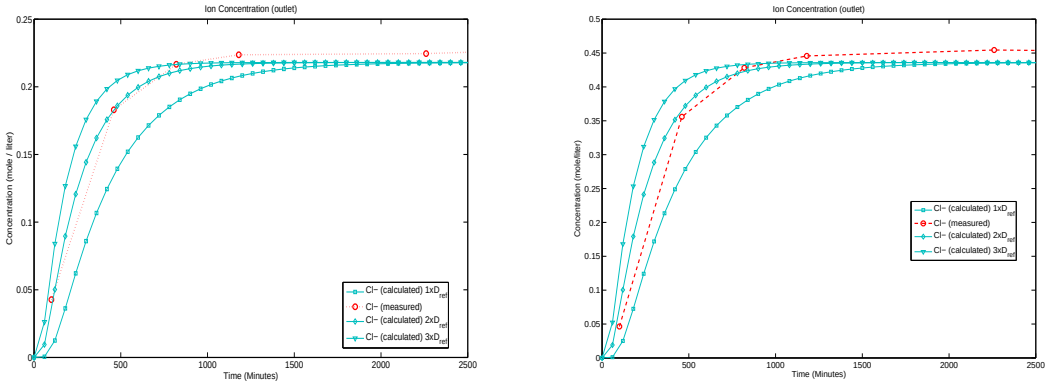

Figure 9.1: Comparison of Cl^- concentrations at outlet with different values of D. Left: injection of 0.109 M $MgCl_2$. Right: injection of 0.218 M $MgCl_2$

$MgCl_2$ and of 0.218 M $MgCl_2$. All simulations here use a time step of 1 hr. The reference value for D in the figure 9.1 is

$$ref = 0.6 \cdot 10^{-7} m^2/s \tag{9.4}$$

which was used in [23].

It is seen that 2 times the reference value makes the best fit in both cases. When we compare this to the experiment of injecting 0.657 M $NaCl$ seen in Fig 9.2 we see that it makes a better fit than D=1 ref, but that it could also be higher.

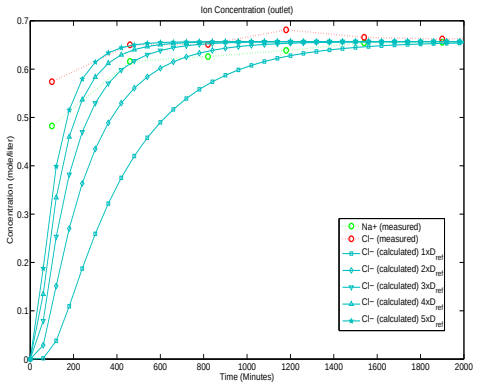

Figure 9.2: Comparison of Cl^- and Na^+ concentrations at outlet with different values of D.

Note that we have only included simulation of Cl^- for the reason that the theoretical distribution of the 2 ions should be identical for $NaCl$ injection into nonionic water. The spread in the 2 experimental curves can indicate the uncertainty in the measurements or perhaps that the ions have a different diffusion coefficient.

We conclude then that

$$D = 1.2 \cdot 10^{-7} m^2/s \quad D' = \frac{D}{\widehat{D}_m} = \frac{12.00}{5.671} = 2.116 \tag{9.5}$$

Assuming

$$D_m = 3.5 \cdot 10^{-9} m^2/s \quad D'_m = \frac{D_m}{\widehat{D}_m} = \frac{3.5}{56.71} = 0.0617 \tag{9.6}$$

as discussed in App C and that the porosity is equal to the initial during these short experiments (D is fit to data mostly before 1 d =1440 min) we calculate

$$D' = D'_m \phi + \frac{\mu J}{\phi} \tag{9.7}$$

$$\mu = (D' - D'_m \phi)\frac{\phi}{J} = (2.116 - 0.0617 \cdot 0.48)\frac{0.48}{0.624} = 1.605 \tag{9.8}$$

$$\alpha = \mu L = 1.605 \cdot 0.07 = 0.112m \tag{9.9}$$

From the numbers above it is seen that the convective diffusion part is dominant in the considered flowing case. If there is no convective flow the diffusion is purely molecular. Both these cases are demonstrated in the test of the convection/diffusion solver for constant porosity in subsection 7.3.3.

9.4 Test of assumption: uniform V

Consider the water phase equation in consistent units

$$\frac{\partial}{\partial t}(\phi C) + \frac{\partial}{\partial x}(CV) = \phi \sum_{ions} \dot{r}_i \tag{9.10}$$

Now transform this equation into dimensionless units

$$\frac{\partial}{\tau \partial t'}(\phi C) + \frac{\partial}{L \partial x'}(C \frac{\widehat{k}\widehat{p}}{L\nu} V') = \phi \sum_{ions} \dot{r}_i \tag{9.11}$$

$$\frac{\partial}{\partial t'}(\phi C) + \frac{\partial}{\partial x'}(C \varepsilon V') = \phi \tau \sum_{ions} \dot{r}_i \tag{9.12}$$

Our assumptions of constant porosity and incompressibility simplifies the equation and we can solve for $\partial_{x'} V'$

$$\frac{\partial}{\partial x'}(V') = \frac{\phi \tau}{C \varepsilon} \sum_{ions} \dot{r}_i \tag{9.13}$$

The ion rates are given by

$$\dot{r}_{ca} = \dot{r}_c + \dot{r}_g + \dot{r}_d, \quad \dot{r}_{so} = \dot{r}_g, \quad \dot{r}_{mg} = \dot{r}_m + \dot{r}_d, \quad \dot{r}_{na} = 0, \quad \dot{r}_{cl} = 0 \tag{9.14}$$

so that

$$\sum_{ions} \dot{r}_i = \dot{r}_{ca} + \dot{r}_{so} + \dot{r}_{mg} + \dot{r}_{na} + \dot{r}_{cl} = \dot{r}_c + 2\dot{r}_g + \dot{r}_m + 2\dot{r}_d \tag{9.15}$$

If we divide eq (9.13) by V' and use that $J \equiv \varepsilon V'$ we get

$$\frac{\partial V}{V \partial x'} = \frac{\partial V'}{V' \partial x'} = \frac{\phi \tau}{CJ}(\dot{r}_c + 2\dot{r}_g + \dot{r}_m + 2\dot{r}_d) \tag{9.16}$$

The left-hand side of eq (9.16) is the gradient of V divided by V, so if this number is small we get that the variation in V over the core is negligible compared to its average value and it is reasonable to assume it is uniform. ϕ, τ, C, J are known quantities at the beginning of the simulation, while the rate terms must be evaluated at specific points and times.

9.5 Determination of rate parameters

All that is left to determine in the model are the rate constants k_c, k_m, k_g, k_d that control the speed of the reactions and their relative importance. Note that since all the rate expressions are of the form

$$\dot{r} = sgn(\rho)F^+ - F^-, \qquad F = k\phi\tau(1-\Omega) \tag{9.17}$$

the rate constants do not express the reactions rates relative to each other in general but expresses how fast dissolution of one mineral occurs relative to another.

All simulations for determining rate constants use a simulation time of 5 days with 48 time steps, so that $\Delta T = 2.5$ hr, unless otherwise specified. The experiments typically last more than 5 days, but a clear trend is observed long before then.

9.5.1 Magnesite model

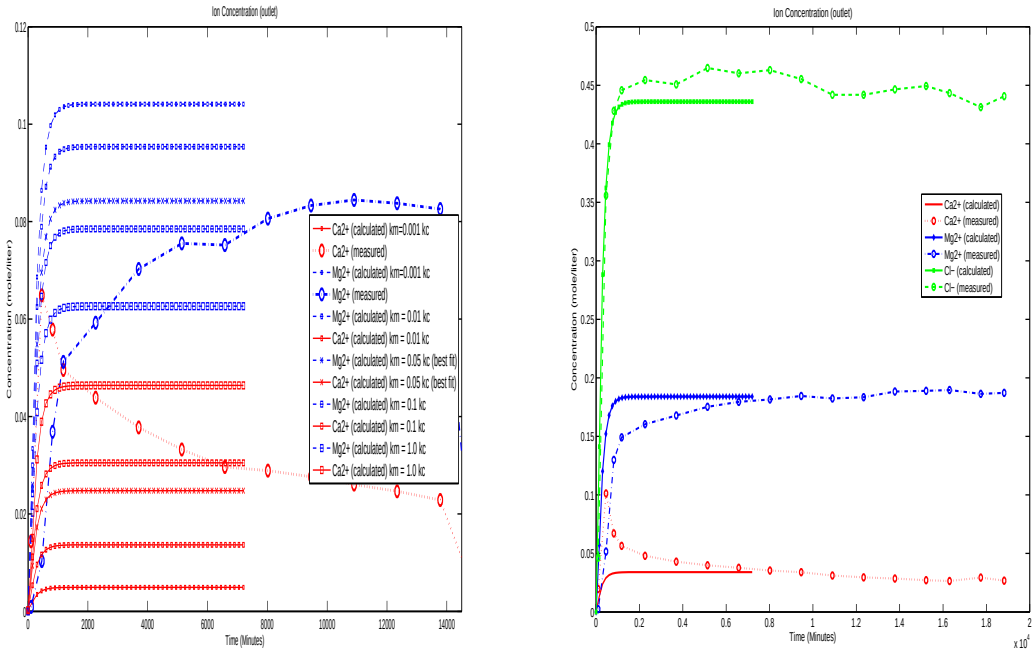

Figure 9.3: Left: Fitting the parameter k_m to data from 0.109 M $MgCl_2$ injection when k_c is already specified to $1.3 \cdot ref$. Right: Comparing the new parameters with data from 0.218 M $MgCl_2$ injection. Ca-curves are red, Mg-curves are blue.

Our starting point is the parameters given in the paper [23]:

$$k_c = 3.125 \cdot 10^{-6} \text{ (mol/liter)/sec}, \quad k_g = 0.03k_c, \quad k_m = 0.09k_c, \quad k_d = 0.00k_c \tag{9.18}$$

From this we define a reference value

$$ref = 3.125 \cdot 10^{-6} \tag{9.19}$$

and express k_c as a multiple of ref and the remaining constants as a multiple of k_c. Since we only consider magnesite among magnesium minerals dolomite is eliminated by keeping $k_d = 0$.

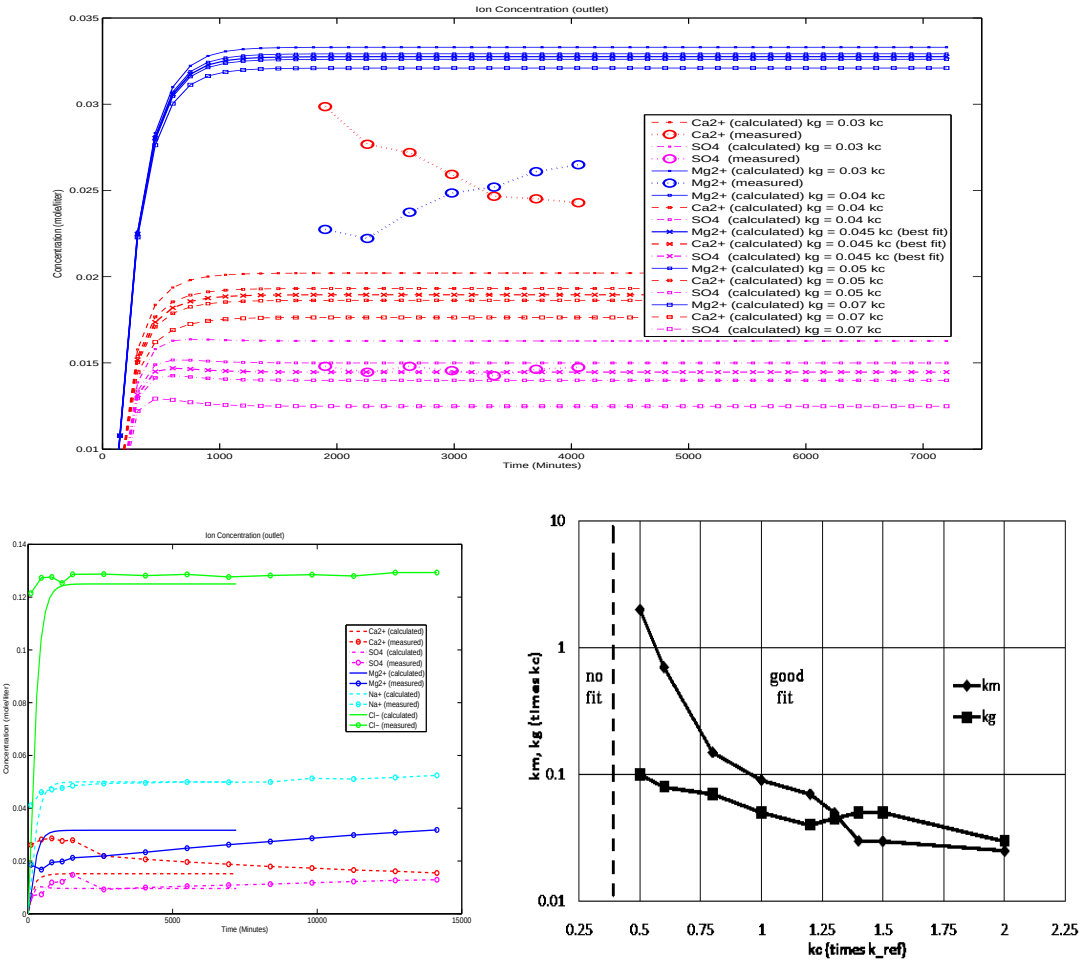

Figure 9.4: Top: Fitting the parameter k_g to data from seawater SW1 injection when $k_c = 1.3 \cdot ref$ and $k_m = 0.05 \cdot k_c$ are already specified. Left: Comparing the new parameters ($k_c = 1.3ref$, $k_m = 0.05k_c$, $k_g = 0.045k_c$) with data from seawater SW2 injection. Right: Parameter combinations. Ca is red, Mg blue, So purple, Na light blue and Cl green.

Choosing the parameters from the experiments goes accordingly:

We select a value for k_c, in this example $k_c = 1.3 \cdot ref$. Then we run simulations with injection of 0.109 M $MgCl_2$ with different values of k_m (note that So-ions are not part of this experiment or simulation so we can set $k_g = 0$ or some other value without changing anything) and select the value that fits best with the effluents of Ca- and Mg-ions (see left in Fig 9.3). We see here that $k_m = 0.05k_c$ makes a good fit compared to the other. Higher values of k_m tends to reduce

the amount of escaping Mg-ions. This means more of the ions are left behind in the core having reacted and formed magnesite.

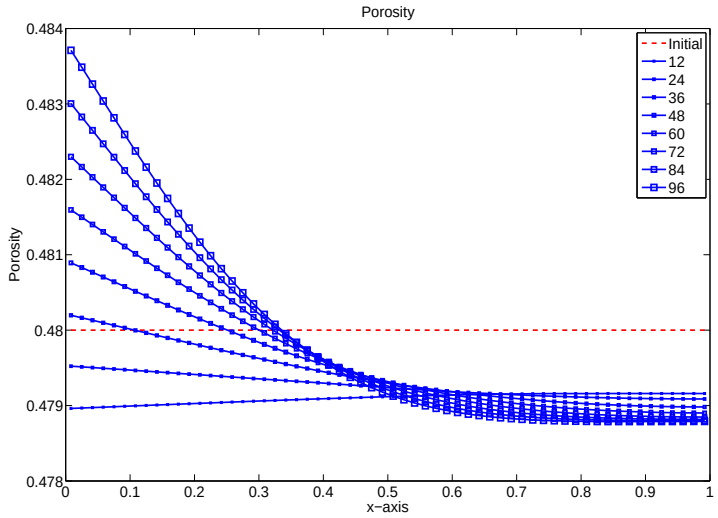

Figure 9.5: Porosity distribution after 2 days with the given number of time steps.

Next the parameters are tested for quality by comparing the simulation with experimental data of injecting 0.218 M $MgCl_2$ (see right in Fig 9.3). The fit is excellent for all involved ions (Na, Ca, Mg). The next step is to determine the last parameter k_g. We then use data from

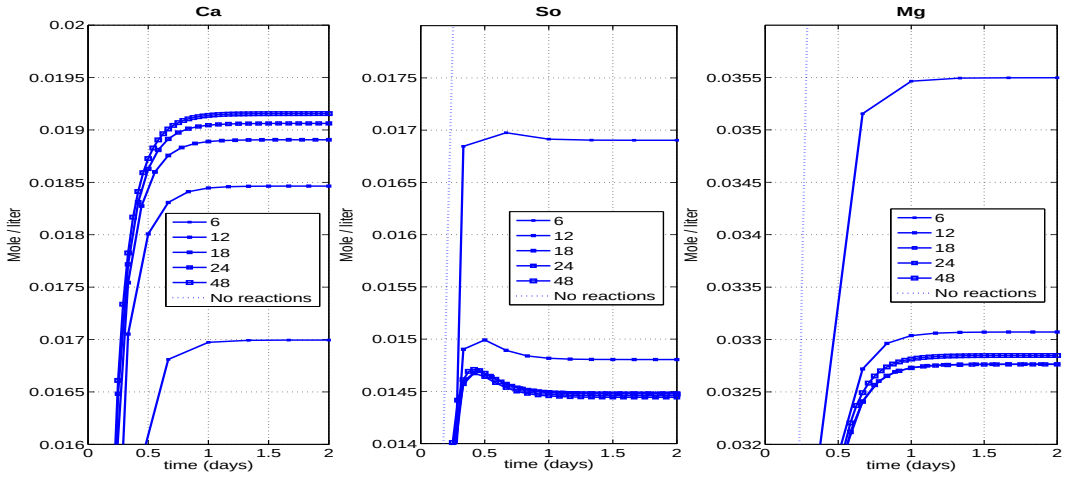

Figure 9.6: Effluents of Ca, So and Mg when injecting SW1 over 2 days. Parameters: $k_c = 1.3ref$, $k_m = 0.05k_c$, $k_g = 0.045k_c$.

injection of seawater SW1 which contains all 5 ions (Ca, So, Mg, Na, Cl) in measurable quantities. As seen top in Fig 9.4 the measured Ca- and Mg- curves have not stabilized and only indicate what they will approach. So-ions have a flat curve and it is better for direct comparison. Using a similar approach as before different values of k_g are tested until a good match is found, in this case $k_g = 0.045 \cdot k_c$.

Finally these parameters are tested against data from seawater SW2 injection. The curves seem to converge to approximately the same values after a long time (left in Fig 9.4).

What is clear after these comparisons is that the model seems to capture the long time behavior quite well, but initially there is a jump in the concentrations of Ca, So and Mg followed by a slow and steady decrease or decline. This is only partially seen in some of the simulated So-curves, but it is clear from a lot of simulations that this transient behavior is not captured by the model.

The choice of k_c may seem arbitrary and it was, although relatively close to the value ref. Actually a lot of different choices of parameters give just as good fit to the data, but as demonstrated: when a specific value of k_c has been selected the values of k_m and k_g are uniquely determined. Several simulation resulted in the different combinations given right in Fig 9.4 (note the logarithmic scale on the y-axis). It was impossible to find a k_m to fit the 0.109 M $MgCl_2$ injection for k_c equal to 0.1 or 0.3 times ref, but higher k_c values always resulted in a good fit with the experiments. Increasing k_c reduces k_m rapidly to a few percent of k_c, while k_g shows less variation. Typical values are then

$$k_c = (0.5 - 2.0)ref, \quad k_m = (0.03 - 2)k_c, \quad k_g = (0.03 - 0.10)k_c \tag{9.20}$$

To test whether the solution is sound we perform a sensitivity analysis on the numerical discretization. For the parameters $k_c = 1.3ref$, $k_m = 0.05k_c$, $k_g = 0.045k_c$ we inject seawater SW1 and vary the time step ΔT (by keeping the time constant to 2 days and varying the number of steps from 12 to 96). We then observe how the porosity distribution changes (Fig 9.5).

There is a difference in the solutions with the time step (the scale of variation is very limited though) and we see that a large time step gives a relatively flat distribution as expected. Increasing the number of steps gives a more heterogeneous distribution and given enough steps the curves will eventually converge to the point that cell 1 has constant reaction rates given by the injection composition (this is correct if we also refine the grid). We see that a time step of 0.5 hr (96 steps) could be preferable, but the solution is also heterogeneous with a time step of 1 hr and this timestep will be used. This also fits well with the time required for transporting the ions from cell 1.

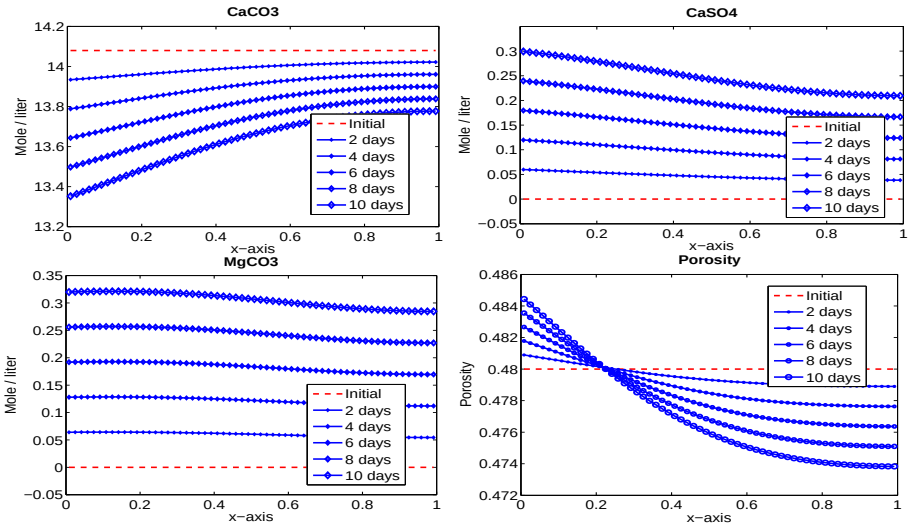

Figure 9.7: Mineral and porosity distributions after 2-10 days of injecting SW1.

When fitting the parameters we have used the flat part of the concentration-time curves resulting from the simulations to compare with experimental data. It is important that these values do not change significantly with the choice of the discretization so the same case above is tested

by comparing effluents of Ca, So and Mg over 2 days when we use 6,12,18,24 and 48 time steps, corresponding to time steps of 8, 4, 2.67, 2 and 1 hrs.

As seen from Fig 9.6 when the time step is coarse the curves look similar to the solution without reactions. When it decreases the curves converge quickly: the last curve is given with twice as many steps, but the difference between it and the one before is less than the previous pair. The curves with 24 and 48 steps deviate with less than 0.0001 mole / liter. Even the 12 step curve could be used which is less than 0.0004 mole / liter from the 48 step curve. Using time steps of a few hours is therefore acceptable, but in simulations where the rate constants are higher the error could increase.

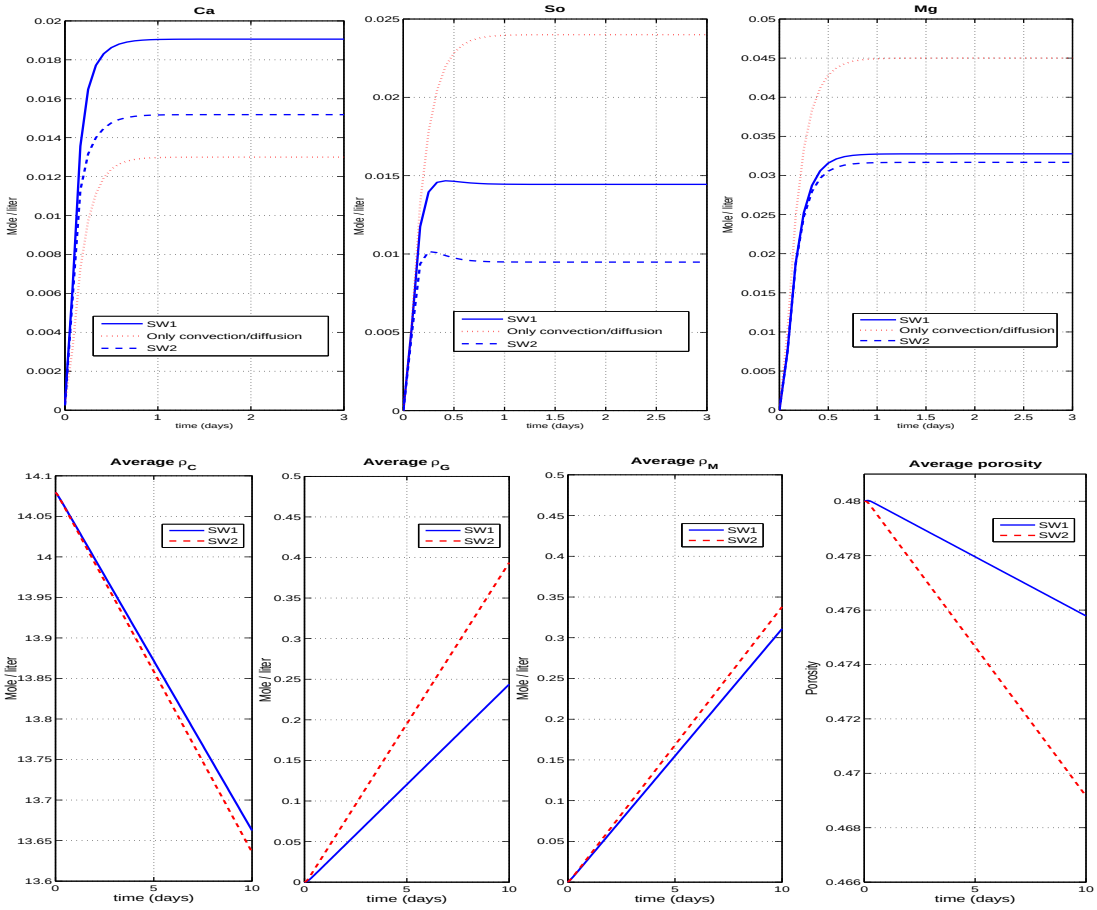

Figure 9.8: Top: Effluent of Ca, So, Mg comparing injection with SW1 vs SW2 and if there are no reactions (only 3 first days shown). Bottom: Average mineral concentrations and porosity vs time.

It is interesting to get predictions from the model and we are especially interested in how the injection of a reactive fluid impacts the composition of the chalk rock. Continuing our case with $k_c = 1.3ref$, $k_m = 0.05k_c$, $k_g = 0.045k_c$, we inject SW1 and observe the mineral and porosity distribution with time (Fig 9.7). Timestep is 1 hr.

What is quite noticeable is that calcite dissolves, while magnesite and anhydrite precipitate over the entire core. The process is most rapid near the inlet and less intense further into the core, but magnesite and anhydrite seem to precipitate more uniformly than calcite dissolves. The result is increased porosity at the inlet and reduced porosity further into the core. Surprisingly there seems to be a fixed point which does not change porosity.

Even when we look at the extreme values of the porosity distribution there is little deviation

from the initial porosity. Our assumption of a constant and uniform porosity then seems to be good.

If we change the brine from SW1 to SW2 there is a noticeable difference in both the outlet concentrations and the rock development (Fig 9.8). We let the simulation run over 10 days with a time step of 1 hr.

Remember that the composition of SW1 and SW2 are identical in Ca, So and Mg, but not in Na and Cl and the ionic strength and activity coefficients (which depends on ionic strength) differ as a result. Since Na and Ca do not participate in the reactions the simulated change is a result of the difference in ionic strength.

The solution without reactions reaches the composition of the injection fluid after about a day and the solutions with reactions stabilize after approximately the same time, but at different levels. Especially SW2 causes the core to retain more Ca and So, resulting in a higher degree of anhydrite precipitation. Apart from that there is little difference in the mineral developments and so the porosity is reduced more with SW2 than with SW1.

Although there is little change in the overall porosity (from 0.48 to about 0.47) there are noticeable changes in the core composition and it should be possible to observe precipitated grains of anhydrite and magnesite in a microscope.

9.5.2 Dolomite model

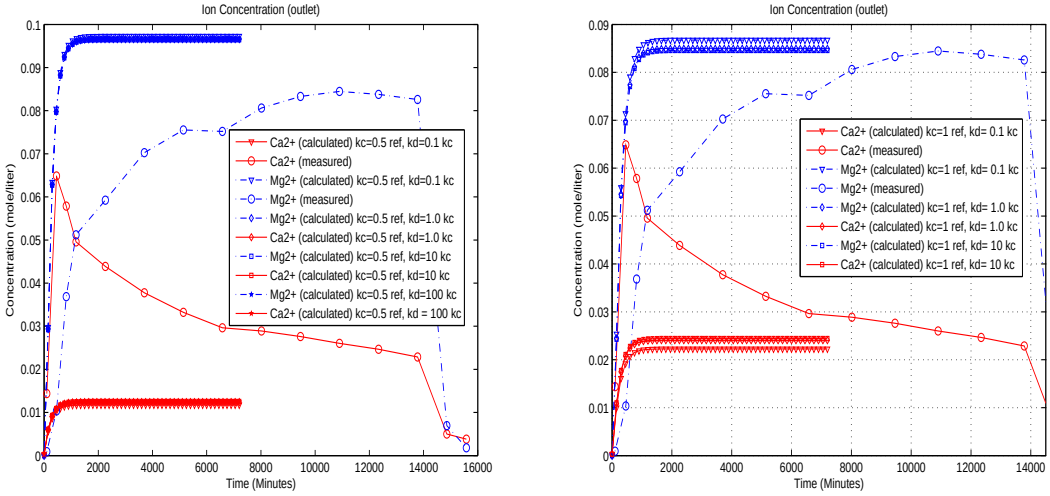

Figure 9.9: Left: No possible k_d if k_c is too low. Right: If k_c is low k_d will be high.

Also this model is based on selecting k_c as a multiple of ref and the remaining parameters k_d and k_g as multiples of k_c. Note that dolomite takes the role of magnesite in this model and we set $k_m = 0$. When we try to fit k_d to the 0.109 M $MgCl_2$ injection there is a problem if we start with small k_c. Let $k_c = 0.5ref$. Then as seen left in Fig 9.9 there is no value for k_d that will fit the experimental data.

Even though k_d is varied from $0.1k_c$ to $100k_c$ there is little change in the curves except if k_d is low and then the curves fit even worse. This limitation on k_c was also observed in the magnesite model producing a lower bound also there.

When k_c is increased to $1.0ref$ there is a fit for $k_d = 10k_c$ (right in Fig 9.9), marking the first k_c with possible match. The procedure continues just as with magnesite. The 0.218 M $MgCl_2$ experiment is checked and found to match the values of k_c, k_d (Fig 9.10). In other simulations performed the experimental data of the 0.218 M solution was always reproduced.

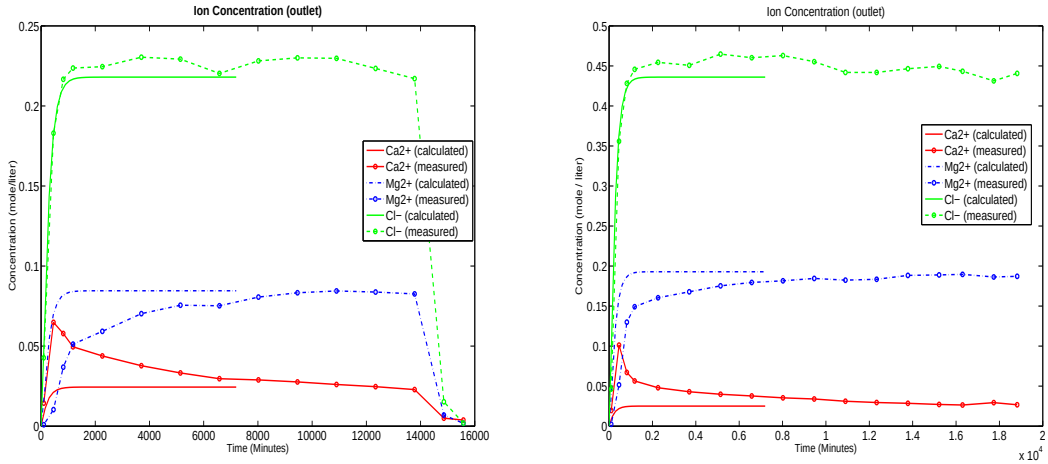

Figure 9.10: Left: Fit data to 0.109 M solution. Right: Comparison to 0.218 M solution.

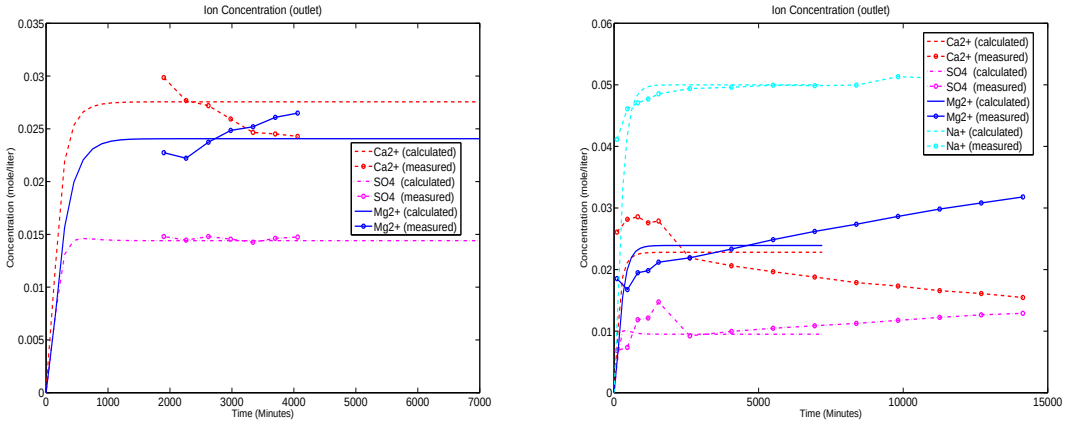

Figure 9.11: Left: Fit to SO-curve with SW1. Right: Comparison with SW2.

Then k_g is determined to 0.04 k_c by fitting the simulated So-curve with the experimental. The corresponding Ca- and Mg- curves do not really follow the trend in SW1. The following check with SW2 (which had more long term data) verify that the parameters are not very good (see Fig 9.11). Similar results was the case in other simulations so finding parameters in the dolomite model is more constrained than in the magnesite model. However for higher values of k_c it is possible to get a good fit to all the data.

Considering the parameters

$$k_c = 1.8ref, \quad k_d = 0.007k_c, \quad k_g = 0.025k_c \tag{9.21}$$

there is a good fit for all the curves, although with SW2 (left in Fig 9.13) the deviations are a bit higher than in the magnesite example.

Right in Fig 9.13 the parameters resulting from fitting the given data are presented. For k_c between 1 and 1.6 times ref we can find parameters to fit the $MgCl_2$ cases and the So-curves in the seawater brines, but the simulated Ca- and So- curves are not close enough to call it a match. When k_c is 1.8 or 2.0 times ref also this fit is good (best for SW1) and we accept the parameters.

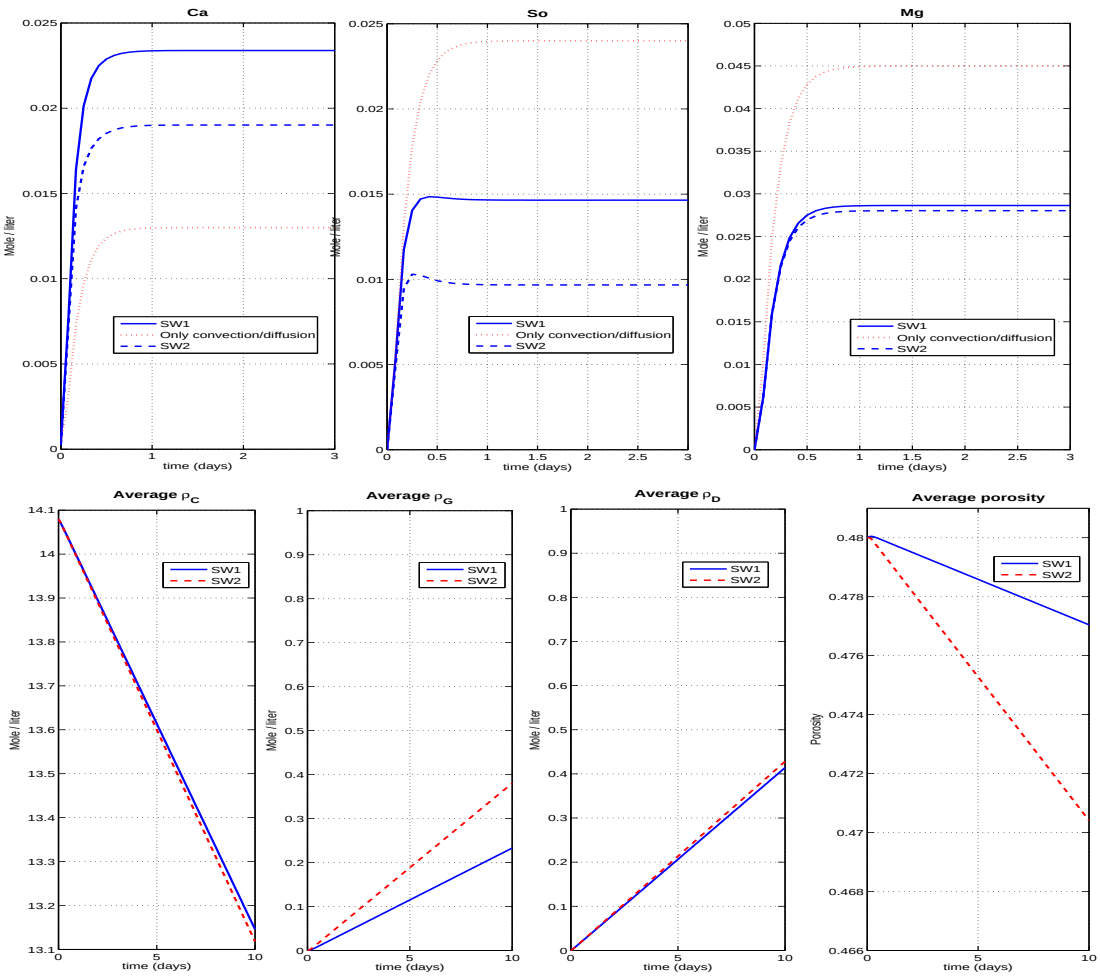

Figure 9.12: Top: Effluent of Ca, So, Mg comparing injection with SW1 vs SW2 and if there are no reactions (only 3 first days shown). Bottom: Average mineral concentrations and porosity vs time.

Since there were possible parameter combinations for the dolomite model it can explain the present experimental data, making dolomite a possible magnesium-based candidate mineral.

Flooding with SW1 and SW2 were performed in the dolomite case (Fig 9.12) and we see the same trends as in the magnesite model: calcite dissolves and the outlet concentration of Ca is greater than the one injected. The opposite is true for Mg and So which are held back in the core to precipitate anhydrite and dolomite. The amount of each mineral changes linearly after a very short time causing the porosity to act the same way. Also in this case there is a porosity reduction.

Note that the Ca curves do not stabilize at the same levels as those for magnesite, while those for Mg and So are very similar. It is because the last 2 were fitted to the same experimental data while the Ca curve followed from the parameters and the fit with experiments is evaluated good if it is in a certain range.

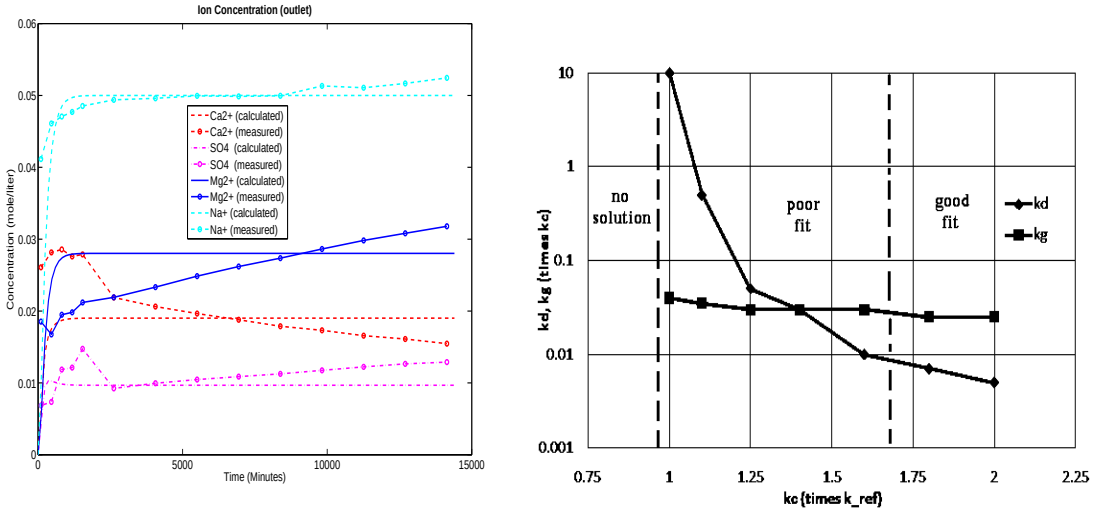

Figure 9.13: Left: Comparison against SW2 with parameters $k_c = 1.8ref$, $k_d = 0.007k_c$, $k_g = 0.025k_c$. Right: Evaluation of different parameters.

9.5.3 Comparison of models

The simulations show that the fit with experiments is good for both models, but more choices are possible with magnesite and a best fit can be selected if requested. However, it is apparent that the rate expressions used in the model do not explain the observations properly. After a day or so the simulated effluent has stabilized its composition and there is no change after that. We have considered especially 2 cases: one for magnesite where $k_c = 1.3ref$, $k_m = 0.05k_c$, $k_g = 0.045k_c$ and one for dolomite where $k_c = 1.8ref$, $k_d = 0.007k_c$, $k_g = 0.025k_c$.

In both the tests we injected SW1. Top in Fig 9.14 we compare the distributions of mineral concentrations and porosity after 10 days. There are some variations in the absolute values, but the trends are more or less the same. Down in Fig 9.14 we have plotted the expressions for dV/Vdx' as given in eq (9.16). It shows that the gradient is less than 8.5% of V and since x' can be no more than 1 we have that V can not vary with more than 8.5%. Thus a constant V is a reasonable assumption.

9.5.4 Inclusion of both minerals

Since there exist parameters that fit the experimental data when $k_d = 0$ and when $k_m = 0$ we have already found solutions to the general model.

However we also would like to have similar amounts of precipitated magnesite and dolomite to recreate the SEM analysis discussed in subsection 3.5.3. Initially the following process was tried:

- Select a value for k_c while all other constants are initially 0.
- Choose k_m so that the simulated Mg-curve falls exactly between the experimental data and the case if $k_m = 0$. In this way half the injected magnesium ions that are lost to the core will precipitate to magnesite.
- Choose k_d so that the simulated and experimental magnesium curves overlap. Then just as many Mg-ions will have been retained in the core
- Select k_g by fitting So curve with SW data.

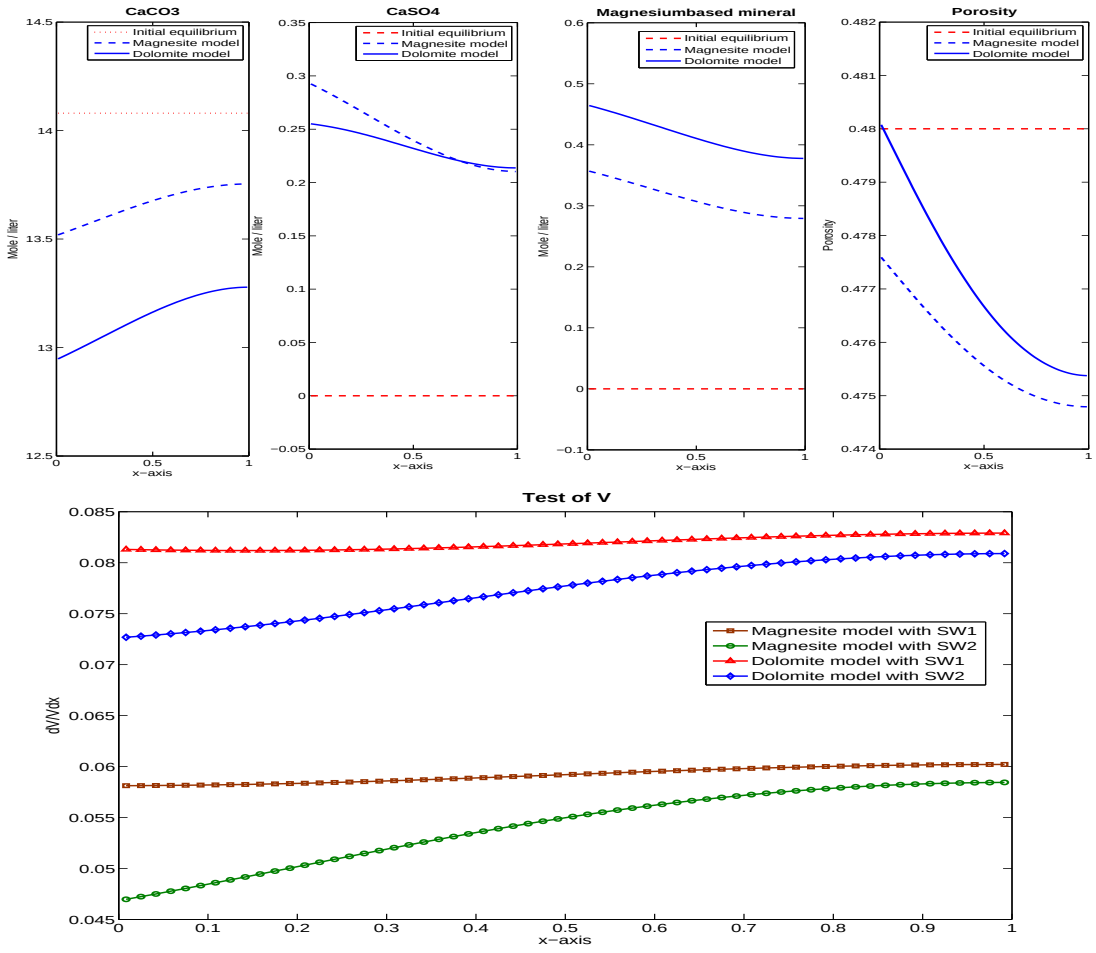

Figure 9.14: Top: distribution of minerals and porosity after 10 days. Bottom: Check of uniform velocity assumption for magnesite and dolomite model, with SW1 and SW2.

However this process has a considerable drawback and that is to not consider the coupling of the system. When k_d was increased from 0 to its supposed value the simulation showed that the average concentration of magnesite and dolomite were an order apart.

A more basic procedure was selected to see if we could find a typical ratio between k_m and k_d that would result in similar amounts of precipitated moles. Basically we kept $k_c = 1$, chose $k_m = 0.005$ and varied k_d to see how the amounts varied in an $MgCl_2$ case. The average mineral concentration as a function of time is very linear (see right in Fig 9.15) so the end values were used for comparison.

From the results presented in Fig 9.15 the ratio $k_d : k_m = 0.1$ seems very good and is supported by simulations with other values of k_m. Only at low values of k_c does this ratio have to be changed.

The parameter determination proceeds similar to the magnesite model:

- Select a value for k_c while all other constants are initially 0.
- Choose k_m with k_d taking the value $0.1k_m$ so that the simulated Mg-curve falls on the experimental data for 0.109 M $MgCl_2$.
- Compare 0.218 M $MgCl_2$ simulation with these parameters.

km (kc)	kd (kc)	rho_m (mol/liter)	rho_d (mol/liter)
0.005	0.01	0.03	0.35
0.005	0.001	0.09	0.17
0.005	0.0005	0.12	0.12
0.05	0.005	0.26	0.20
0.5	0.05	0.37	0.29
0.01	0.001	0.15	0.14

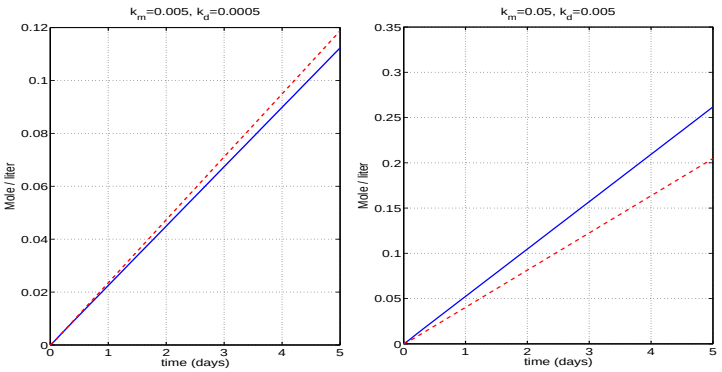

Figure 9.15: Left: Determining k_d : k_m ratio to get similar amount moles precipitation. Right: Average dolomite and magnesite concentrations vs time for two parameter choices.

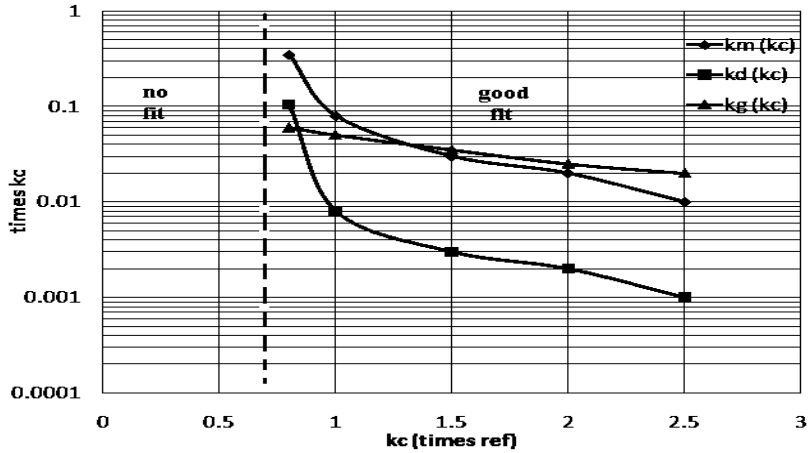

Figure 9.16: Parameters that fit the experiments and give similar precipitation of dolomite and magnesite.

- Select k_g by fitting the So curve with SW1 data. Check that Mg- and Ca- curves follow the correct trend.
- Test parameters on simulation with SW2.

Given a specific k_c the resulting parameters are presented in Fig 9.16. For k_c less than 0.8 it was not possible to keep magnesite and dolomite on the same level and still fit the experimental data. The parameter determination is illustrated for the case

$$k_c = 1.5ref, \quad k_m = 0.03k_c, \quad k_d = 0.003k_c, \quad k_g = 0.035k_c \tag{9.22}$$

in Fig 9.17.

A simulation of injecting SW1 for several days was performed. The time step was 2 hrs. The fluid concentrations at the outlet are given in Fig 9.18. The pH and the ions taking instant equilibrium are included this time and are seen to change fast compared to the other ions, quickly adapting the new environment.

The mineral and porosity concentration changes with time. As before calcite dissolves, while the other minerals precipitate throughout the core. In this case the effect on porosity is the same, a

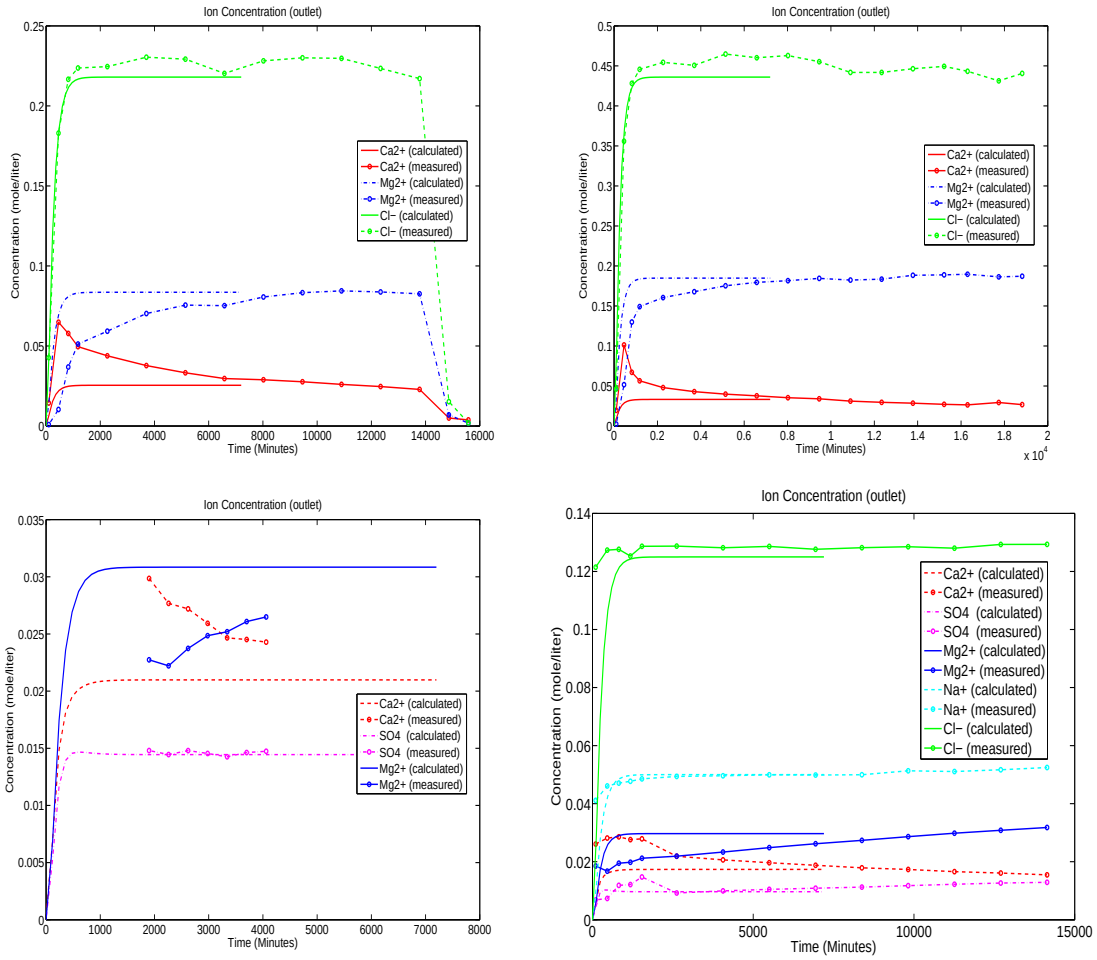

Figure 9.17: a: Find k_m and k_d with 0.109 M $MgCl_2$ data. b: Compare with 0.218 M $MgCl_2$ test. c: Find k_g from SW1. d: Compare with SW2 data.

reduction, but it is most significant farthest from the inlet. Note how the average concentrations of each mineral and also the porosity behaves as a linear function with time. Dolomite and magnesite (and coincidentally anhydrite) precipitate moles of the same magnitude as wanted and are plotted together.

The rates and relative gradient of V are given at different times in Fig 9.20. They all converge to distinct curves after a few days indicating that the system has reached a steady state with convection, diffusion and reactions. This will continue until there is a point in the core where calcite does not exist. This should first happen at the inlet. However the model will also predict a very low porosity at the outlet and given enough time it should reach zero.

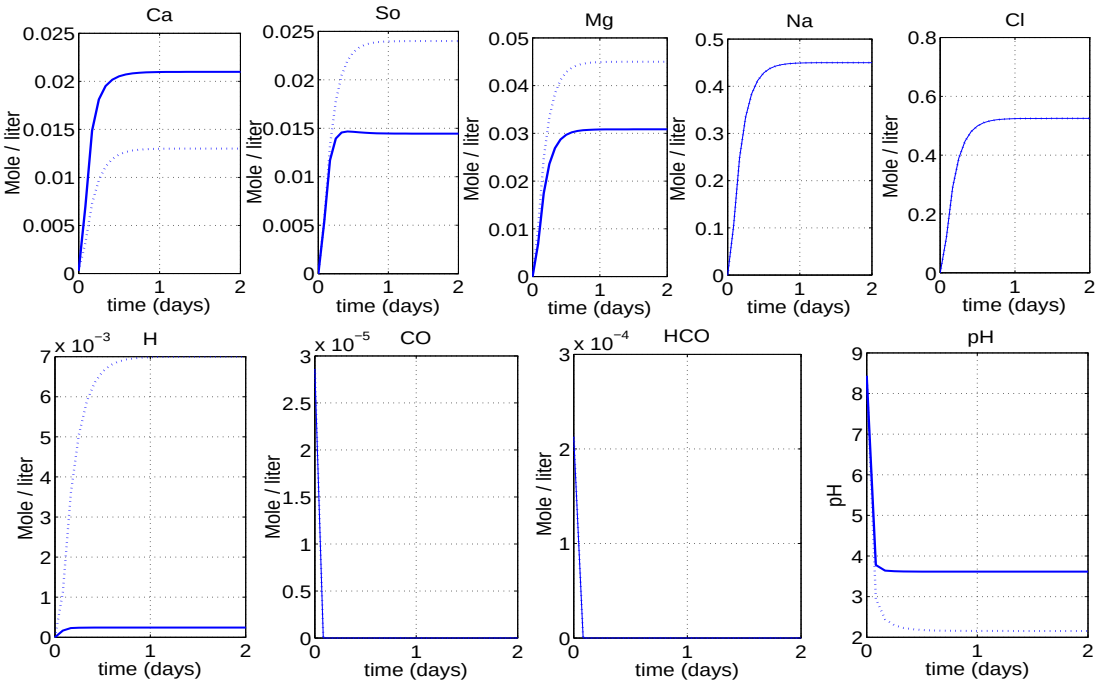

Figure 9.18: Effluents vs time. Dotted lines are the solution without reactions.

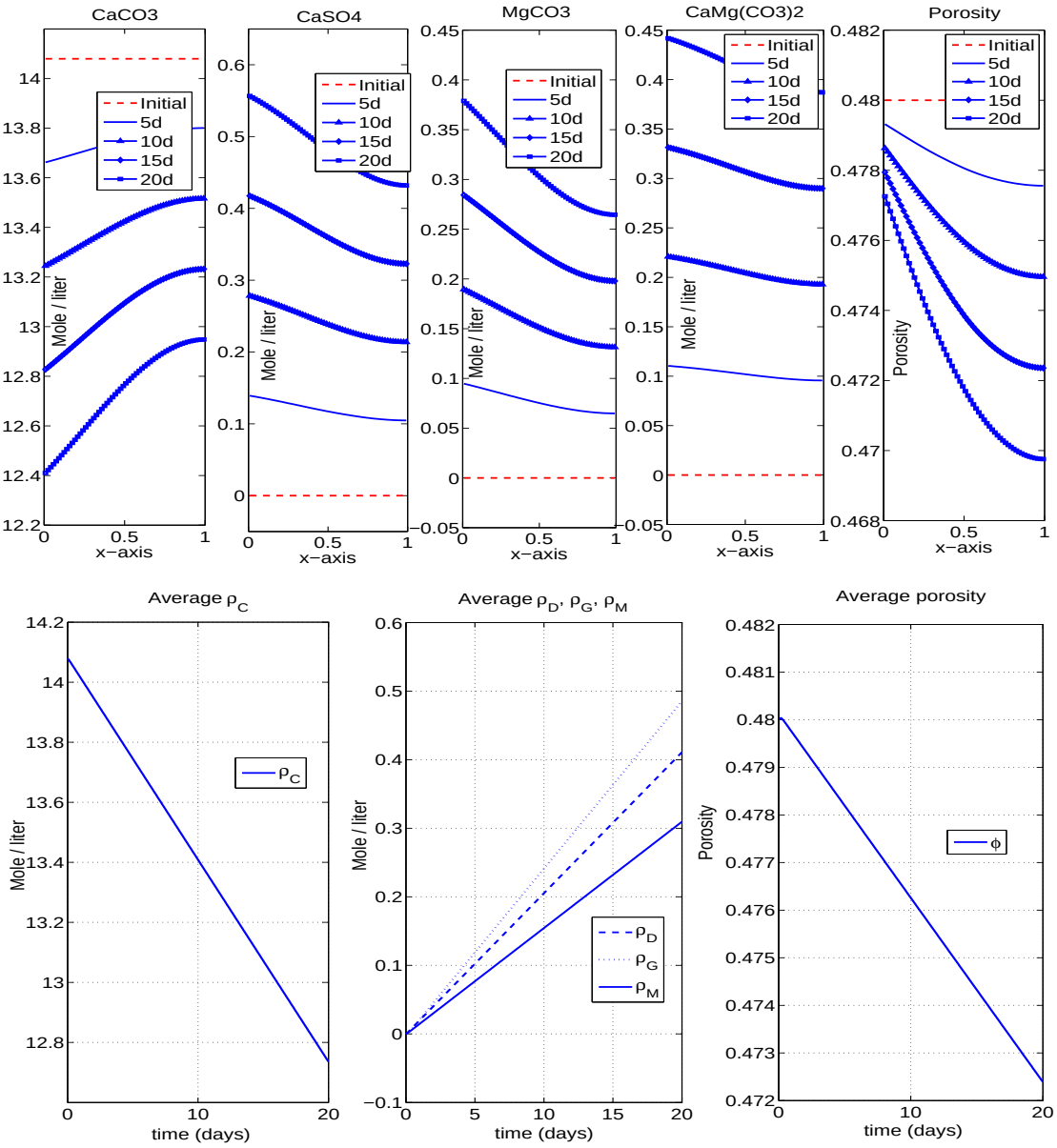

Figure 9.19: Top: Distribution of mineral concentration and porosity at different times. Bottom: Average mineral concentrations and porosity vs time.

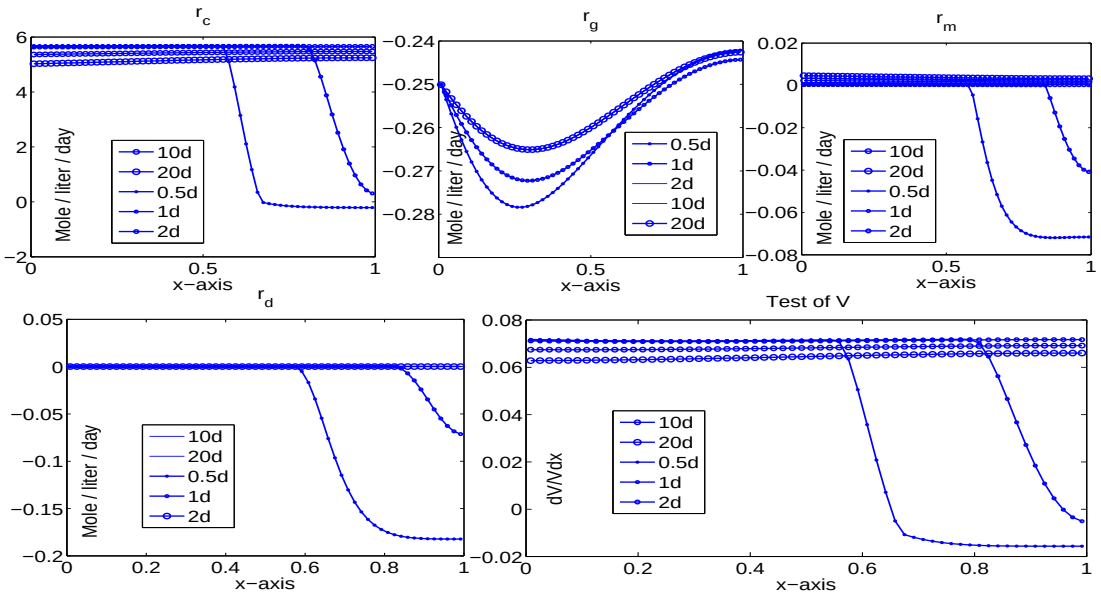

Figure 9.20: Rates and relative gradient of V

Chapter 10

Case II: Variable porosity and permeability

10.1 Assumptions

The most important assumptions here are that the porosity now is updated in the equation system, permeability varies locally with porosity, and the seepage velocity can be considered uniform over the core.

10.2 Theoretical permeability calculations

We can calculate the distribution of permeability given the distribution of porosity using

$$k(x,t) = k_0(x) f(\frac{\phi(x,t)}{\phi_0}) \tag{10.1}$$

From Darcys law we have

$$V(t) = \frac{Q(t)}{A} = -\frac{k(x,t)}{\nu}\frac{\partial p}{\partial x}(x,t) = -\frac{k_{tot}(t)}{\nu}\frac{\Delta P(t)}{L} \tag{10.2}$$

At any given time t we must have

$$k(x)\frac{\partial p}{\partial x}(x) = k_{tot}\frac{\Delta P}{L} \tag{10.3}$$

Numerically this is expressed as

$$k_i\frac{\Delta p_i}{\Delta x} = k_{tot}\frac{\Delta P}{L} \tag{10.4}$$

which can also be written as

$$\Delta p_i = \Delta P\frac{k_{tot}}{k_i}\frac{\Delta x}{L} \tag{10.5}$$

Since pressure drops are additive

$$\Delta P \equiv \sum_i \Delta p_i = \sum_i \Delta P\frac{k_{tot}}{k_i}\frac{\Delta x}{L} = \Delta P k_{tot}\frac{\Delta x}{L}\sum_i \frac{1}{k_i} \tag{10.6}$$

$$\Rightarrow \quad k_{tot}\frac{\Delta x}{L}\sum_i \frac{1}{k_i} = 1 \tag{10.7}$$

The overall permeability measured over the core is then

$$k_{tot} = \frac{L}{\Delta x \sum_i \frac{1}{k_i}} \tag{10.8}$$

Note that this expression is most sensitive to the lowest values of the permeability distribution as expected indicating that a small region of low permeability can markedly reduce the overall permeability.

The pressure drop is simply

$$\Delta P(t) = -\frac{L\nu Q(t)}{Ak_{tot}(t)} \tag{10.9}$$

For the pressure distribution we can use an upwind formulation to simplify

$$\Delta p_i = -\frac{\Delta x \nu Q(t)}{Ak_i} \tag{10.10}$$

$$\Delta p_i = p_i - p_{i-1} \tag{10.11}$$

$$\Delta p_1 = p_1 - \Delta P \tag{10.12}$$

$$\Delta p_I = p_I - p_{i-1} \tag{10.13}$$

With these equations it is possible to derive the pressure distribution. This discussion is not further investigated due lack of experimental data.

10.3 Test of assumption: Uniform V

Again we are interested in testing our assumptions by evaluating if the gradient of V really is 0. The transformed water phase equation has the form

$$\frac{\partial}{\partial t'}(\phi C) + \frac{\partial}{\partial x'}(C\varepsilon V') = \phi\tau \sum_{ions} \dot{r}_i \tag{10.14}$$

We use that C is constant and solve for $\partial_{x'} V'$

$$\frac{\partial}{\partial x'}(V') = \frac{1}{C\varepsilon}(\tau\phi \sum_{ions} \dot{r}_i - C\frac{\partial \phi}{\partial t'}) \tag{10.15}$$

where

$$\sum_{ions} \dot{r}_i = \dot{r}_c + 2\dot{r}_g + \dot{r}_m + 2\dot{r}_d \tag{10.16}$$

Divide by V' and use that $J \equiv \varepsilon V'$ to get

$$\frac{\partial V}{V \partial x'} = \frac{\partial V'}{V' \partial x'} = \frac{1}{CJ}(\tau\phi \sum_{ions} \dot{r}_i - C\frac{\partial \phi}{\partial t'}) \tag{10.17}$$

The expression $\frac{\partial \phi}{\partial t'}$ is evaluated by taking the difference in porosity at step n and $n-1$ and divide by the timestep.

10.4 The reaction solver

The most important difference in the reaction solver is that the porosity used in the calculations is not the constant initial, but is updated with the solutions of the minerals in the ode solver. A simple test with SW1 (which is a reactive brine) as initial water moving towards equilibrium is given with the constants from [23]:

$$k_c = ref, \quad k_m = 0.09k_c, \quad k_g = 0.03k_c, \quad k_d = 0 \tag{10.18}$$

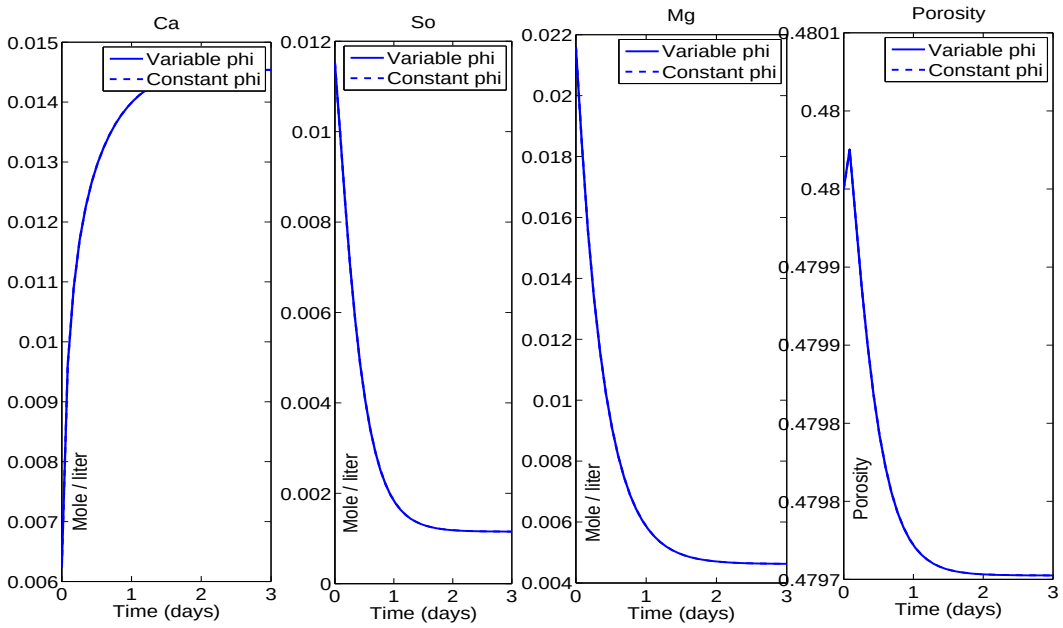

Figure 10.1: Variable porosity does not impact this equilibrium calculation.

It is compared against the same data with the solver using the initial porosity in the equations.

As seen in Fig 10.1 the solutions are impossible to distinguish. Only at small levels are there any differences. The reason is that the porosity changes so little from the initial (0.0003 compared to 0.48) that it does not impact the solution.

10.5 The convection/diffusion solver

Since the stability criterion for this solver was not really proven to be TVD we want to test how robust it is by checking if extreme conditions are solved in a stable manner. The following parameters were used for the simulation:

$$C_{initial} = 10 \quad C_{inj} = 50 \quad \phi_{average} = 0.5 \quad q = 1 \quad J = q\phi_{average} = 0.5 \quad dx = 0.01 \tag{10.19}$$

$$\phi = \begin{cases} 0.7, & 0 < x < 0.3 \\ 0.3, & 0.3 < x < 0.6 \\ 0.5, & 0.6 < x < 1 \end{cases} \qquad D = \begin{cases} 1, & 0 < x < 0.3 \\ 0, & 0.3 < x < 0.6 \\ 1, & 0.6 < x < 1 \end{cases} \tag{10.20}$$

Both the harmonic mean and the arithmetic mean were tested for D, while ϕ used the arithmetic mean. The simulation results after 0.5, 1.0, 1.5 and 2.0 days together with the initial distribution are given in Fig 10.2. Note that the solution shows total concentration and not pore concentration.

The solution with the arithmetic mean seems unphysical while the one with the harmonic mean seems more correct. Since the jumps in ϕ and D were extreme it is assumed the algorithm will handle smoother conditions.

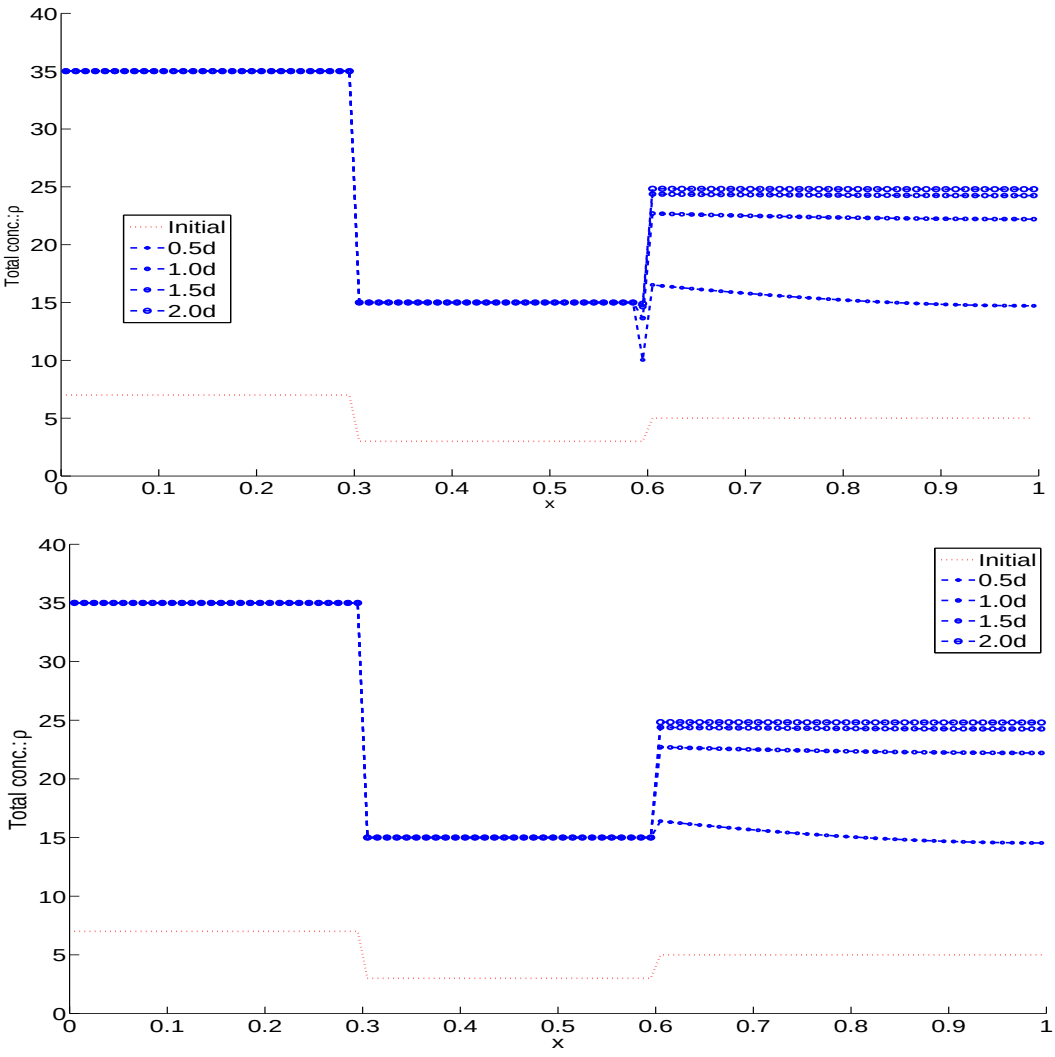

Figure 10.2: Test of the convection / diffusion solver with arithmetic mean (top) and harmonic mean (bottom) for the diffusion coefficient D.

10.6 Full scale simulation

In the previous chapter we argued that the small change in porosity would not impact the solution, but now we want to test if these assumptions are true and if the estimates are correct. To do this we first performed a small test of injecting 0.109 M $MgCl_2$ for 1 day, with a time step of 2 hrs. The parameters were those from [23]:

$$k_c = ref, \quad k_m = 0.09k_c, \quad k_g = 0.03k_c, \quad k_d = 0 \tag{10.21}$$

We compare the effluent of Mg and Ca and observe the distribution in porosity after 1 day (see Fig 10.3). For a reference scale they are compared to the solution without reactions and the initial distribution. What is clear is that also this case is identical to its counterpart with constant porosity, because the porosity is so close to constant during the simulation.

This also illustrates that the parameters found using the constant porosity assumption is sound.

Next we repeated the simulation of injecting SW1 for several days with the parameters

$$k_c = 1.5ref, \quad k_m = 0.03k_c, \quad k_d = 0.003k_c, \quad k_g = 0.035k_c \tag{10.22}$$

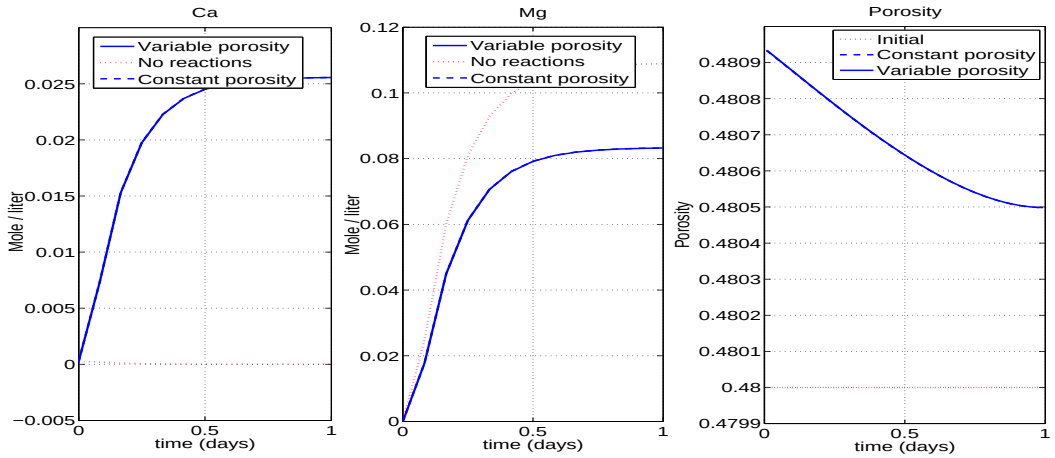

Figure 10.3: Comparing constant and variable porosity models with injection of 0.109 M $MgCl_2$.

(identical to the case in the previous chapter). The timestep was 2 hrs.

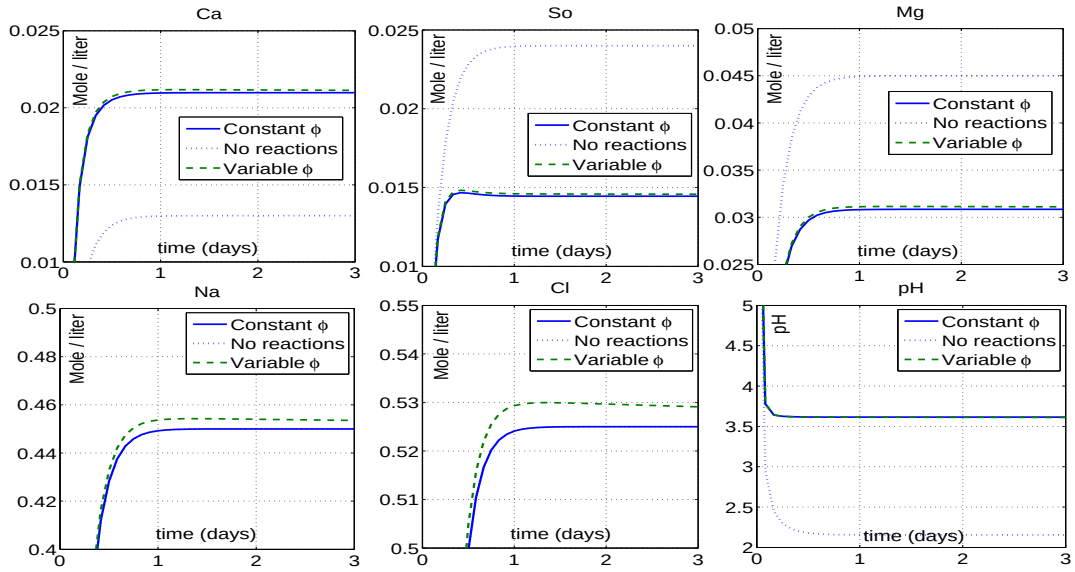

Figure 10.4: Comparison of constant and variable porosity models by considering effluents from injecting SW1

The effluents of Ca, So, Mg, Na, Cl and pH are given in Fig 10.4 comparing with the case of constant porosity. For scale we have included solutions without reactions (they are identical to the case with no reactions for Na and Cl). There is a small, but noticeable difference already from the start. The solutions make a peak value, before slowly descending towards the flat level of the constant porosity solution. This is most clearly seen for Cl in this case. The lab data often had such effects, but on a much larger scale. Several simulations did not reproduce anything similar to that scale.

Since D can vary in this case we plot its distribution with time in Fig 10.5. It is seen that the diffusion coefficient increases with time, and mostly near the outlet. The change is not very

significant (from initial 2.115 to a maximum of 2.16 after 20 days).

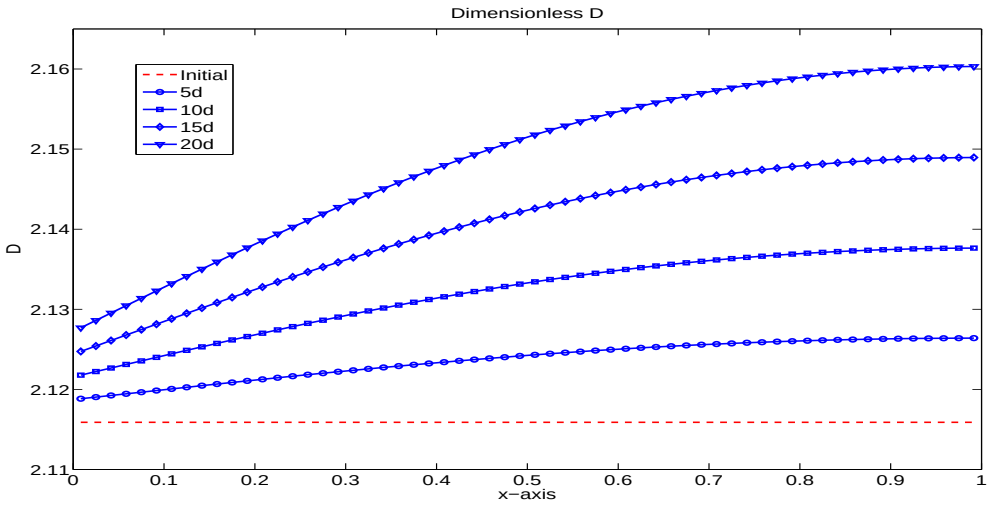

Figure 10.5: Distribution of diffusion coefficients.

Again this can be connected back to a small change in porosity. A seen in Fig 10.6 the porosity has not changed to more than 0.47 from an initial 0.48 after 20 days. The solutions with constant and variable porosity are very similar. When zooming in at the last 5 days of the simulation it is possible to see some variation in the average concentrations and porosity. Looking at the distributions on a normal scale the impression is they are not affected.

Finally we consider the rate expression and the test for uniform V. These distributions at different times are given in Fig 10.7. When comparing this figure with Fig 9.20 we see that the distributions do not converge, but each point seems to move with a constant speed along the y-axis. The reason is probably the linear decrease in porosity so that although the fluid composition is the same there is less pore volume to create minerals and so the rate drops. The values for the relative gradient of V are less than 0.073 a number that is less than for constant porosity, perhaps indicating that this model is better. Since this distribution approaches 0 the assumption seems to improve with time.

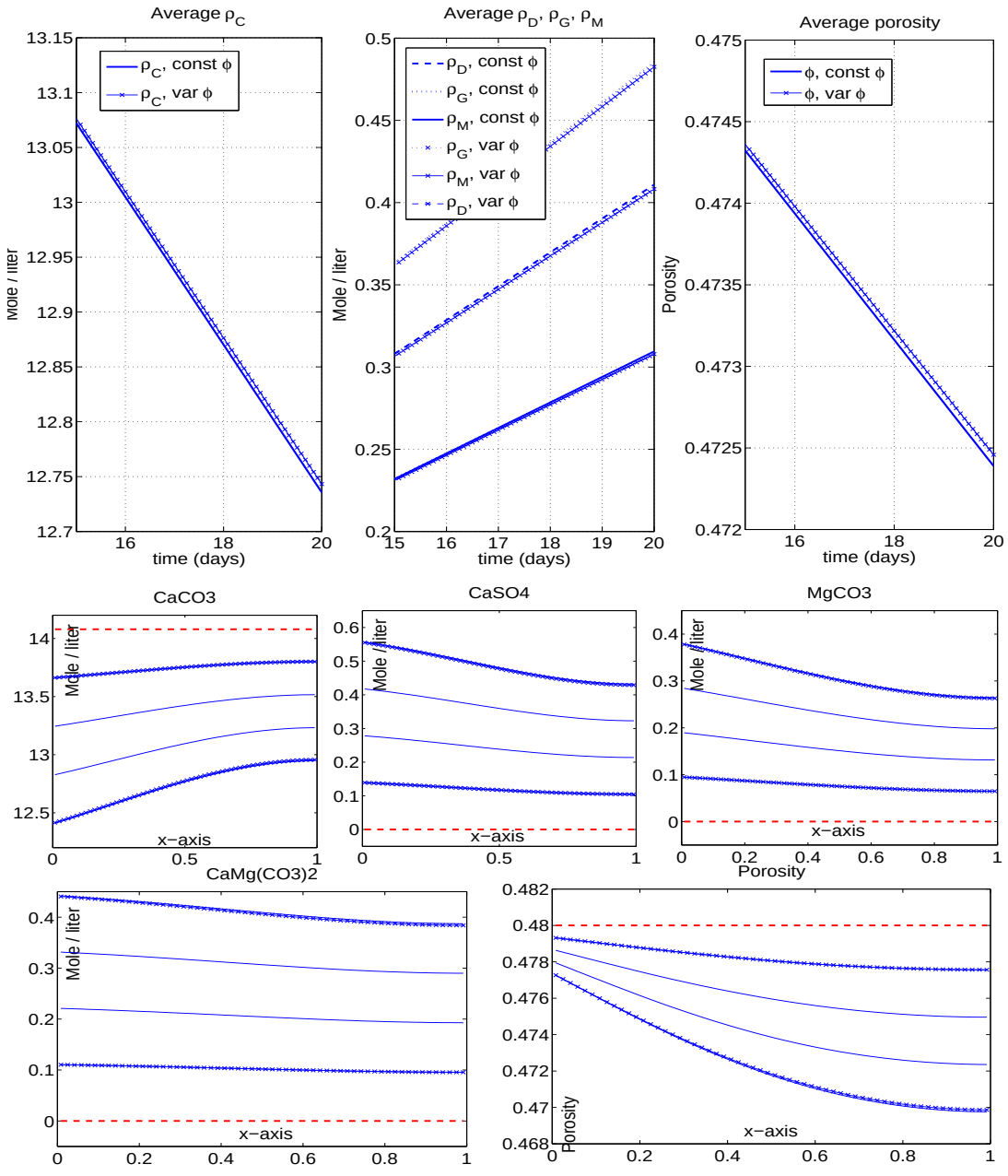

Figure 10.6: Top: average mineral concentrations and porosity with time for variable and constant porosity. Bottom: Mineral and porosity distributions at initial (dotted lines), 5, 10, 15 and 20 days. Solution for variable porosity is given only at 5 and 20 days with crossed points.

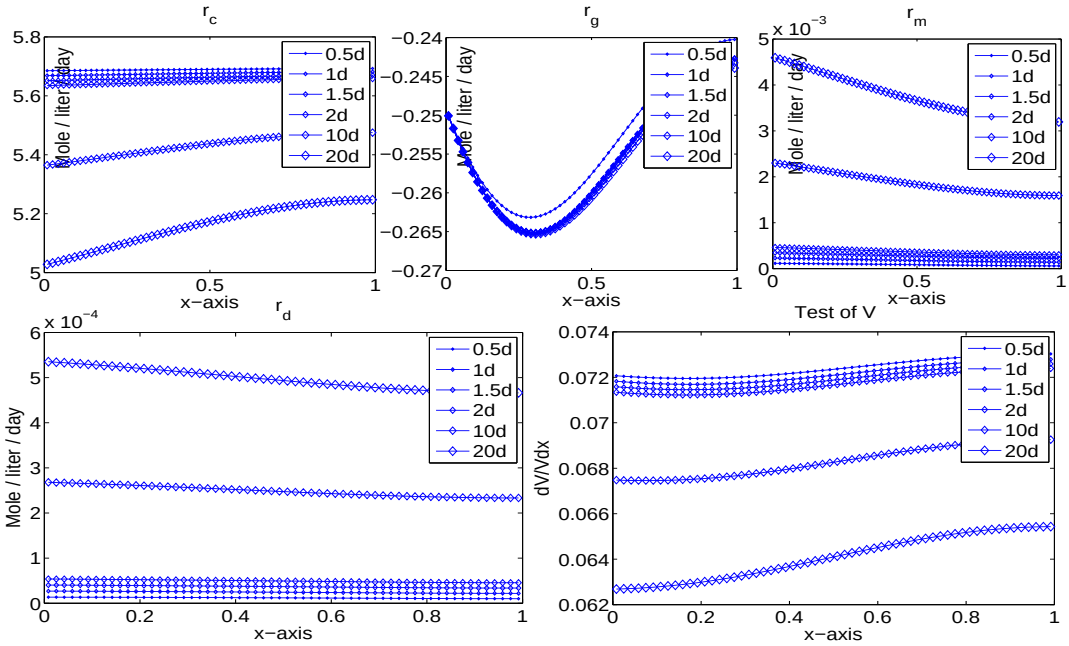

Figure 10.7: Distributions of the rates of each mineral and the relative gradient of V

Chapter 11

Discussion

We will review some of the most important assumptions made in the model and evaluate them

- Na and Cl are not reactive: This is a very good assumption since their experimental effluents match very closely with the simulated values.
- Ca, Mg and So are reactive ions: The experiments and simulations indicate that they are because the effluent is different from the injected brine.
- The diffusion coefficient is the same for all ions: From the slopes of some of the curves we see that this could be a rough assumption (see the $NaCl$ data for example), but and it rarely matches with the early time effluents of ions such as Ca, Mg and So. This is believed to be related to the next point, though.
- Constant rate coefficients: This is a rough assumption. Initially there should a lot of available surface area of calcite causing a high reaction rate, while after a period of precipitation of other minerals the injected brine does not come into contact so easily with the calcite, reducing the observed dissolution. This gradual precipitation on the rock surface could also explain why the effluents are steadily decreasing or increasing in the experimental cases and hopefully also the initial jump in effluent.
- Neglecting C_{co} in expression for charge balance: ideally this should be fixed, although finding C_h then becomes solving a 3rd degree polynomial.
- Constant and uniform porosity: For the data we have considered this is a very good assumption, since the maximum estimated change in porosity is just 0.01.
- Constant seepage velocity V: The simulated data suggest that V would change no more than 8% which is considered little enough to be constant.
- Constant viscosity ν: it could change with composition, but this is not considered.
- Initial composition: We have assumed the entire core is composed of calcite and that everything is uniform initially. It is reasonable for a core plug.

Bibliography

[1] Jon Gluyas, Richard Swarbrick; *Petroleum geoscience*; Chapter 4; Blackwell Publishing, 2004

[2] Knut Bjørlykke; *Sedimentologi og petroleumsgeologi*; Chapter 8, 13; Gyldendahl Forlag, 2001

[3] Tore Prestvik; *Mineralogi, 2. utgave*; Chapters 10, 12; Forlaget Vett og Viten AS, 2005

[4] Jann-Rune Ursin ; *Natural Gas Engineering* ; Chapter 1; UiS, 2008

[5] Edward Tarbuck, Frederick Lutgens ; *Earth science, 11. edition* ; Chapters 2, 3; Pearson Prentice Hall, 2006

[6] E. Fjær, R. Holt, P. Horsrud, A. Raaen, R. Risnes; *Petroleum related rock mechanics, 2. edition*; Chapters 1, 2, 7; Elsevier, 2008

[7] Don W. Green, G. Paul Willhite; *Enhanced oil recovery, SPE textbook series vol. 6*; Chapter 3; Society of Petroleum Engineers, 1998

[8] Malcolm Rider; *The geological interpretation of well logs, 2. edition* Chapter 6; Rider-French consulting Ltd, 2002

[9] Pål Andersen; *Two phase flow in porous media*; Chapters 3, 4, 5; Bachelor Thesis at University of Stavanger, 2009

[10] Antonio Lasaga; *Kinetic theory in the earth sciences* Chapters 1, 2, 4; Princeton University Press, 1998

[11] Masterton and Hurley; *Chemistry; Principles and reactions, 5th edition* Chapter 11; Thomson Learning, 2004

[12] Donald Langmuir; *Aqueous environmental geochemistry* Chapter 4; Prentice-Hall, 1997

[13] (ARMA 01-0121) D. W. Rhett, C. J. Lord; *Water weakening in sedimentary rocks*; DC Rocks 2001, The 38th US symposium on rock mechanics, July 7-10, 2001

[14] (56426-MS) J. Sylte, L. Thomas, D. Rhett, D. Bruning, N. Nagel; *Water induced compaction in the Ekofisk field*; SPE annual technical conference and exhibition, Houston, Texas, 3-6 october, 1999

[15] (18278-PA) I. Ruddy, M. Andersen, P. Pattillo, M. Bishlawi, N. Foged; *Rock compressiblity, compaction and subsidence in a high-prosity chalk reservoir: a case study of Valhall field*; Journal of petroleum technology, Volume 41, number 7, p. 741-746, July, 1989

[16] M. Madland et. al; *Rock fluid interactions in chalk exposed to seawater, MgCl2 and NaCl brines with equal ionic strength*; 15th European symposium in improved oil recovery - Paris, France, 27-29 April 2009

[17] M. Madland, A Hiorth; *Chemical processes in chalk relevant for water weakening*; CoP 13. october, 2009

[18] (31062-PA) J Mortensen, F. Engstrøm, I. Lind; *The relation among porosity, permeability and specific surface of chalk from the Gorm field, Danish North Sea*; SPE Reservoir Evaluation and Engineering Journal, Vol. 1, No. 3, p. 245-251, June 1998

[19] (12636-MS) S. Chen, D. Allard, J. Anli; *Factors affecting solvent slug size requirements in hydrocarbon miscible flooding*; SPE Enhanced Oil Recovery Symposium, Tulsa, Oklahoma, 15-18 April, 1984

[20] (14416-PA) Jan Ypma, G. Koninklijke; *Compositional effects in gravity dominated nitrogen displacements*; SPE Reservoir Engineering Journal, Vol 3, No 3, p. 867-874, August 1988

[21] (118431-PA) T. Austad, M. Madland, T. Puntervold, R. Korsnes; *Seawater in chalk; An EOR and compaction fluid*; SPE Reservoir Evaluation and Engineering Journal, Vol 11, No 4, p 648-654, August 2008

[22] (MR2552169) Steinar Evje, Aksel Hiorth, Merete Madland, Reidar Korsnes; A mathematical model relevant for weakening of chalk reservoirs due to chemical reactions; *Networks and Heterogeneous Media, No. 4, p. 755-788, 2009*

[23] Steinar Evje, Aksel Hiorth, Merete Madland, Reidar Korsnes; *Chemical reactions and weakening of chalk reservoirs: Modeling and experiments*; 20 October 2009

[24] (84303-MS) B Z Shang, J G Hamann H L Chen, D H Caldwell; *A model to correlate permeability with efficient porosity and irreducible water saturation*; SPE Annual technincal conference and exhibition, Denver, Colorado, 5-8 October, 2003

[25] (5646-PA) H S Fogler, K Lund, C C McCune; *Predicting the flow and reaction of HCl/HF acid mixtures in porous sandstone cores*; SPE journal, Vol 16, no 5, p 248-260, 1976

[26]

`http://www.mindat.org/min-1951.html`

[27]

`http://en.wikipedia.org/wiki/Thermal_expansion`

`http://en.wikipedia.org/wiki/Magnesite`

`http://en.wikipedia.org/wiki/Anhydrite`

`http://en.wikipedia.org/wiki/Calcite`

`http://en.wikipedia.org/wiki/Periodic_table`

Appendix A

General model in 3D

The following equations model the distribution of $C, C_{na}, C_{cl}, C_{ca}, C_{so}, C_{mg}, \rho_c, \rho_g, \rho_m, \rho_d, p$ with position x, y, z and time t.

$$\partial_t(\phi C) + \nabla(C\overrightarrow{V}) = \phi(\dot{r}_c + 2\dot{r}_g + \dot{r}_m + 2\dot{r}_d) \quad \text{(A.1)}$$

$$\partial_t(\phi C_{na}) - \nabla(D\phi\nabla C_{na}) = -\nabla(C_{na}\overrightarrow{V}) \quad \text{(A.2)}$$

$$\partial_t(\phi C_{cl}) - \nabla(D\phi\nabla C_{cl}) = -\nabla(C_{cl}\overrightarrow{V}) \quad \text{(A.3)}$$

$$\partial_t(\phi C_{ca}) - \nabla(D\phi\nabla C_{ca}) = \phi(\dot{r}_c + \dot{r}_g + \dot{r}_d) - \nabla(C_{ca}\overrightarrow{V}) \quad \text{(A.4)}$$

$$\partial_t(\phi C_{so}) - \nabla(D\phi\nabla C_{so}) = \phi\dot{r}_g - \nabla(C_{so}\overrightarrow{V}) \quad \text{(A.5)}$$

$$\partial_t(\phi C_{mg}) - \nabla(D\phi\nabla C_{mg}) = \phi(\dot{r}_m + \dot{r}_d) - \nabla(C_{mg}\overrightarrow{V}) \quad \text{(A.6)}$$

$$\partial_t\rho_c = -\phi\dot{r}_c \quad \text{(A.7)}$$

$$\partial_t\rho_g = -\phi\dot{r}_g \quad \text{(A.8)}$$

$$\partial_t\rho_m = -\phi\dot{r}_m \quad \text{(A.9)}$$

$$\partial_t\rho_d = -\phi\dot{r}_d \quad \text{(A.10)}$$

$$\frac{M_w}{\omega_w}\phi C + \frac{M_c}{\omega_c}\rho_c + \frac{M_g}{\omega_g}\rho_g + \frac{M_m}{\omega_m}\rho_m + \frac{M_d}{\omega_d}\rho_d = 1 \quad \text{(A.11)}$$

$$D \equiv (D_m\phi + \alpha\frac{|\overrightarrow{V}|}{\phi})I \quad \text{(A.12)}$$

$$V \equiv -\frac{kI}{\nu}\nabla(p - \omega_w g z) \quad \text{(A.13)}$$

The most significant differences from 5.7.3 are that

- we use the ∇ operator instead of a single space-derivative
- D and k are now in tensor form since they in general can be anisotropic. Above we have assumed isotropic conditions, and therefore the identity matrix I has been used.
- Darcys law for V must be expressed as the gradient of the pressure potential since hydrostatic pressure difference does not produce flow.

All else (rates, aqueous concentrations, etc) can be considered the same as defined in chapter 5. Note especially that the same simplifying assumptions apply.

Appendix B

Basis for $k - \phi$-correlations

B.1 Correlations based on direct estimation

In [24] several correlations are evaluated to predict overall permeability k from different parameters. One correlation including only porosity ϕ is

$$logk = a\phi + b \Leftrightarrow k = 10^{a\phi+b} = 10^b * 10^{a\phi} = a_0 e^{b_0\phi} \tag{B.1}$$

It had a low average of correlation coefficients ($R^2_{avr} \approx 0.3$) for the different sets and ϕ is therefore not a very good predictor by itself. This was expected since many permeabilities can correspond to the same porosity.

By using a variable called effective porosity ϕ_e there was a clear relation to overall permeability given by

$$\log k = a \log(\phi_e) + b \Leftrightarrow k = 10^{a \log(\phi_e)+b} = 10^b \phi_e^a = a_0 \phi_e^{b_0} \tag{B.2}$$

giving very good agreement between estimated and measured permeability ($R^2 \approx 0.9$). ϕ_e is given by

$$\phi_e = \frac{c_k \phi(1 - S_{wr})}{(1 - \phi(1 - S_{wr}))^2 + c_k} \tag{B.3}$$

where S_{wr} is irreducible water saturation and c_k is efficiency of pore structure modified by irreducible water saturation. The input parameters are really formation resistivity factor F, ϕ and S_{wr}. Assuming ϕ is high (good assumption for chalk) and S_{wr} is low we get

$$\phi_e = \frac{c_k \phi(1 - S_{wr})}{(1 - \phi(1 - S_{wr}))^2 + c_k} \approx \frac{c_k \phi}{(1 - \phi)^2 + c_k} \approx \frac{c_k \phi}{c_k} = \phi \tag{B.4}$$

showing that the correlation

$$k = a\phi^b \tag{B.5}$$

might be good. Especially if the porosity is uniform such a correlation should give a good estimate.

B.2 Correlations based on changes in structure

In this case we consider a porous rock that has its properties changed heterogeneously by chemical reactions. We are especially interested in chalks reaction to seawater or similar injection fluids, but in lack of such data we consider acid cleaning of porous rocks. Although these reactions are more violent and can create new channels, the operation is per definition below the fracture pressure and should work by expanding the pores the acid flows through. The correlations differ from another in absolute values, but we are primarily interested in the type of correlations that can be applied to the chemical cleaning.

In [25] the following suggestions (left side) are used by Fogler and coauthors:

$$\frac{k}{k_0} = F(\frac{\phi}{\phi_0})^g \quad \Leftrightarrow \quad k = a\phi^b \tag{B.6}$$

$$\frac{k}{k_0} = e^{\beta(\frac{\Delta\phi}{\Delta\phi max})} \quad \Leftrightarrow \quad k = ae^{b\phi} \tag{B.7}$$

A good reason for only using porosity as a variable is that we can consider the pore throats as a region of locally low porosity. When a distribution of permeability k was assumed (given by a relation such as above) an overall permeability k_t could be calculated and in [25] the experimental results were in reasonable agreement with prediction.

[18] also mentions a $k-\phi$ relation as $k = c\phi^3/s^2$ where c is Kozeny's constant (found by Kozeny to be 0.22-0.24 for porous materials) and s is grain surface area per bulk volume. For a given rock it would seem all we needed to determine was a representative value of s, however we do not know how how this value will change when chemical reactions alter the microstructure itself and assuming it to be constant here seems unreliable.

B.3 Comparison

The 2 methods above differ between a direct correlation of overall permeability with overall porosity and that of treating both porosity and permeability as nonuniform and giving overall estimates based on these distributions. It is believed that the last method is the best and most relevant for this application.

B.4 Correlations between local permeability and local porosity

As described in section 5.4 we require a correlation $f(\cdot)$ such that $k/k_0 = f(\phi/\phi_0)$ which fits

$$f(1) = 1 \quad f(0) = 0 \quad f' > 0 \quad f'' < 0 \tag{B.8}$$

B.4.1 Suggestion I: $f = ax^b + c$

Going through the requirements we can restrict the values of a, b and c.

$$f(0) = c = 0 \tag{B.9}$$

$$f(1) = a = 1 \tag{B.10}$$

$$f' = bx^{b-1} > 0 \rightarrow b > 0 \tag{B.11}$$

$$f'' = b(b-1)x^{b-2} < 0 \rightarrow b - 1 < 0 \tag{B.12}$$

A possible relation that fits the requirements is then

$$f(x) = x^b, 0 < b < 1 \tag{B.13}$$

Note that this correlation would be unphysical since a doubling of the porosity would not even double the permeability.

B.4.2 Suggestion II: $f = ae^{bx} + c$

$$f(0) = a + c = 0 \rightarrow c = -a \tag{B.14}$$

$$f(1) = ae^b + c = ae^b - a = a(e^b - 1) = 1 \rightarrow a = \frac{1}{e^b - 1} \tag{B.15}$$

$$f' = abe^{bx} = \frac{be^{bx}}{e^b - 1} > 0 \rightarrow \frac{b}{e^b - 1} > 0 \tag{B.16}$$

$$f'' = ab^2e^{bx} = b\frac{be^{bx}}{e^b - 1} < 0 \rightarrow b < 0 \text{ since } \frac{b}{e^b - 1} > 0 \tag{B.17}$$

$$b < 0 \rightarrow e^b < 1 \rightarrow e^b - 1 < 0 \tag{B.18}$$

$$e^b - 1 > b \rightarrow b > 0 \tag{B.19}$$

The last implication is true since the two expressions have equal value and derivative at $b = 0$ and the derivative of the left expression is increasing to the right and decreasing to the left, while the left side has constant slope. Since the only possible value for b then is 0 we get $f = \frac{e^x - 1}{e - 1}$ leaving little room for experimental fitting.

B.4.3 Suggestion III: Stepwise smooth f

We assume a function of the form

$$f = f_1(x) \text{ for } 0 < x < 1 \text{ and } f = f_2(x) \text{ for } x > 1 \tag{B.20}$$

$$\text{Both } f_i = a_i x^{b_i} + c_i \text{ or both } f_i = a_i e^{b_i x} + c_i \tag{B.21}$$

The reason for ([?]) is that the processes of cleaning (increased porosity) and filling (decreasing porosity) have or should at least be permitted to have different effects on permeability. ([?]) is used so that equal behavior can be reflected in equal functions. We modify our requirements accordingly:

- $f(0) = 0 \rightarrow f_1(0) = 0$
- $f(1) = 1 \rightarrow f_1(1) = f_2(1) = 1$
- $f' > 0 \rightarrow f_1', f_2' > 0$
- $f_2'' < 0$ if cleaning widens pore throats effective
- $f_1'' > 0$ if grain deposition fills the pores to a higher degree than plugging pore throats

As shown the first 3 requirements on f_1 gives a function of the form x^{b_1} with $b_1 > 0$. The last requirement is that $f_1'' = b_1(b_1 - 1)x^{b_1 - 2} > 0$ which leads to $b_1 > 1$. Regarding $f_2 = a_2 x^{b_2} + c_2$ we have

$$f_2(1) = a_2 + c_2 = 1 \tag{B.22}$$

$$f_2' = a_2 b_2 x^{b_2 - 1} > 0 \rightarrow a_2 b_2 > 0 \tag{B.23}$$

$$f_2'' = a_2 b_2 (b_2 - 1) x^{b_2 - 2} < 0 \rightarrow b_2 < 1 \tag{B.24}$$

The total expression for f is then

$$f = \begin{cases} x^a & 0 < x < 1 \\ bx^c + 1 - b & x > 1 \end{cases} \tag{B.25}$$

with

$$a > 1; b > 0; 0 < c < 1 \tag{B.26}$$

$$\text{or } a > 1; b, c < 0 \tag{B.27}$$

With the other functional form $f_i(x) = a_i e^{b_i x} + c_i$ we get

$$
\begin{aligned}
f_1(0) &= a_1 + c_1 = 0 && \text{(B.28)}\\
f_1(1) &= a_1 e^{b_1} - a_1 = 1 \rightarrow a_1 = \frac{1}{e^{b_1} - 1} && \text{(B.29)}\\
f_1' &= a_1 b_1 e^{b_1 x} > 0 \rightarrow a_1 b_1 > 0 && \text{(B.30)}\\
f_1'' &= a_1 b_1^2 e^{b_1 x} > 0 \rightarrow \frac{1}{e^{b_1} - 1}, b_1 > 0 \rightarrow b_1 > 0 && \text{(B.31)}\\
f_2(1) &= a_2 e^{b_2} + c_2 = 1 && \text{(B.32)}\\
f_2' &= a_2 b_2 e^{b_2 x} > 0 \rightarrow a_2 b_2 > 0 && \text{(B.33)}\\
f_2'' &= a_2 b_2^2 e^{b_2 x} < 0 \rightarrow a_2, b_2 < 0 && \text{(B.34)}
\end{aligned}
$$

In this case f is

$$
f = \begin{cases} \frac{e^{ax}-1}{e^a-1} & 0 < x < 1 \\ be^{cx} + 1 - be^c & x > 1 \end{cases} \qquad \text{(B.35)}
$$

with

$$
a > 0; b, c < 0 \qquad \text{(B.36)}
$$

Note that either of these formulas require determination of 3 parameters and need sufficient measurements of permeability and porosity from both a cleaning process and a deposition process. The formula should be used to describe the local permeability since the porosity distribution can develop heterogeneously. One could also simplify by applying it to the minimum porosity since this is what effectively determines the flow resistance.

A more complex approach that includes hysteresis effects between porosity and permeability would be to look at a differential of the form

$$
dk = \begin{cases} r_+(\phi, k)d\phi & , d\phi > 0 \\ r_-(\phi, k)d\phi & , d\phi < 0 \end{cases} \qquad \text{(B.37)}
$$

where r_+ and r_- are positive functions describing the rate of change of permeability if porosity increases or decreases. As seen the rates should depend on the instant porosity and permeability.

B.4.4 Selected correlation

Since pressure data is not available for the given experimental data and no attempt has been made to produce such results we can rather guess a correlation and show how this would affect the overall permeability and pressure response.

B.4.5 Suggested experimental investigation of relation between k and ϕ

We want to find out how the permeability of a core of chalk will be affected by a change in its porosity. The porosity alteration is made by exposing the core to a chemically reactive fluid (for example $MgCl_2$-solution). This involves keeping a constant temperature and pressure since different states will result in different reaction behavior.

- First measure initial porosity and permeability
- The fluid should be pumped through the core at a slow rate since newly deposited grains may be removed by the flow. Density and viscosity of the fluid can be measured separately or be computed and the permeability can be calculated by measuring the pressure drop and length over the core and knowing the volume rate:

$$
q = -\frac{kA}{\mu}\frac{\Delta P}{\Delta x} \qquad \text{(B.38)}
$$

- The porosity can be measured by weighing the wet core after the permeability test, dry it and then weigh the dry core.
- The injection can proceed and when a significant increase/decrease in the pressure drop over the core has been reached a new measurement can be performed.

Appendix C

The effective diffusion coefficient D

C.1 Definition of D

Given an imaginary surface drawn through a fluid phase. If there is a concentration gradient over the surface there will be a diffusive flux across the surface given by Ficks first law [10, 7]:

$$\text{Diffusive flux} = -\text{Diffusion coefficient} \cdot \text{Concentration gradient} \tag{C.1}$$

$$Cv = -D \cdot \frac{\partial C}{\partial x} \tag{C.2}$$

C is concentration, D which is the proportionality constant is defined as the diffusion coefficient and v is the induced component velocity across the surface.

C.2 Experimental determination of D

Given 2 fluids of same phase but unequal concentration C of a substance we can consider a displacement process. Experiments conducted with constant interstitial velocity v and constant effective diffusion coefficient D can analytically be shown to obey the differential equation

$$\frac{\partial C}{\partial t} = -v\frac{\partial C}{\partial x} + D\frac{\partial^2 C}{\partial x^2} \tag{C.3}$$

If we take constant porosity and no chemical reactions in the transport equations for our model we get the same

$$\partial_t(\phi C_i) - \partial_x(D\phi\partial_x C_i) = \phi\dot{r}_i + \partial_x(C_i\frac{k}{\nu}\partial_x p) \tag{C.4}$$

$$\phi\partial_t(C_i) - D\phi\partial_x^2(C_i) = -\partial_x(C_i V) \tag{C.5}$$

$$\phi\partial_t(C_i) = -\phi v\partial_x(C_i) + D\phi\partial_x^2(C_i) \tag{C.6}$$

$$\partial_t(C_i) = -v\partial_x(C_i) + D\partial_x^2(C_i) \tag{C.7}$$

The differential equation above with initial conditions $C(x,0) = 0$ for all $x > 0$ and boundary conditions $C(0,t) = 1$, $C(\infty,t) = 0$ for $t > 0$ has the analytical solution

$$C(x,t) = \frac{1}{2}\left[1 - erf\left(\frac{x - vt}{2\sqrt{Dt}}\right)\right] \tag{C.8}$$

for normalized concentration C and $erf(\cdot)$ is the error-function. By comparing the profile at the outlet with the error function we can estimate D for a certain porosity and interstitial velocity. The procedure is explained in better detail in [7].

Some important assumptions in the derivation of this solution and thus estimation of D are that the fluid is one-phase (which holds for different brines), but also equal densities and mobilities. The density assumption typically concerns gravity override (this is negligible when the densities are as close as they are) and mobility ratio effectively means viscosity ratio (since the fluids are single phase). High salinity can increase viscosity. If the displacing fluid is less viscous it can finger through and increase the dispersion. It is assumed such effects are negligible by using a constant viscosity ν.

C.3 Correlations for D

According to [7] the effective dispersion coefficient D can be written as the sum of an apparent molecular diffusion component D_{ma} and a convective-dispersive component D_{cd}

$$D = D_{ma} + D_{cd} \tag{C.9}$$

The D_{ma} is a correction of the molecular diffusion coefficient D_m due to the porous paths the ions travel to move a horizontal distance depending on formation (resistivity) factor F_R and porosity ϕ. D_{cd} depends on interstitial velocity v, the formation inhomogeneity factor F_I and the average particle diameter d_p. Viscous fingering depends on the presence of a pressure drop and should be related to the convective part, but we assume a constant viscosity and ideal behavior.

The Perkins-Johnston correlation states that

$$D = \frac{D_m}{F_R \phi} + \frac{v F_I d_p}{2} \tag{C.10}$$

The formation factor F_R is defined as the resistivity measured over a core saturated with a given fluid, divided by the resistivity of the fluid itself. According to [8] F_R can be correlated to porosity and lithology by an expression of the form

$$F_R = a\phi^m \tag{C.11}$$

Especially for chalk and tight formations the relation is given by

$$F_R = \frac{1}{\phi^2} \tag{C.12}$$

To determine useful values for the other parameters we consider the literature.

- A study of the North Sea chalk field Gorm in [18] discusses Gorms formation properties. Over the depth of 6989 to 7330 feet the porosity varies between $23 - 43\%$, permeability between $0.1 - 4.6$ mD and average particle diameter varies from 1.0 to 3.0 μm for the different zones.
- In [19] a carbonate system is considered where several models are compared to optimize slug size to displace oil. It is assumed $F_I d_p = 0.0036\ m$, D_m for oil/solvent is $2 * 10^{-9}\ m^2/s$ and D_m for gas/solvent is $1 * 10^{-7}\ m^2/s$.
- [20] describes an immiscible displacement, but mentions that the homogeneity factor particle diameter product for sandstone typically has a value in the range $F_I d_p = 0.001 - 0.006$ m. Also D_m is ca $10^{-9}\ m^2/s$ for liquids and $10^{-7}\ m^2/s$ for gases.

[10] provides the Robinson-Stokes formula for the tracer molecular coefficient D_A of species A (which is interpreted as the molecular diffusion coefficient):

$$D_A = \frac{RT\lambda_A^0}{F^2|z_A|} \tag{C.13}$$

where R is the gas constant, F is the Faraday constant, z_A is the ionic charge, T is absolute temperature and λ_A^0 is the equivalent limiting conductance of the ion. A table of values for D_A

is given in [10] at 3 different temperatures: 0, 18 and 25 degrees Celsius. The data seems to be linear, meaning that also λ_A^0 is constant over that range. Extrapolating these data to 130 degrees (see Fig C.1) we get different values, but the average (we have assumed one coefficient for all ions in the model) is approximately $35 \cdot 10^{-6} cm^2/s = 3.5 \cdot 10^{-9} m^2/s$. This value is similar to that used in the other sources, the uncertainty is only the validity of the stated assumptions.

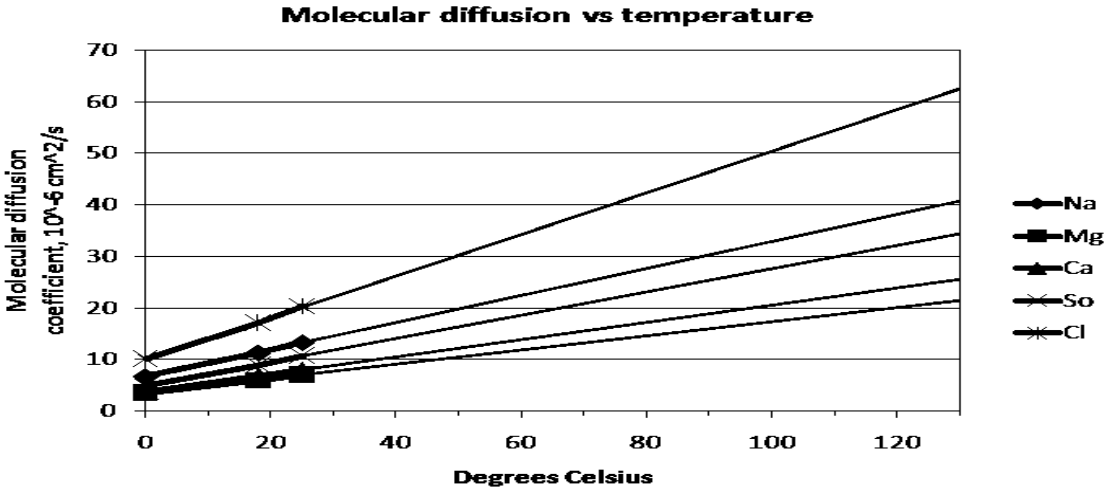

Figure C.1: Extrapolated data of tracer molecular coefficients.

We are mostly looking for typical values and their appropriate magnitude. For a given sample of core data these values should be found more accurately as described above. With no experimental information we would settle with $D_m = 3.5 \cdot 10^{-9}\ m^2/s$ and $F_I d_p = 0.004\ m$. These values are assumed constant although chemical alterations may suggest otherwise. The resulting correlation is then

$$D = D_m \phi + \frac{V}{\phi} \frac{F_I d_p}{2} \tag{C.14}$$

When we estimate this correlation more closely we will measure the initial porosity ϕ, the molecular diffusion coefficient is assumed $D_m = 3.5 \cdot 10^{-9} m^2/s$, V is determined by the injection rate and the overall diffusion coefficient D is adjusted to fit experimental data. Then $\frac{F_I d_p}{2}$ which will also be called α can be determined directly.

In the numerical programming low values of ϕ will increase D greatly and may cause numerical instabilities. In practice we could therefore give a lower limit to the value of ϕ in the denominator.

Appendix D

TVD-analysis

D.1 The convection/diffusion solver for constant porosity

From subsection 7.3.2 we derived a numerical expression for the convection/diffusion solver:

$$\rho_i^{n+1} = \rho_i - \lambda\left([V\rho_i - D_0\frac{\rho_{i+1}-\rho_i}{\Delta x}] - [V\rho_{i-1} - D_0\frac{\rho_i-\rho_{i-1}}{\Delta x}]\right) \tag{D.1}$$

From this we can express the neighbor cell as

$$\rho_{i+1}^{n+1} = \rho_{i+1} - \lambda\left([V\rho_{i+1} - D_0\frac{\rho_{i+2}-\rho_{i+1}}{\Delta x}] - [V\rho_i - D_0\frac{\rho_{i+1}-\rho_i}{\Delta x}]\right) \tag{D.2}$$

Taking the difference we get

$$\begin{aligned}\rho_{i+1}^{n+1} - \rho_i^{n+1} &= \rho_{i+1} - \rho_i - \lambda\left([V\rho_{i+1} - D_0\frac{\rho_{i+2}-\rho_{i+1}}{\Delta x}] - [V\rho_i - D_0\frac{\rho_{i+1}-\rho_i}{\Delta x}]\right) \\ &\quad +\lambda\left([V\rho_i - D_0\frac{\rho_{i+1}-\rho_i}{\Delta x}] - [V\rho_{i-1} - D_0\frac{\rho_i-\rho_{i-1}}{\Delta x}]\right) \qquad \text{(D.3)} \\ &= (\rho_{i+2}-\rho_{i+1})[\lambda\frac{D_0}{\Delta x}] + (\rho_{i+1}-\rho_i)[1-\lambda V - 2\lambda\frac{D_0}{\Delta x}] \\ &\quad +(\rho_i - \rho_{i-1})[\lambda V + \lambda\frac{D_0}{\Delta x}] \qquad \text{(D.4)}\end{aligned}$$

Assume first that

$$|1-\lambda V - 2\lambda\frac{D_0}{\Delta x}| = 1-\lambda V - 2\lambda\frac{D_0}{\Delta x} \geq 0 \tag{D.5}$$

Then

$$\begin{aligned}&|\rho_{i+1}^{n+1} - \rho_i^{n+1}| \leq \\ &|\rho_{i+2}-\rho_{i+1}|(\lambda\frac{D_0}{\Delta x}) + |\rho_{i+1}-\rho_i|(1-\lambda V - 2\lambda\frac{D_0}{\Delta x}) + |\rho_i - \rho_{i-1}|(\lambda V + \lambda\frac{D_0}{\Delta x})\end{aligned} \tag{D.6}$$

From the definition we have

$$TV^{n+1} = \sum_{i=-\infty}^{\infty} |\rho_{i+i}^{n+1} - \rho_i^{n+1}|\Delta x \qquad TV^n = \sum_{i=-\infty}^{\infty} |\rho_{i+i}^{n} - \rho_i^{n}|\Delta x \tag{D.7}$$

so summing eq (D.6) over all i we get

$$\begin{aligned}TV^{n+1} &\leq TV^n(\lambda\frac{D_0}{\Delta x}) + TV^n(1-\lambda V - 2\lambda\frac{D_0}{\Delta x}) + TV^n(\lambda V + \lambda\frac{D_0}{\Delta x}) \qquad \text{(D.8)} \\ &= TV^n \qquad \text{(D.9)}\end{aligned}$$

Note that eq (D.5) is the same as the criterion (7.112).

Our next assumption is

$$|1-\lambda V-2\lambda\frac{D_0}{\Delta x}|=-(1-\lambda V-2\lambda\frac{D_0}{\Delta x})\geq 0 \tag{D.10}$$

Then

$$\begin{aligned}&|\rho_{i+1}^{n+1}-\rho_i^{n+1}|\leq\\&|\rho_{i+2}-\rho_{i+1}|(\lambda\frac{D_0}{\Delta x})-|\rho_{i+1}-\rho_i|(1-\lambda V-2\lambda\frac{D_0}{\Delta x})+|\rho_i-\rho_{i-1}|(\lambda V+\lambda\frac{D_0}{\Delta x})\end{aligned} \tag{D.11}$$

$$\begin{aligned}TV^{n+1} &\leq TV^n(\lambda\frac{D_0}{\Delta x})-TV^n(1-\lambda V-2\lambda\frac{D_0}{\Delta x})+TV^n(\lambda V+\lambda\frac{D_0}{\Delta x}) &\text{(D.12)}\\ &= TV^n[\lambda\frac{D_0}{\Delta x}-1+\lambda V+2\lambda\frac{D_0}{\Delta x}+\lambda V+\lambda\frac{D_0}{\Delta x}] &\text{(D.13)}\\ &= TV^n[-1+4\lambda\frac{D_0}{\Delta x}+2\lambda V] &\text{(D.14)}\end{aligned}$$

For the variation to remain bounded we require

$$-1+4\lambda\frac{D_0}{\Delta x}+2\lambda V\leq 1 \tag{D.15}$$

$$-2+4\lambda\frac{D_0}{\Delta x}+2\lambda V\leq 0 \tag{D.16}$$

$$-(1-\lambda V-2\lambda\frac{D_0}{\Delta x})\leq 0 \tag{D.17}$$

When we compare this with eq (D.10) we see that only one value of Δt is useful. This same value is the upper limit of the interval given by (D.5). In conclusion we have that the method is TVD if

$$1-\lambda V-2\lambda\frac{D_0}{\Delta x}\geq 0 \tag{D.18}$$

D.2 The convection/diffusion solver for variable porosity

When porosity can vary our convection/diffusion solver looks like

$$\begin{aligned}\rho_i^{n+1} &= \rho_i+\lambda\left([D_{0,i+1/2}\phi_{0,i+1/2}(\partial_x\frac{\rho}{\phi_0})_{i+1/2}]-[D_{0,i-1/2}\phi_{0,i-1/2}(\partial_x\frac{\rho}{\phi_0})_{i-1/2}]\right)\\ &\quad -\lambda\left(J(\frac{\rho}{\phi_0})_{i+1/2}-J(\frac{\rho}{\phi_0})_{i-1/2}\right) &\text{(D.19)}\\ &= \rho_i+\frac{\lambda}{\Delta x}\left([D_{0,i+1/2}\phi_{0,i+1/2}(\frac{\rho_{i+1}}{\phi_{0,i+1}}-\frac{\rho_i}{\phi_{0,i}})]-[D_{0,i-1/2}\phi_{0,i-1/2}(\frac{\rho_i}{\phi_{0,i}}-\frac{\rho_{i-1}}{\phi_{0,i-1}})]\right)\\ &\quad -\lambda J\left(\frac{\rho_i}{\phi_{0,i}}-\frac{\rho_{i-1}}{\phi_{0,i-1}}\right) &\text{(D.20)}\end{aligned}$$

Taking differences we get

$$\begin{aligned}\rho_{i+1}^{n+1}-\rho_i^{n+1} &= \rho_{i+1}-\rho_i\\ &\quad +\frac{\lambda}{\Delta x}\left([D_{0,i+1.5}\phi_{0,i+1.5}(\frac{\rho_{i+2}}{\phi_{0,i+2}}-\frac{\rho_{i+1}}{\phi_{0,i+1}})]-[D_{0,i+0.5}\phi_{0,i+0.5}(\frac{\rho_{i+1}}{\phi_{0,i+1}}-\frac{\rho_i}{\phi_{0,i}})]\right)\\ &\quad -\frac{\lambda}{\Delta x}\left([D_{0,i+0.5}\phi_{0,i+0.5}(\frac{\rho_{i+1}}{\phi_{0,i+1}}-\frac{\rho_i}{\phi_{0,i}})]-[D_{0,i-0.5}\phi_{0,i-0.5}(\frac{\rho_i}{\phi_{0,i}}-\frac{\rho_{i-1}}{\phi_{0,i-1}})]\right)\\ &\quad -\lambda J\left((\frac{\rho_{i+1}}{\phi_{0,i+1}}-\frac{\rho_i}{\phi_{0,i}})-(\frac{\rho_i}{\phi_{0,i}}-\frac{\rho_{i-1}}{\phi_{0,i-1}})\right) &\text{(D.21)}\end{aligned}$$

Now let

$$D_0^+ \equiv \max_i(D_{0,i}^n) \qquad \phi_0^+ \equiv \max_i(\phi_{0,i}^n) \qquad \phi_0^- \equiv \min_i(\phi_{0,i}^n) \tag{D.22}$$

Assume for simplicity that we can replace D and ϕ by D_0^+ and ϕ_0^+ in the factors and ϕ_0^- in the denominators. This transfers all the variation to the variation in ρ, but enhances it if the porosity distribution is nonuniform. Then

$$\begin{aligned}
\rho_{i+1}^{n+1} - \rho_i^{n+1} &= \rho_{i+1} - \rho_i \\
&\quad + \frac{\lambda}{\Delta x}\left([D_0^+\phi_0^+(\frac{\rho_{i+2}}{\phi_0^-} - \frac{\rho_{i+1}}{\phi_0^-})] - [D_0^+\phi_0^+(\frac{\rho_{i+1}}{\phi_0^-} - \frac{\rho_i}{\phi_0^-})]\right) \\
&\quad - \frac{\lambda}{\Delta x}\left([D_0^+\phi_0^+(\frac{\rho_{i+1}}{\phi_0^-} - \frac{\rho_i}{\phi_0^-})] - [D_0^+\phi_0^+(\frac{\rho_i}{\phi_0^-} - \frac{\rho_{i-1}}{\phi_0^-})]\right) \\
&\quad - \lambda J\left((\frac{\rho_{i+1}}{\phi_0^-} - \frac{\rho_i}{\phi_0^-}) - (\frac{\rho_i}{\phi_0^-} - \frac{\rho_{i-1}}{\phi_0^-})\right)
\end{aligned} \tag{D.23}$$

$$\begin{aligned}
&= \rho_{i+1} - \rho_i \\
&\quad + \frac{\lambda D_0^+\phi_0^+}{\Delta x\phi_0^-}([\rho_{i+2} - \rho_{i+1}] - [\rho_{i+1} - \rho_i]) \\
&\quad - \frac{\lambda D_0^+\phi_0^+}{\Delta x\phi_0^-}([\rho_{i+1} - \rho_i] - [\rho_i - \rho_{i-1}]) \\
&\quad - \frac{\lambda J}{\phi_0^-}([\rho_{i+1} - \rho_i] - [\rho_i - \rho_{i-1}])
\end{aligned} \tag{D.24}$$

$$\begin{aligned}
&= (\rho_{i+2} - \rho_{i+1})[\lambda\frac{D_0^+\phi_0^+}{\Delta x\phi_0^-}] \\
&\quad + (\rho_{i+1} - \rho_i)[1 - \lambda\frac{J}{\phi_0^-} - 2\lambda\frac{D_0^+\phi_0^+}{\Delta x\phi_0^-}] \\
&\quad + (\rho_i - \rho_{i-1})[\lambda\frac{J}{\phi_0^-} + \lambda\frac{D_0^+\phi_0^+}{\Delta x\phi_0^-}]
\end{aligned} \tag{D.25}$$

Note that eq (D.25) has exactly the same form as eq (D.4) and following a similar analysis as in section D.1 the resulting stability criterion becomes

$$\lambda\frac{J}{\phi_0^-} + 2\lambda\frac{D_0^+\phi_0^+}{\Delta x\phi_0^-} \le 1 \qquad \Leftrightarrow \qquad \Delta t \le \frac{\phi_0^-\Delta x^2}{J\Delta x + 2D_0^+\phi_0^+} \tag{D.26}$$